

**CHARGE DISSIPATION MECHANISM
OF LOW-COST ANTISTATIC ADDITIVE
LIGNIN IN CONTACT CHARGED
POLYMERS**

A THESIS SUBMITTED TO
THE GRADUATE SCHOOL OF ENGINEERING AND
SCIENCE
OF BILKENT UNIVERSITY
IN PARTIAL FULFILLMENT OF THE REQUIREMENTS FOR
THE DEGREE OF
MASTER OF SCIENCE
IN CHEMISTRY

By

Mertcan ÖZEL

July 2019

CHARGE DISSIPATION MECHANISM OF LOW-COST ANTISTATIC ADDITIVE LIGNIN IN CONTACT CHARGED POLYMERS

By Mertcan ÖZEL

July 2019

We certify that we have read thesis and that in our opinion it is fully adequate, in scope and in quality, as a thesis for the degree of Master of Science.

Bilge BAYTEKİN (Advisor)

Ali ÇIRPAN

Burak ÜLGÜT

Yunus Emre TÜRKMEN

Salih ÖZÇUBUKÇU

Approved for the Graduate School of Engineering and Science:

Ezhan KARAŞAN

Director of the Graduate School

ABSTRACT

**CHARGE DISSIPATION MECHANISM OF
LOW-COST ANTISTATIC ADDITIVE LIGNIN IN
CONTACT CHARGED POLYMERS**

Mertcan ÖZEL

M.S. in Chemistry

Advisor: Bilge BAYTEKİN

July 2019

Contact electrification (C.E.), a phenomenon studied for millennia, develops contact charges on material surfaces, when two materials are contacted and then separated. Accumulation of contact charges and their uncontrolled sudden discharges on dielectric polymers pose major drawbacks in industries i.e. pharmaceutical, (micro)electronics, and space, causing million-dollar losses annually. The overall mechanism of C.E. is unclear until now, however, recent efforts have proven that chemical bond-breakages on polymer surfaces result in mechanoions – which are indeed the contact charges on the surfaces. These studies also showed that removing mechanoradicals (co-formed upon bond-breaking) by molecular radical scavengers destabilizes the mechanoions (charges) and render the doped polymer material antistatic. This method of static charge mitigation has an advantage over the conventional methods (e.g. doping with metals, carbon powder, conductive polymers, or surface humidity enhancers) because it is not based on an increase in surface conductance and smaller doping concentrations are needed to achieve

antistatic behavior. However, currently used molecular radical scavenger doping is generally not cost effective method to be upscaled for industrial use.

Lignin; however, is a “low-cost” material (the second most abundant polymer on earth, a by-product of paper production) that can act as a radical scavenger. In this thesis work, lignin was extracted from some examples of both hard and softwood. Firstly, it was verified that lignin doping in low concentrations (1 – 5% w/w) reduce the contact charge accumulation on common polymers such as on a crosslinked elastomer polydimethylsiloxane, and on thermoplastics polypropylene, polyethylene, polylactic acid, and polystyrene. Then, the mechanism of the observed charge dissipation was discussed in the light of the results obtained from surface conductance of polymers upon doping, ³¹P NMR and solid state ¹³C-NMR spectroscopy, total phenol content, and the reacted number of radicals before and after grinding - which was shown essential to get homogeneous doping- of lignin.

The results pointed out a mechanism involving a radical scavenging activity without any change in the surface conductance of the material, similar to that with molecular radicals. The understanding of lignin’s charge dissipation mechanism will be helpful in industrial utilization of lignin as an antistatic additive and in assessment of the limitations of this utilization.

Keywords: *antistatic additives, contact electrification, polydimethylsiloxane, thermoplastic polymers, radical scavengers, static electricity, triboelectricity.*

ÖZET

DOKUNMA İLE ELEKTRİKLENEN POLİMERLERDE DÜŞÜK MALİYETLİ ANTİSTATİK KATKI MALZEMESİ OLARAK KULLANILAN LİGNİN'İN YÜK SÖNÜMLEME MEKANİZMASI

Mertcan ÖZEL

Kimya, Yüksek Lisans

Tez danışmanı: Bilge Baytekin

Temmuz 2019

Dokunma ile elektriklenme (D.E.) iki yüzeyin birbirine dokundurulup ayrılması sonucu yüzeylerin elektriksel yüklenmesidir ve binlerce yıldır neden ve nasıl oluştuğu sorgulanmaktadır. Yüzeylerde yük birikmesi, ilaç, mikroelektronik ve uzay gibi bir çok endüstride ciddi bir problem yaratmakta ve yıllık milyonlarca dolarlık zararlara sebep olmaktadır. D.E. mekanizması hala daha tam olarak ortaya konamamıştır ancak yakın zamanda malzemelerin bir araya gelip ayrılmaları sırasında yüzeyde oluşan bağ kırılmaları sonucu oluşan mekanoiyonların yüzeydeki yükleri oluşturduğu gösterilmiştir. Oluşan mekanoiyonlar, onlarla beraber oluşan ve onları daha kararlı kılan mekanoradikallerin ortamdaki radikal tuzaklayıcıları ile uzaklaştırılması ile kararsız hale getirilebilir ve bu sayede polimer malzeme antistatik özellik kazanır. Bu yöntemin, klasik yöntem olan (metal, karbon tozu ve iletken polimerler ya da nem artırıcılar gibi katkılarla) iletkenlik artırma yöntemine göre avantajı doplama miktarının çok az olmasıdır. Yine de halihazırda kullanılan moleküler radikal

tuzaklayıcılarının pahalı olmaları nedeniyle bu yöntemin endüstride kullanılması mümkün değildir.

Radikal tuzaklayıcısı olarak kullanılabilen lignin ise dünyada en çok bulunan ikinci polimerdir ve kağıt endüstrisinin de bir atığı olduğundan “masrafsız” bir malzemedir. Bu tez çalışmasında lignin bazı sert ve yumuşak kereste kaynaklarından elde edilmiştir. Kütlece az (%1-5 arası) bir katkı oranının bile uygulamada işe yaradığı, polimer yüzeylerde elektriksel yüklerin birikmesinin engellendiği ve zamanla yüklerin yüzeyden yok olma hızlarının arttığı, çapraz bağlı polidimetilsiloksan, termoplastik polipropilen, polietilen, polilaktik asit ve polistren örneklerde gösterilmiştir. Daha sonra da gözlemlenen yük sönümlenmenin mekanizması; yüzey iletkenlik ölçümleri, ³¹P NMR, katı hal NMR’ı, toplam fenol ölçümü, ligninin homojen bir şekilde katılanması için gerekli olan soğuk öğütme işlemi öncesi ve sonrasında yapılan radikal miktarı ölçümü gibi yöntemlerden elde edilen sonuçlar ışığında tartışılmıştır.

Sonuçlar, moleküler radikal tuzaklayıcılarda görülene benzer şekilde, mekanizmanın iletkenlik artışı içermeyen bir radikal tuzaklama içerdiğini göstermektedir. Ligninin yük sönümlenme mekanizmasının aydınlatılması, hem ligninin endüstride antistatik bir katkı malzemesi olarak kullanımına, hem de bu kullanımın sınırlarının çizilmesine yardımcı olacaktır.

Anahtar kelimeler: anti-statik katkı malzemeleri, dokunma ile elektriklenme, polidimetilsiloksan, termoplastik polimerler, radikal tuzaklayıcılar, statik elektriklenme, triboelektriklenme.

ACKNOWLEDGEMENT

First of all, I would like to express my special thanks and sincere gratitude to my advisor Assist. Prof. Bilge Baytekin for all the feedbacks, her guidance, support and encouragement. I also want to thank her for being such a role-model and for her company in and out of the lab day and night. Also, Assoc. Prof. Tarık Baytekin for his priceless feedback and help in instrumentation.

I am grateful to all the jury members Prof. Ali Çırpan, Assist. Prof. Burak Ülgüt, Assist. Prof. Yunus Emre Türkmen, and Assist. Prof. Salih Özçubukçu for their time and valuable feedbacks.

Also, I would like to thank all of my colleagues in our research group especially Dr. Fatma Demir for her support and help in the project and Dr. Joanna Kwiczak Yiğitbaşı for her support and assistance. I thank other Baytekin Group members, Mohammad Morsali for his help during photo shooting, Doruk Cezan and Turab Ali Khan for all their support.

I acknowledge The Scientific and Technological Research Council of Turkey (TUBITAK) for financial support under project no: 116Z523. Also, I would like to thank all the members of Bilkent University, Department of Chemistry.

Last but not least, I would like to express my gratitude to my beloved parents Güzin and Mehmet Cengiz Özel for their endless support, patience and strong encouragement. I also would like to thank to my beloved one, Gözde Aydın, for her unlimited support, feedback, patience and her faith in me during this work.

TABLE OF CONTENTS

1. INTRODUCTION.....	1
1.1. Contact Electrification Phenomenon	1
1.1.1. Charge Mitigation: Radical Scavengers/Antioxidants	5
1.1.2. Triboelectric Series	7
1.2. Lignin	9
1.2.2. The Chemistry of Lignin	11
1.2.3. Lignin Extraction Methods.....	16
1.3. PDMS and Thermoplastic Polymers	18
1.4. Aim of The Thesis	19
2. EXPERIMENTAL	22
2.1. Materials	22
2.2. Experimental Procedures	23
2.2.1. General Lignin Extraction and Particle Size Reduction Pathway	23
2.2.2. Lignin Extraction Procedure.....	24
2.2.3. Particle Size Reduction Procedure.....	24

2.2.4. Structural and Chemical Characterization of Lignin	25
2.2.4.1. FTIR Spectroscopy	26
2.2.4.2. Prussian Blue Method for Total Phenol Content (TPC) Determination	26
2.2.4.3. Mechanoradical Content Determination by DPPH Test.....	28
2.2.4.4. Solubility Enhancement by Acylation of Lignin	28
2.2.4.5. GPC Measurements for Molecular Weight Determination.....	30
2.2.4.6. ¹³ C-CP/MAS NMR Spectroscopy.....	30
2.2.4.7. ³¹ P-NMR Spectroscopy	31
2.2.4.8. Thermal Stability Analyses (TGA/DSC) of Lignin.....	31
2.2.4.9. X-Ray Diffraction (XRD) Analysis	32
2.2.4.10. Scanning Electron Microscopy (SEM) Analyses.....	32
2.2.5. Lignin Doping to The Polymers	32
2.2.5.1. Lignin Doping to PDMS (Polydimethylsiloxane)	33
2.2.5.2. Lignin Doping to Thermoplastics (PE, PP, PS, PLA).....	34
2.2.6. Preparation of Lignin-Free Wood	35
2.2.7. Electrical Measurements	36
2.2.7.1. Charge Density Measurements.....	36
2.2.7.2. Charge Decay Measurements	37
2.2.7.3. Surface Conductance Measurements	38

3. RESULTS & DISCUSSION	40
3.1. Characterization of Extracted, Cryomilled and Acylated Lignin	40
3.1.1. Particle Size Measurement Results	41
3.1.2. Structural Analyses of Lignin by FTIR Spectroscopy	43
3.1.3. Total Phenol Content (TPC) Determination	49
3.1.4. Mechanoradical Content Determination.....	52
3.1.5. Molecular Weight Determination of Acylated Lignins.....	55
3.1.6. ¹³ C-CP/MAS NMR Results	55
3.1.7. ³¹ P-NMR Results	57
3.1.8. Thermal Stability Results	58
3.1.9. XRD Analysis of Lignin.....	60
3.1.10. Surface Morphology Analysis of Cryomilled Lignin	60
3.2. Contact Charge Density and Charge Decay Measurements.....	61
3.2.1. Contact Charge Density of Thermoplastics and the Effect of Lignin Doping	61
3.2.2 Contact Charge Density of PDMS and The Effect of Lignin Doping	64
3.2.2.1. The Effect of Milling Time of Lignin on Contact Charging of PDMS ..	64
3.2.2.2. The Effect of Lignin Sources on Contact Charging of PDMS.....	68
3.2.2.3. The Effect of Total Phenol Content of Lignin on Contact Charging of PDMS	70
3.2.3. Contact Charge Decay on PDMS and the Effect of Lignin Doping	71

3.2.4. Why Does Wood Not Get Charged? Does Lignin Have Any Effect?.....	73
3.2.5. The Effect of Lignin Doping on The Surface Conductance of PDMS	76
3.3. Mechanism of Charge Dissipation by Radical Scavenging.....	77
4. CONCLUSION	81
5. REFERENCES.....	83

TABLE OF FIGURES

Figure 1. Applications of contact electrification by controlling, decreasing, and increasing the surface charges.	3
Figure 2. Previously proposed possible charge transfer mechanisms. (a) Transfer of an electron. (b) Transfer of an ion.	4
Figure 3. (a) Surface charge lowering in polydimethylsiloxane (PDMS) by doping radical scavengers DPPH, tocopherol, and HALS. (b) proposed interaction of frontier molecular orbitals between mechanoradicals and mechanocations (left), and, mechanoradicals and mechanoanions (right) on contact-charged surfaces [2].	6
Figure 4. A triboelectric series of materials.	8
Figure 5. Illustration of a plant cell wall. Taken from [47].	11
Figure 6. Standard three monolignol monomers of lignin. p-coumaryl alcohol (H), coniferyl alcohol (G), and sinapyl alcohol (S).	12
Figure 7. Most common linkages found in lignin. a) β -O-4, b) β -5, c) β - β' , d) 5-5', e) 4-O-5, f) β -1.	13
Figure 8. Proposed chemical structure of a lignin.	14
Figure 9. Resonance stability of phenoxy radicals on monolignols [48].	15
Figure 10. Chemical structure radical species of lignin at different pH conditions. .	15
Figure 11. Outline of lignin extraction processes from lignocellulosic biomass.	17

Figure 12. Chemical structure of polydimethylsiloxane (PDMS).....	18
Figure 13. Chemical structure of polyethylene (PE), polypropylene (PP), polystyrene (PS), and polylactic acid (PLA).	19
Figure 14. Extraction and particle size reduction flow-chart used in this thesis to obtain lignin from the mentioned sources.	23
Figure 15. Acylation reaction scheme of lignin with trimethylacetylchloride.	29
Figure 16. Acylated lignin samples dissolved in THF (Concentration: 1 mg/1 mL). ..	29
Figure 17. Images of Pure (undoped) PDMS, non-cryomilled lignin doped PDMS and 60 min. cryomilled lignin doped PDMS.....	34
Figure 18. Illustration of Contact Electrification Measurement Setup-1. Determination of maximum net charge density on the polymer surfaces after contact.....	37
Figure 19. Illustration of Contact Electrification Measurement Setup-2. Determination of surface electric potential upon contact and separation events...	37
Figure 20. (a) Illustration of surface conductance measurement setup. (b) Electrical circuit scheme of the two probe method.	39
Figure 21. Particle size vs cryomilling time of cryomilled nutshell lignin. Error bars were calculated from 3 independent measurements of each sample.	41
Figure 22. Particle size vs. ultrasonication time for lignin samples from different sources, namely nutshell, maple, pine, and birch. 0 min sonication refers to previously 60 min. cryomilled lignin. Error bars were calculated using 3 independent measurements of each sample.....	42
Figure 23. FTIR spectra of lignin (nutshell, maple bark, pine bark and birch bark). All spectra were given as normalized transmittance percentage vs wavenumber. (a)	

Extracted lignin, (b) 60 min cryomilled lignin, (c) 5-10-30-60 min. cryomilled nutshell lignin, (d) acylated lignin.....	45
Figure 24. Stacked spectra (shifted on the vertical axis for clarity) of extracted-cryomilled (60 min)-acylated lignin samples. (a) Nutshell lignin, (b) maple lignin, (c) pine lignin, and (d) birch lignin.	47
Figure 25. FTIR spectrum of lignin removal from limba wood.....	48
Figure 26. “Prussian Blue test” reactions of polyphenols (PP).	49
Figure 27. (a) UV-Vis spectra of Methyl Gallate standard solutions with concentrations 0.1 mM-0.5 mM used in Prussian Blue test for polyphenols showing an increase of the absorption band at 700 nm (the absorption maximum for Prussian blue that forms upon oxidation of polyphenols) and (b) the generated calibration curve. For details of the solution preparations and the test, see section 2.2.4.2. ...	49
Figure 28. UV-Vis spectra recorded during Prussian blue test: Nutshell (a), maple (b), pine (c), and birch lignin (d). N(1-5), M(1-5), P(1-5), and B(1-5) indicate each of 5 identical experiments performed in order to calculate standard deviations for nutshell, maple, pine, and birch lignin respectively.	51
Figure 29. UV absorption changes of Prussian Blue reaction of (a) lignin and (b) blank control sample (lignin-free) solution initial and after 24 hours.....	51
Figure 30. Prussian blue reaction. Visual comparison of the blank sample (without lignin) and lignin contained sample (polyphenol) after 24 hours	52
Figure 31. UV-Vis spectrum of DPPH-lignin mixtures at given reaction times. (a) Non-cryomilled, (b) 5 minutes, (c) 10 minutes, (d) 30 minutes, and (e) 60 minutes cryomilled samples, (f) control sample having no lignin but only DPPH.	54

Figure 32. The reacted number of radicals per gram of lignin sample cryomilled for the given milling times at the given reaction times. The reaction between DPPH radical scavenger and the lignins continue at even prolonged times.....	54
Figure 33. ¹³ C-CP/MAS NMR spectra of 60 minutes cryomilled lignins.	56
Figure 34. The reaction of 2-Chloro-1,3,2-dioxaphospholane with active hydroxyl groups. R = phenol residues, alcohols, aldehydes and carboxylic acids.	57
Figure 35. ³¹ P-NMR spectrum of the phosphorylated nutshell lignin.....	58
Figure 36. (a) Thermogravimetric Analysis (TGA) curve of all lignin samples. (b) TGA/DTG curve shows the decomposition rate of the samples.	59
Figure 37. XRD diffractogram of cryomilled nutshell lignin and cellulose (cotton). .	60
Figure 38. SEM images of non-cryomilled and 5 to 60 minutes cryomilled lignins. .	61
Figure 39. a) The signals of lignin-free and lignin-doped wood, b) the voltage signals of undoped and doped PS against PTFE, collected from the homemade tapping device. c-d) Surface charges of wood and thermoplastics.	63
Figure 40. Open circuit voltages obtained as a result of tapping and contact-charging of the samples of selected undoped and doped with 5% (w/w) thermoplastic polymers. Lignin was 60 min cryomilled before doping. PP, PLA, PE and PS refer to pure polymers and L-PP, L-PLA, L-PE and L-PS refer to polymers doped with lignin	63
Figure 41. Contact Electrification results of 5 % lignin-doped PDMS. Undoped PDMS vs 5-10-30-60 min cryomilled doped PDMS.....	66
Figure 42. Charge density of PDMS and particle size of lignin as a function of cryomilling time.	68
Figure 43. Charge density vs number of touches on the surface of PDMS and L-PDMS (1% and 5% doping) samples prepared with lignin extracted from nutshell, maple,	

pine, and birch. All samples extracted from the sources are cryomilled for 60 min before doping.	69
Figure 44. Charge density of undoped and doped PDMS versus total phenol content of lignin.	70
Figure 45. Charge decay plot of undoped and doped PDMS samples (a). The solid lines represent the average of at least 3 measurements. Semi-logarithmic plots of charge vs time (b).	73
Figure 46. Charge density vs number of touches on the surface of PDMS and Pine bark wood against aluminum foil.	74
Figure 47. Lignin extraction and wood bleaching (a-b), lignin-free wood after 5 min cryomilling and lignin doping of wood by cryomilling (c-d).	75
Figure 48. Lignin (pine bark) doping to lignin-free wood from 1% to 50% (w/w) by cryomilling. The samples were doped with lignin by 5 minutes of cryomilling.	75
Figure 49. Contact Electrification of lignin-free wood and lignin doping concentration to wood by 1-3-5-50% (w/w). 100% doping concentration refers to pure lignin.	76
Figure 50. Surface conductance results of PDMS and 5% lignin doped PDMS samples. Conductance of the samples were calculated from surface resistivities measured via two-probe method. For experimental details see section 2.2.7.3.	77
Figure 51. The mechanism of contact charge formation and stabilization on polymer surface of an undoped polymer.	80
Figure 52. The mechanism of contact charge dissipation by removal of mechanoradicals by radical (re)combination or H-transfer via lignin doping.	80

LIST OF TABLES

Table 1. Current (2019) prices of molecular antioxidants (radical scavengers) used as antistatic additive in the recent studies. Data taken from Sigma-Aldrich website.....	6
Table 2. Total phenol content determination of the lignin samples. Standard deviations and mean values were calculated using the data from 5 different samples prepared by using identical procedure ^(a) . Methyl gallate standard ^(b)	52
Table 3. Molecular weights of acylated polymers. *Polydispersity index	55
Table 4. Contact Electrification results of lignin doping to wood and thermoplastics	64
Table 5. Comparison of the effects of cryomilling time on particle size, reacted number of radicals in lignin and charge density of PDMS. Reacted number of radicals were calculated after the complete reaction of lignin radicals with DPPH radicals (144 hours).....	67
Table 6. Comparison of lignin total phenol content and charge density of lignin doped PDMS.	71

CHAPTER 1

1. INTRODUCTION

1.1. Contact Electrification Phenomenon

Contact Electrification (CE), also known as triboelectrification, or static charging, is a natural event that occurs in our lives anytime and anywhere, whenever two surfaces touch each other. Electrical charge development emerges, when two materials are brought into contact (e.g. touched or rubbed) and then separated [1–3]. For instance, clinging of clothes, slight electrical shock when one touches a door handle in a dry day and sticking of dust and tiny particles on cell phone or computer screens occur due to static charge accumulation generated by contact electrification [4]. Static charge (or contact charge) accumulation causes not only these trivial frustrations, but also it leads to shocks and explosions [5,6], it damages satellites [7], electronic devices and circuits [8]. In industry (e.g., chemical, petrochemical, semiconductor and packaging), accumulated charges can spoil the production yields and product quality.

In particular, pharmaceutical industry, it is claimed that charged drug particles can undesirably aggregate and ruin the uniformity of end-products. Especially for powders and liquids, static charging can pose fire and explosion hazards as well [9]. Contact electrification has also many positive outcomes, if the phenomenon is handled properly [10]. It has many useful applications including electrophotography, electrostatic separation of particles, electrostatic spray coating and electrostatic self-assembly [11,12]. Recently, the most attractive application of contact electrification has become triboelectric nanogenerators (TENG). TENGs are mechanical energy harvester devices, which were first described by Wang group [13–15] as a promising approach to harvest mechanical energy and convert it into electricity, since triboelectrification is a universal and ubiquitous effect that is widely encountered in everyday life. The strategies for the utilization and control of CE are based on three different points: Controlling, increasing and decreasing the surface charges. The applications based on these approaches are shown in Figure 1.

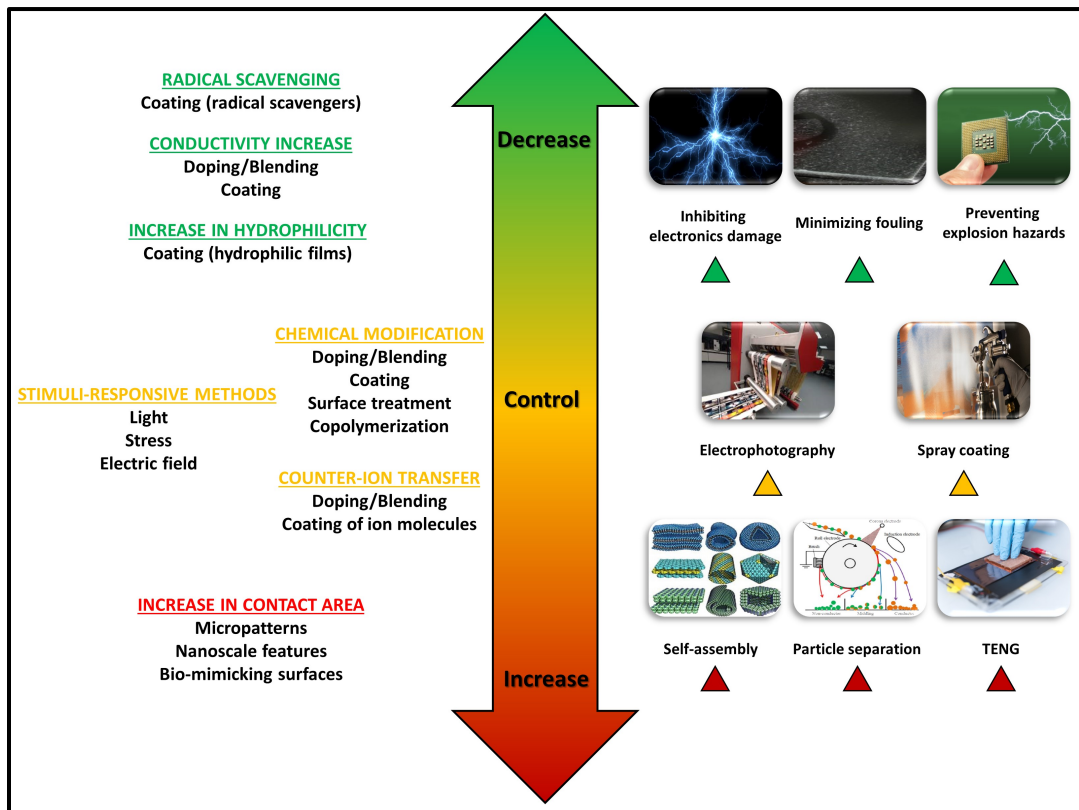


Figure 1. Applications of contact electrification by controlling, decreasing, and increasing the surface charges.

Contact electrification offers variety of applications as summarized in Figure 1 however, challenges still exist and cannot be dispelled unless contact electrification mechanism is totally understood. As chemical mechanism of contact electrification, two different mechanisms had been proposed in the previous decade: electron transfer and ion transfer [16,17]. The possible mechanisms of charge transfer upon contact are shown in Figure 2 below.

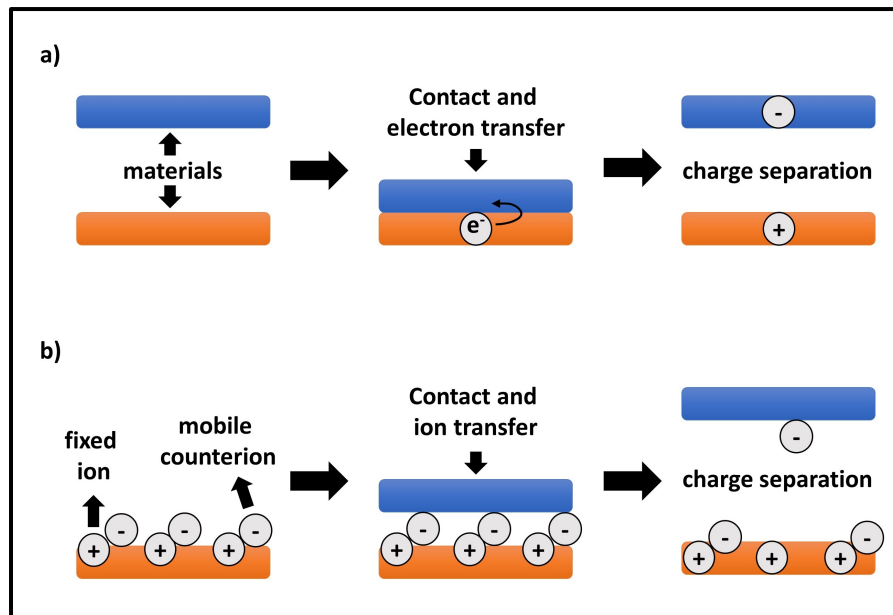


Figure 2. Previously proposed possible charge transfer mechanisms. (a) Transfer of an electron. (b) Transfer of an ion.

Material transfer on the other hand, plays a significant role in the mechanism of contact electrification. The reports in the last decade proved that, the mechanism is not solely based on electron and/or ion transfer. Evidently, the combination of charge and microscopic amount of material (approximately microgram per square centimeter) exchange between the contacting surfaces [18–20]. As these reports point out this material transfer upon contact can only happen, if the chemical bonds in the polymers are broken as a result of mechanical treatment (mechanochemical bond-cleavage) and bits of material is transferred between the surfaces. The species that form as products of the mechanochemical bond-cleavages are called as *mechanoions* and *mechanoradicals* [2].

1.1.1. Charge Mitigation: Radical Scavengers/Antioxidants

As it is mentioned before, surface charge accumulation-based hazards can be eliminated by doping the dielectric materials with conductive materials (e.g. metals, carbon powder, carbon nanotubes, and conductive polymer) or with additives to increase surface humidity (e.g. ions) [21,22]; however, distinct mechanical or electrical properties of the polymers are lost upon doping of the additive because of high doping concentrations required to achieve the percolation.

A newly introduced mechanism-based method for charge mitigation is the addition of radical scavengers into commonly used polymers. As mentioned above, mechanochemical bond-cleavages that occur during contact produces mechanoions and mechanoradicals. These mechanoradicals that are formed as a result of homolytic bond cleavage upon electrification are mostly peroxy radicals ($\text{ROO}\cdot$) [18] stabilized by resonance contributors [23]. These mechanoradicals can stabilize the co-formed mechanoions (“the charges”) via interaction of frontier molecular orbitals [2,24]. When the mechanoradicals are chemically scavenged by the radical scavenger additives, the mechanoions are destabilized and decay quickly (through commonly accepted mechanisms such as by reactions with molecules of air or migration into the bulk). Several radical scavenger compounds have been studied for this purpose and revealed remarkable results as shown in Figure 3 [2,18,25]. As stated above, radical scavenging method is superior to the conventional charge mitigation methods because the doping does not need conductive percolation and therefore smaller doping amounts can be used, which help to retain intrinsic properties of the native polymers [2].

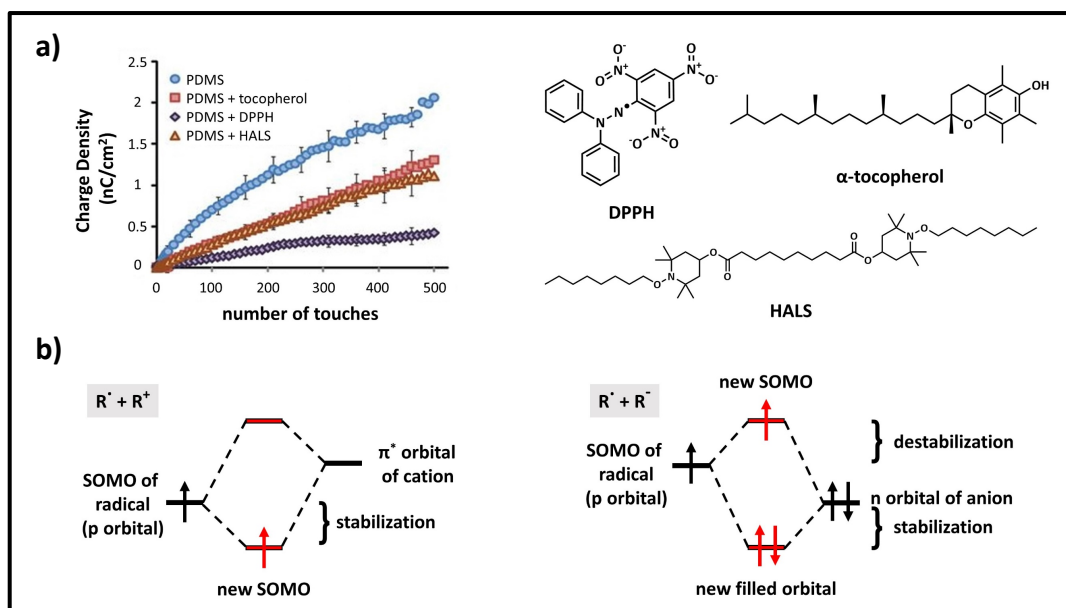


Figure 3. (a) Surface charge lowering in polydimethylsiloxane (PDMS) by doping radical scavengers DPPH, tocopherol, and HALS. (b) proposed interaction of frontier molecular orbitals between mechanoradicals and mechanocations (left), and, mechanoradicals and mechanoanions (right) on contact-charged surfaces [2].

Table 1. Current (2019) prices of molecular antioxidants (radical scavengers) used as antistatic additive in the recent studies. Data taken from Sigma-Aldrich website.

ANTIOXIDANTS	PRICE (per kg)
Catechin	21.600.000 €
Taxifolin	2.700.000 €
Quercetin	26.500 €
DPPH	600.000 €
α-tocopherol	1000 €
Tannic acid	200 €
Dopamine	4500 €
HALS	11000 €
Lignin	0 €

The examples of radical scavenger molecules used in charge mitigation on polymer surfaces are DPPH (2,2-diphenyl-1-picrylhydrazyl), (±)-α-tocopherol (Vitamin E), HALS (bis(1-octyloxy-2,2,6,6-tetramethyl-4-piperidyl)) sebacate [2], tannic acid, and polydopamine [26]. Nevertheless, those chemical compounds are relatively expensive (see Table 1) so that limits their applications in industry. The world plastic

production has reached 350 million tons in 2017 according to Plastics Europe Market Research Group (PEMRG) report, thus listed radical scavengers are not feasible for such huge amount of demand, since their costs are not affordable in industry.

Scientists working to find industrially applicable additives for charge mitigation should target to a cheap and readily available material. Therefore, naturally abundant chemicals in the biomass are ideal candidates for such a purpose .

1.1.2. Triboelectric Series

Triboelectric series is a list of materials ranked by their tendencies to gain or lose net charges upon CE. The materials are sorted from the top as decreasing trend to charge positively (electron loss) and increasing trend to charge negatively (electron gain) upon contact with each other. There are also materials in the middle of the list, which do not show any propensity to either charge positively or negatively. Lists made from contact electrified materials date back to ancient Greece - the word “electricity” is derived from the Greek word ἤλεκτρον, which means amber (one of the materials used in the early experiments performed by Thales of Miletus more than 2500 years ago) [27]. Many different triboelectric series have been reported over the past 150 years [28–31], and Diaz and Felix Navarro have compiled the four published series in their report [32]. Although trends can be found in these lists, i.e. polar materials usually becoming positively charged and nonpolar ones becoming negatively charged upon contact with each other [17], the rankings of materials in triboelectric series are occasionally debated. Furthermore, there are sets of materials that produce a

cyclic triboelectric series [33] showing one physical property or one mechanism cannot explain all the examples of contact electrification. The idea of ranking triboelectric series has recently been completely refuted by contact charging of identical materials [34] and the reversal of sign of net charge on polymers by material transfer [19].

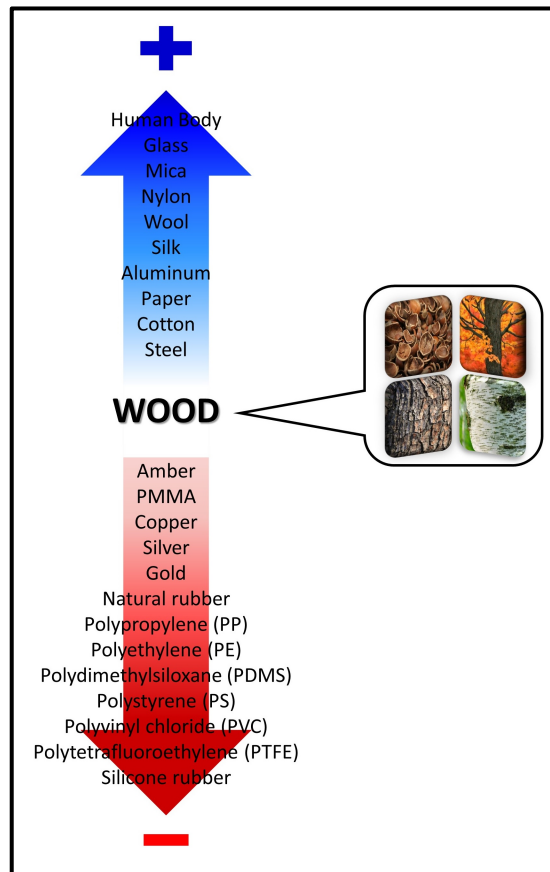


Figure 4. A triboelectric series of materials.

As can be seen in the triboelectric series, most materials get charged upon contacting each other – their sign of net charge may vary for different conditions, which is the source of ambiguities in different triboelectric series. However, there is one common material that appear at the middle of the list, as a non-charging material in all triboelectric series: “wood”. Recently, wood and its products has attracted great

attention due to their abundance in nature and owing to their sustainability. *Why does wood not get contact charged?* If the underlying reason of the case is examined, it can open a new pathway to obtain sustainable and cheap antistatic additives that can be used also at an industrial scale and lignin might be a reason for this special behavior of wood as we investigate in a following section.

1.2. Lignin

Lignin is one of the three main components of wood and it can be responsible for inability of contact charging in wood. Lignin is an antioxidant [35–37] with radical scavenging property [38–41] arising from its polyphenolic structure.

Lignin was discovered in 1838 by Anselme Payen, a French chemist who discovered cellulose for the first time by extracting it from wood using nitric acid and alkaline solutions. Payen did not only discover cellulose, he also isolated lignin and called it “incrustant”. In 1857, lignin was given its name “lignin” by German scientist Schulze [42].

Wood or lignocellulosic biomass is mainly composed of three constituents: cellulose, hemi-cellulose and lignin. Cellulose covers 30% – 50%, hemi-cellulose 20% – 30% and lignin is 15% – 30% of the lignocellulosic feedstock; the rest are pectin, wax, fats, and moisture. Lignin is the second most abundant bio-polymer after cellulose, and it consists of cross-linked polyphenolic units. Lignin is the most abundant natural aromatic polymer and is the main chemical source of aromatic building blocks on earth. Enzyme-mediated dehydrogenation polymerization, also called as lignification, is responsible for in-vivo production of lignin. Lignification results in an

amorphous cross-linked material with ether and carbon-carbon bonds (Figure 8) [43]. Cell tissues of primitive plants (e.g. algae) do not contain any lignin because of the fact that lignin is mainly located in the secondary cell walls (Figure 5), deposited during cell differentiation, which is responsible for the structural robustness of each cell, and also, for the integrity of whole plant. Lignin is a hydrophobic material responsible for water and nutrient transportation and provides protection against insects and microbial attack.

Lignin is a by-product of paper industry because lignin residues cause quality problems in paper production. Efficient lignin removal from the wood enhances the quality of the produced paper, so that millions of tons of lignin are discarded as waste each year in pulping industry. Waste lignin has so far only limited applications and it is usually burned for its caloric value. Recently, there are attempts to use lignin as the major source and starting material for the production of aromatic building blocks (benzene, toluene and xylene); however, only 2% of waste-lignin is converted to high-valued chemicals (organic compounds, biofuels, etc.) [44–46]. Disappointingly, the potential of lignin in terms of renewability and sustainability is still far from being fully used.

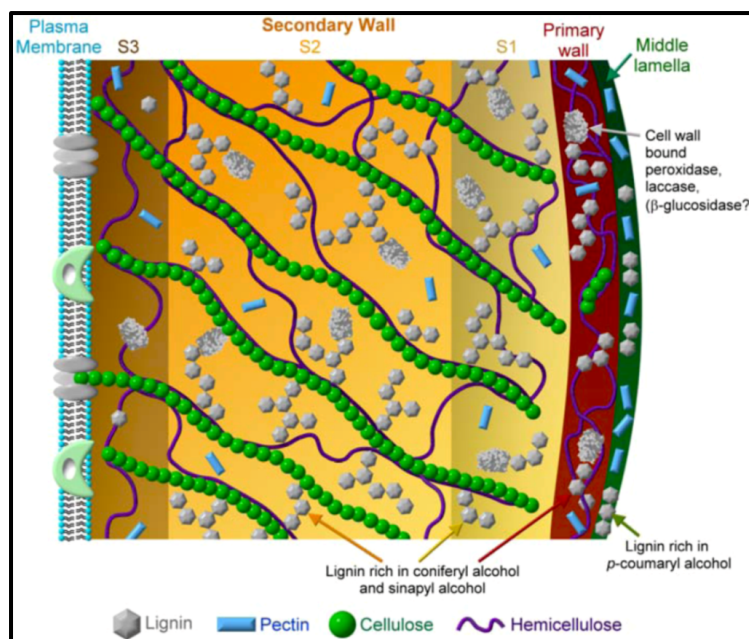


Figure 5. Illustration of a plant cell wall. Taken from [47].

1.2.2. The Chemistry of Lignin

Lignin contains three different cinnamyl alcohol monomers including *p*-coumaryl alcohol, coniferyl alcohol, and sinapyl alcohol (Figure 6). These monomers are found in lignin as the phenylpropanoid forms *p*-hydroxyphenyl (H), guaiacyl (G), and syringyl (S), respectively. The monomer ratios differ on the basis of lignin source. Grassy plants contain all three monolignol monomers, while softwoods (e.g. pine and spruce tree) contain mainly coniferyl alcohol (G), and hardwoods (maple and birch tree) both coniferyl (G) and sinapyl alcohol (S) [46]. Chemical bonds, monomer content and radical polymerization steps of monolignols diversify the chemical structure of lignin from one origin to another and exact structure of each extracted (or isolated) lignin is extremely hard to be determined.

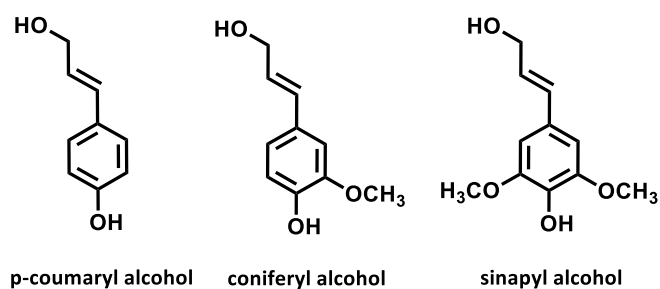


Figure 6. Standard three monolignol monomers of lignin. p-coumaryl alcohol (H), coniferyl alcohol (G), and sinapyl alcohol (S).

Chemical reactions between monomers enable the formation of vast variety of inter-unit linkages [45,48]. Lignin has plenty of the so called β -O-4 linkage (a bond between β -carbon of one monolignol unit and phenolic hydroxyl of the other) that accounts for 50% of all linkages in softwood. The rest of the bonds between the lignols are formed by other types of ether bonds involving α -O-4, 4-O-5, and C-C bonds β - β , 5-5, β -5 and β -1 (Figure 7) in addition, more complex lignin structures contain dibenzodioxocin linkages.

Lignin content of lignocellulosic biomass feedstocks varies from 2% to 40% by weight. Origin of lignin should be chosen wisely in order to achieve efficient extraction of lignin from its biomass source. Nutshell, maple, pine and birch have been used in this study as sources of lignin, which possess high weight percentages of lignin; 30% – 40%, 29.1%, 27.3%, 22%, respectively [49].

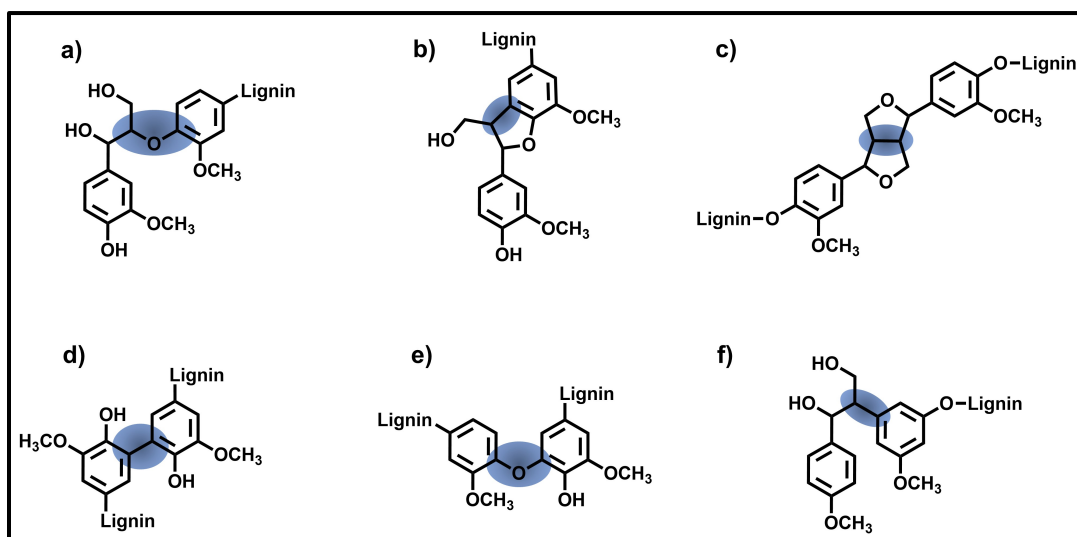


Figure 7. Most common linkages found in lignin. a) β -O-4, b) β -5, c) β - β' , d) 5-5', e) 4-O-5, f) β -1.

Stability and degradation insusceptibility of lignin originate from the existence of plenty of covalent bonds in the polymer backbone, as well as strong presence of intermolecular interactions such as hydrogen bonding. Both the physical and chemical properties of lignin are dependent on the extraction method (pulping process) from the lignocellulosic material. There are several methods known for lignin isolation. The details of the lignin extraction methods are described in section 1.2.3. Softwood lignins have comparatively higher T_g (glass transition temperature) values between 138 °C – 160 °C due to greater amount of intermolecular hydrogen bonds and condensed aromatic structures besides hardwood lignins show lower T_g range (110 °C – 130 °C) [50]. Kraft lignin, which is a polymeric material obtained from native lignin by kraft pulping process, has a thermal stability that has been investigated. It was found that major weight loss (approx. 40 %) is in the range of 200 °C – 600 °C and the maximum weight loss is observed around 400 °C. 15% of the weight of the lignin is lost before reaching 300 °C. T_g varies between 124 °C – 174 °C for kraft lignin, soda lignin has T_g values observed in the range of 150 °C – 155 °C, on

the other hand organosolv lignins (extracted lignin via organic solvents) have relatively lower T_g ranging between 91 °C – 97 °C [51].

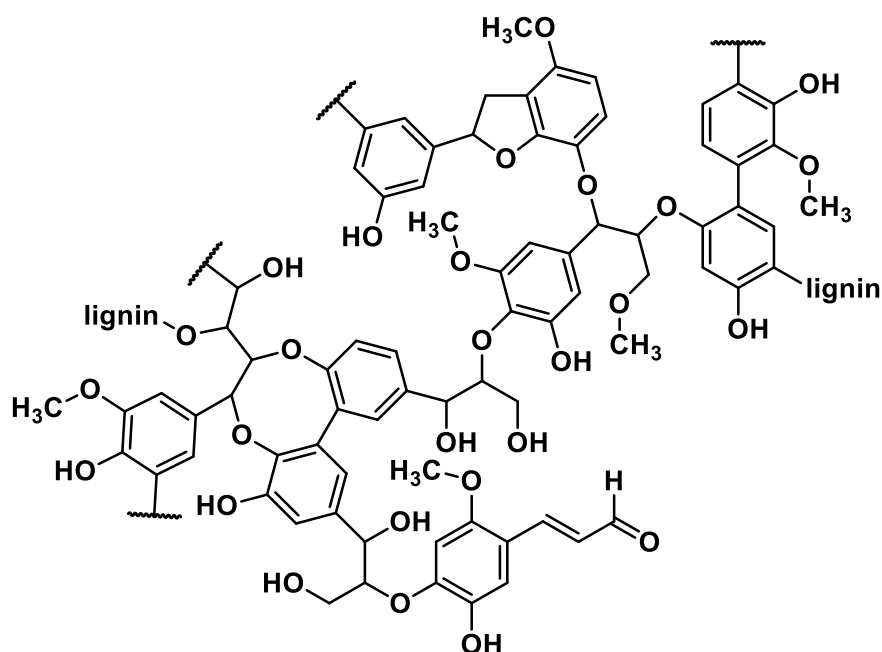


Figure 8. Proposed chemical structure of a lignin.

Figure 8 shows the proposed chemical structure of a lignin; however, as it is mentioned before it is hard to elucidate the exact chemical structure of any lignin due to linkages that change from one lignin source to another and the whole structure varying with the extraction method of lignin from biomass. There are several spectroscopic techniques (e.g. ^1H -, ^{13}C -, ^{31}P -NMR), used for disclosing the structure of lignin. Even though the types of bonding and the amounts of sub-groups can be determined by these methods, there is no method that reveals the exact structure explicitly due to numerous bonding schemes and branching possibilities of the sub-units.

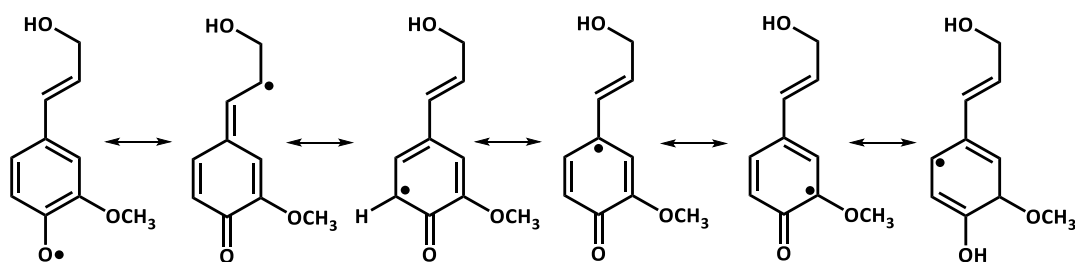


Figure 9. Resonance stability of phenoxy radicals on monolignols [48].

Lignins inherently have radicalic groups in the structure owing to the stability of the phenoxy radical (due to many resonance contributors as shown in Figure 9) that can form at the phenolic ends. These stable organic radicals in lignin have been studied comprehensively in terms of botanical origin, natural processes, pH dependence, mechanical, and temperature effects [52]. The results of these studies demonstrate different radicalic content depending on the origin of lignin and extraction methods, also proposed radicals as substituted o-semiquinone type species can exist in different protonation states (Figure 10).

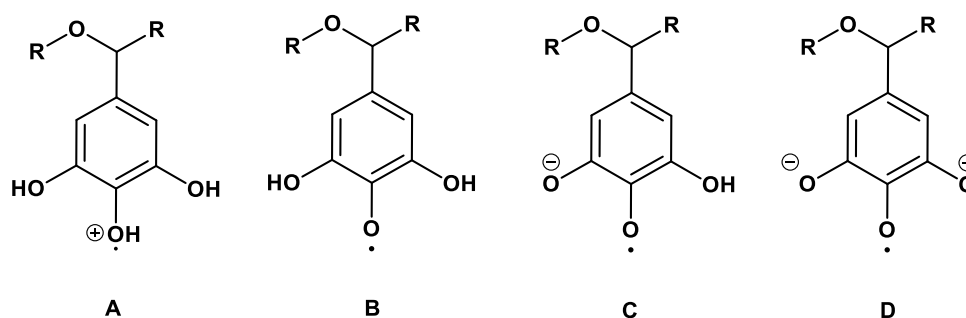


Figure 10. Chemical structure radical species of lignin at different pH conditions.

The pH value is the most influencing factor affecting the chemical structure of the radical species during extraction, different radical species can be determined by X-band EPR spectroscopy. In Figure 10, A, B, C, and D are referred to protonated,

deprotonated, and neutral radical structures. The EPR results proved that the protonated form is more pronounced at pH 1 while the deprotonated species C and D are the main species at pH 13. The neutral form B is dominant in mildly acidic conditions (pH 3.7 – pH 8.6) on the other hand the other species can be detectable as well in that pH range [53].

1.2.3. Lignin Extraction Methods

There are several techniques to isolate lignin from lignocellulosic biomass. These are classified into two based on the significant or mild structural modification of lignin during the isolation (Figure 11). Pulping methods including Kraft [54], Sulfite [55], Alkaline [56], and Klason [57] processes result in significant structural alterations of lignin under comparatively harsh conditions. In addition, Björkman process, ionic liquid treatment, and organosolv process have mild impacts on the chemical structure of lignin. For instance, kraft process modifies the lignin structure by breaking most α - β -aryl ether bonds also, sulfur rich structure forms due to the attack of hydrogen sulfide ions during the process. Sulfite process similarly yields to sulfonate groups on lignin structure, while the structure of lignin obtained through alkaline process becomes more sulfonic acid-rich. The Klason process comprises of sulfuric acid treatment of lignin and leads to major changes to the original structure of lignin. Structural alterations can still be observed under so called 'mild isolation processes' such as Björkman process, where isolation of lignin is obtained by harsh grinding of the material followed by organic/aqueous solvent extraction, which

causes an increase in the number of carbonyl and hydroxyl groups particularly in hardwood lignin. Cellulolytic enzyme, ionic liquid treatment and organosolv processes involve solvent extraction just like Björkman process, however, they less likely affect the lignin structure and yield more native-like lignin [58].

Consequently, it is obvious that all the isolation procedures have both advantages and disadvantages depending on the utilization of the extracted product, so that one should choose the method, which fits the intended/tolerable structural changes according to the desired final application of lignin. The extraction method used in this thesis is a synthetic combination of Klason process and Björkman process. It involves sulfuric acid treatment and extensive grinding (see section 2.2.1).

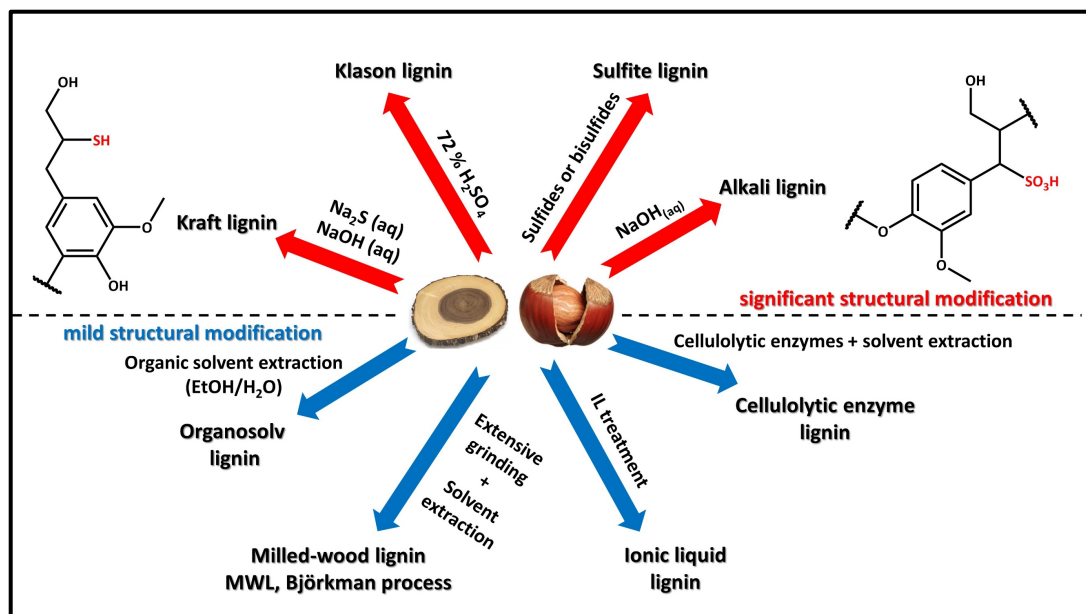


Figure 11. Outline of lignin extraction processes from lignocellulosic biomass.

1.3. PDMS and Thermoplastic Polymers

Polydimethylsiloxane (PDMS) is the most common silicon elastomer [59], which was first synthesized by Wacker Chemie in 1950s. It is a robust, biocompatible and viscoelastic material. It can be easily molded, which enables the PDMS usage in a wide range of applications from medicine and cosmetics to microfluidic devices, and flexible electronics [60,61]. The polymer backbone consists of Si-O-Si bonds as shown in Figure 12. This structure provides flexibility, non-toxicity, non-flammability and electrical resistivity. Once cross-linked, the polymer is set in a defined shape and cannot be remolded.

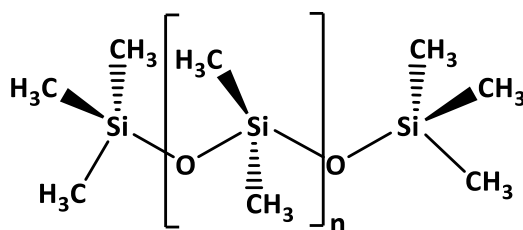


Figure 12. Chemical structure of polydimethylsiloxane (PDMS).

Thermoplastics are type of polymers that can be melted upon heating and solidified upon cooling which makes their remolding possible. There are many thermoplastic polymers in the market and used in daily life. For instance, polyethylene (PE) is commonly used in detergent bottles and portable gasoline cans (high-density polyethylene (HDPE)) or in durable goods boxes and squeeze bottles (low-density polyethylene (LDPE)). Polypropylene (PP) is used in making plastic food containers as well and as electrical cable insulation material. Polystyrene (PS) has variety of applications ranging from disposable cutlery to plastic parts of cars and boats. Polylactic acid (PLA) on the other hand, is a biodegradable thermoplastic produced

from renewable resources especially corn starch and is used in 3D printing. These are the examples of the common thermoplastics that are used in this work. Their chemical structures are shown in Figure 13.

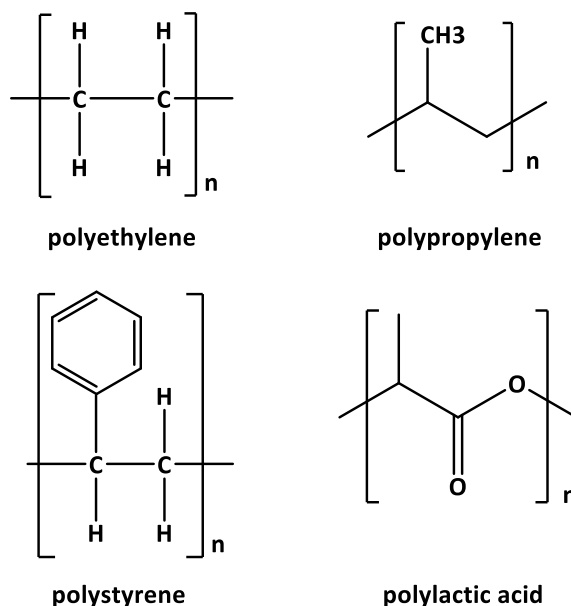


Figure 13. Chemical structure of polyethylene (PE), polypropylene (PP), polystyrene (PS), and polylactic acid (PLA).

1.4. Aim of The Thesis

As mentioned above, finding a cheap, sustainable, and effective material that renders polymers/plastics antistatic without altering the doped material's other characteristics will be beneficial for industrial scale applicability – since no such material exists in the market at the moment. Here, we assert that lignin can be a good candidate for an antistatic additive for common polymers. A recent work from our group showed a brief proof-of-principle [62] for the hypothesis that lignin might indeed may have such a potential as an antistatic additive. However, in this previous

work, there were no details about the mechanism of charge mitigation, without which it is impossible to take the steps towards an industrial product. The clear understanding of this mechanism not only helps understanding of contact charge dissipation but also helps identifying the mechanism of charge formation and the chemistry of the species formed during the contact of two surfaces. For the latter, there exists no chemical or spectroscopic method that can provide a full explanation, since the groups affected form only on the surface and even the surface methods fall too coarse (both spatially and temporally) in following the formation and the later fate of contact charges.

Here, we aim to provide a detailed view on how lignin addition to common polymers, elastomers and thermoplastics, can be used to mitigate contact charges on them. For this purpose, we probe the “usual suspects” in a mechanism for charge mitigation: 1) whether lignin addition increases the conductance of the doped polymers, 2) whether lignin, exhibiting natural radical scavenging property, can show a radical scavenging of mechanoradicals and hence remove them from the environment and destabilize charges, 3) whether the phenolic groups in lignin can act as H atom donors for mechanoradicals.

In order to test these, firstly various lignocellulosic feedstocks, namely nutshell, and maple, pine, birch tree barks (the choice is made from the ones possessing the highest reported lignin content) is investigated, and lignin is isolated from each biomass. Extracted lignins are characterized by several techniques: FTIR, NMR spectroscopy, TGA/DSC, XRD and imaged by SEM. Their radical and total phenol content determinations are pursued by the aid of UV-Vis spectroscopy. Then the

obtained material is doped into elastomeric PDMS and thermoplastics (PP, PLA, PE and PS) by mixing either the prepolymer (PDMS) or the heated thermoplastic with the lignin. The doped material is tested for any conductance increase, and contact charging/charge dissipation behavior in comparison with the undoped controls.

Some work is also devoted to investigate our initial hypothesis that wood does not get charged because of its lignin content. For this purpose, we have isolated lignin from wood and compared the charging/discharging behavior of de-lignified wood with the native, lignin containing sample.

CHAPTER 2

2. EXPERIMENTAL

2.1. Materials

The nutshell was obtained from nuts grown in Gümeli village in the west black sea region, Turkey. Maple tree bark, pine tree bark and birch tree bark were collected from their natural habitat in Bilkent University Campus, Ankara, Turkey. Acids: Sulfuric Acid (95 – 97%), Acetic Acid (99.85%, glacial), Phosphoric Acid (85%), and Hydrochloric Acid (37%) (Sigma Aldrich) were used in the experiments. All the solvents including tetrahydrofuran, ethanol, isopropyl alcohol, 1,4-dioxane, and acetonitrile (Sigma Aldrich) were used without further purification. H₂O₂ solution, FeCl₃, K₃Fe(CN)₆, trimethylacetylchloride, and methyl-3,4,5-trihydroxybenzoate (Sigma Aldrich) were used as obtained. NaOH (pellets) and Na₂SO₃ were purchased from Carlo Erba. Arabic gum was purchased from an herbalist. Autoclave Reactor (30 mL) (PARR Instrument Company) was used in the extraction processes of lignin from nutshell and barks.

Retsch Molecular Test Sieves and Retsch Cryomill Grinder with LN₂ tank were used to decrease the particle size of the samples.

2,2-Diphenyl-1-picrylhydrazyl (DPPH) was purchased from Sigma Aldrich. Chromium(III) acetylacetonate (Sigma Aldrich) relaxation agent, deuterated chloroform with TMS (98%) (Merck KGaA), and extra dry pyridine (99.5%) (Acros) were used in NMR measurements. Cholesterol (Sigma Aldrich) was used as internal standard in ³¹P-NMR. Lignin samples were derivatized with 2-chloro-1,3,2-dioxaphospholane (Sigma Aldrich) prior to ³¹P-NMR. PDMS was prepared by using Dow Corning Sylgard 184 Silicone Elastomer Kit. Thermoplastics (PP, PE, PS and PLA) were purchased from Sigma Aldrich. Aluminium stubs (Agar Scientific) were used to mount the samples for contact charge and decay measurements in the tapping device described below.

2.2. Experimental Procedures

2.2.1. General Lignin Extraction and Particle Size Reduction Pathway

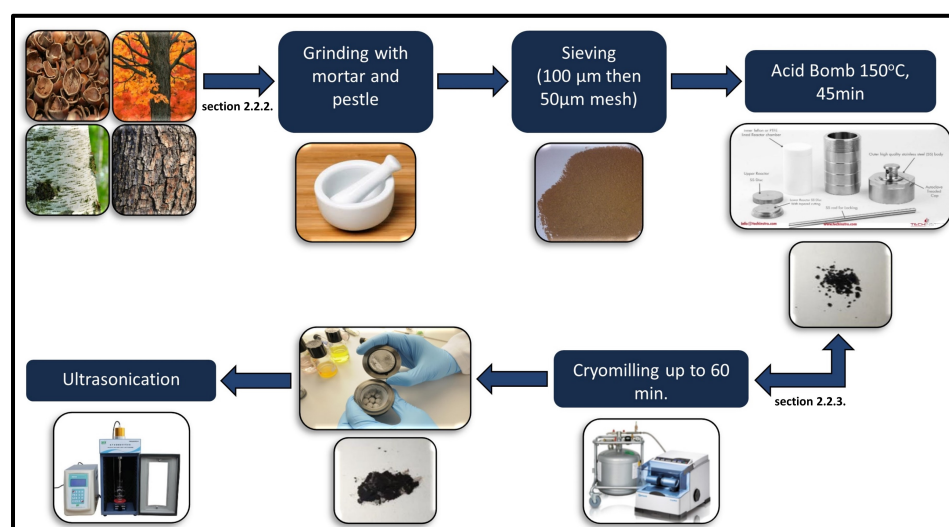


Figure 14. Extraction and particle size reduction flow-chart used in this thesis to obtain lignin from the mentioned sources.

All the lignin samples, regardless of their sources, were prepared using the same process pathway illustrated in Figure 14.

2.2.2. Lignin Extraction Procedure

Lignin sources (nutshell, and maple, birch, pine barks) were grinded with mortar and pestle, then sieved using 100 μm and 50 μm test sieves respectively. 5 g of each sample was taken into the autoclave reactor and 10 mL of 72% H_2SO_4 (diluted from stock solution 95 – 97%) solution was added and mixed. The reactor was sealed and placed in an oven and was kept at 150 $^\circ\text{C}$ for 45 minutes. The extracted samples were then washed with distilled water several times and the solid lignin was collected by suction filtration. A pinch of extracted lignin sample was dissolved in 1,4-dioxane to measure the pH of the solution, which should be around 4 – 5. Extracted samples were dried overnight under vacuum at 40 $^\circ\text{C}$.

2.2.3. Particle Size Reduction Procedure

Extracted lignin samples were placed in a zirconia grinding chamber and milled via Retsch Cryomill device with 6 zirconia balls (diameter: 10.06 mm) at 30 Hz frequency for the given grinding times (5 – 60 min) at -196 $^\circ\text{C}$ (77 K). Low temperature is achieved by circulation of liquid nitrogen around the grinding chamber of the device during grinding operation.

Ultrasonication was performed for further reduction of particle size – which is necessary to get a homogeneous doping and increased surface area of lignin particles- of the cryomilled lignin samples. UP200St Hielscher ultrasonic horn was used and performed at 20 kHz frequency and 200 W at 0 °C. 100 mg of each lignin sample was dissolved (due to low solubility of lignin in 1,4-dioxane, they form a suspension) in 20 mL of 1,4-dioxane and were sonicated for certain time intervals up to 60 minutes. The samples were placed into ice-bath to avoid overheating on the ultrasonic probe, also the sonication was taken a rest for 60 seconds of every 5 minutes.

Malvern Zeta Sizer Nano instrument was used to perform particle size distribution analyses. The instrument allows the determination of the sizes of particles in a range of 0.3 nm to 50 µm by differential light scattering method. Particle size distribution of 10 mg of lignin samples suspended in 10 mL of 1,4-dioxane solution was recorded immediately after preparation of the samples. Each measurement was performed three times and standard deviations were calculated.

2.2.4. Structural and Chemical Characterization of Lignin

Chemical and structural properties of extracted lignin samples were characterized by several techniques: FTIR spectroscopy, Prussian Blue Method for Total Phenol Content Determination, Mechanoradical Content Determination by DPPH test, Gel Permeation Chromatography (GPC), NMR spectroscopy (¹³C-NMR and ³¹P-NMR), TGA/DSC, X-Ray Diffraction (XRD). The samples were also imaged by Scanning Electron Microscopy (SEM).

2.2.4.1. FTIR Spectroscopy

The functional groups of the lignin samples have been investigated by FTIR-ATR using Bruker Alpha FTIR-ATR Spectrometer. All samples were analyzed with spectral width of 4.000 – 400 cm^{-1} and 64 scans at a resolution of 4 cm^{-1} . The spectra were baseline corrected and transmittance percentage was given as normalized data.

2.2.4.2. Prussian Blue Method for Total Phenol Content (TPC)

Determination

Reagents

- 0.02 M FeCl_3 Solution in 0.10 M HCl

8.3 mL of the concentrated HCl was diluted to 1 L with distilled water and 3.24 g anhydrous ferric chloride was dissolved in 1 L of the 0.10 M HCl solution. The solution has a pale-yellow color.

- 0.016 M $\text{K}_3\text{Fe}(\text{CN})_6$ Solution

5.26 g of potassium ferricyanide was dissolved in 1 L of distilled water. The solution has a yellow color.

- Stabilizer Solution

1.0 g gum arabic was dissolved in 80 mL of distilled water by boiling for 25 minutes. The solution was filtered, and the filtrate was diluted to 100 mL. 10 mL 85% H_3PO_4 and 10 mL 1% gum arabic were mixed and the mixture was

diluted to 50 mL with distilled water. The stabilizer solution was refrigerated.
(remains stable for 1 week.)

Procedure

Exactly 5.00 mg of cryomilled lignin (polyphenol) sample was dissolved in 0.1 mL of 1,4-dioxane. 3.00 mL deionized water was added and vortexed. (Poor quality water, particularly iron-containing water may give unacceptable results!) 1.00 mL of freshly prepared FeCl_3 solution was added to the mixture, followed by 1.00 mL of freshly prepared $\text{K}_3\text{Fe}(\text{CN})_6$ solution, just 1 minute after the addition of FeCl_3 solution. The mixture was mixed by stirring bar for exactly 24 hours to complete the reaction. (Reaction duration was followed by UV-Vis Spectra for 0, 24, and 48 hour reactions, then 24 hours was chosen as optimum time according to the maximum absorbance (Figure 29-a)). 5.00 mL of stabilizer (gum arabic solution) was added to terminate the reaction and the absorbance maximum of Prussian blue ($\text{Fe}_4[\text{Fe}(\text{CN})_6]_3$) at 700 nm was recorded. 5 identical preparations for each lignin sample were made and they measured using the same procedure by 10-fold dilution of the final mixture.

For obtaining the standard values of phenol content, methyl gallate (methyl-3,4,5-trihydroxybenzoate) standard was prepared by weighing exactly 5.00 mg of methyl gallate. The standard was tested identically through the procedure described above except that this time only 30 minutes was enough to acquire stable blue color for the standard samples. After 30 minutes the reaction was stopped by addition of 5.00 mL of stabilizer solution then the absorbance of the formed Prussian Blue ($\text{Fe}_4[\text{Fe}(\text{CN})_6]_3$)

at 700 nm was measured by 10-fold dilution of each sample. 5 identical standard samples were prepared for calculation of standard deviation.

2.2.4.3. Mechanoradical Content Determination by DPPH Test

0.2 mg of lignin (5 to 60 min cryomilled) was added into 50 μL , 1.3×10^{-1} M 2,2-diphenyl-1-picrylhydrazyl (DPPH) solution prepared in ACN. The mixture was diluted to 5 mL (a stock DPPH-lignin solution) with ACN and waited for desired hours. Then, 0.5 mL of DPPH-lignin solution was diluted again to 5 mL with ACN just before UV-Vis measurement in each time interval. A control solution of DPPH in ACN was also prepared with the same molarity and the absorbance of the solutions at 517 nm (the absorbance maximum of DPPH) were followed in the solutions' UV-Vis absorption spectra. Each sample was re-measured after indicated waiting times and any decreases in the absorbance were tracked. The consumption of the DPPH by mechanoradicals was monitored from the decrease in the absorbance of DPPH and the number of cryomilling generated mechanoradicals were calculated from this decrease.

2.2.4.4. Solubility Enhancement by Acylation of Lignin

Extracted, cryomilled and ultrasonicated lignin samples are not soluble in any solvent, they form a suspension in 1,4-dioxane and are slightly soluble in pyridine. Their solubility problem prevents their characterization by conventional methods,

e.g. by UV-Vis or GPC). Therefore, we tried to enhance their solubility by acylation with trimethylacetylchloride, as shown in Figure 15. The detailed acylation procedure is also given below.

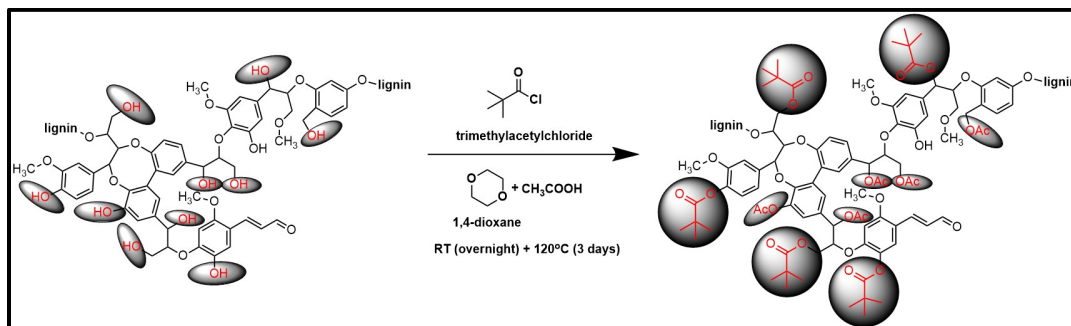


Figure 15. Acylation reaction scheme of lignin with trimethylacetylchloride.

Exactly 20 mg of cryomilled lignin samples were weighed and dissolved in 20 mL of 1,4-dioxane then 5 mL acetic acid was added drop by drop while mixing. The solution was stirred overnight at room temperature. Excess amount of trimethylacetylchloride (10 mL) was added and refluxed for 3 days at 120 °C. Acetic acid and excess of trimethylacetylchloride were evaporated with a rotary evaporator, followed by high vacuum drying of the obtained product at 40 °C for 24 hours.

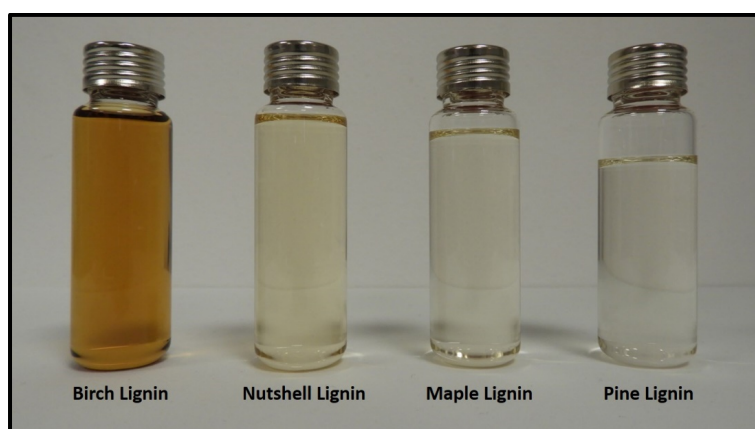


Figure 16. Acylated lignin samples dissolved in THF (Concentration: 1 mg/1 mL).

2.2.4.5. GPC Measurements for Molecular Weight Determination

All acylated lignin samples were dissolved in THF (HPLC grade, without stabilizer) to obtain 1 mg/mL solutions for the GPC analysis (Figure 16). Samples were filtered using a PTFE syringe filter (0.45 μm pore size). After filtration, they were injected into the SEC system. The SEC system (Agilent, Santa Clara, CA, USA) used includes a degasser, isocratic pump, auto sampler, diode array UV detector (Agilent 1200 series ELSD); the mobile phase was THF (HPLC grade, without stabilizer) with a flow rate of 0.6 mL/min. The column used was 6.2 mm \times 250 mm Agilent Zorbax PSM 300-S (particle size: 5 μm). The system was calibrated with polystyrene standards (575, 1530, 3950, 10210, 29510, 72450, 205000, 467000 Da) using ELSD detector.

2.2.4.6. ^{13}C -CP/MAS NMR Spectroscopy

Due to the low solubility of lignin in many deuterated organic solvents (e.g. CDCl_3), solid state ^{13}C -NMR was performed. Lignin samples were analyzed by ^{13}C -CP/MAS (Cross-polarization/Magic angle spinning) NMR (Nuclear Magnetic Resonance). The analyses were carried out using Bruker Avance 300 MHz WB Superconducting FT NMR Spectrometer equipped with 4 mm MAS probe. For acquisition of ^{13}C -CP/MAS NMR spectra, relaxation delay of 4 s, and spin rate of 8.5 kHz were used. The spectrum shown in the results were derived from 7000 scans, with the chemical shifts given as δ ppm in the range of 0 – 210 ppm. The NMR spectrometer was calibrated against pure glycine sample before the measurements.

2.2.4.7. ³¹P-NMR Spectroscopy

The most common procedure for the ³¹P-NMR analysis of lignin samples presented in the literature [63] was adopted in our analysis: 30 – 40 mg lignin was sonicated in CDCl₃ in order to decrease the particle size and enhance the solubility. Then, 500 μL of lignin-CDCl₃ solution were taken into NMR tube and a few drops of dry pyridine was added. The derivatization reagent 2-chloro-1,3,2-dioxaphospholane (100 μL) was added into the NMR tube and the mixture was vortexed for 5 minutes. Cholesterol (10 mg/mL) (an internal standard) and chromium (III) acetylacetonate (5 mg/mL) (a relaxation agent) were dissolved in the mixture of 1.6 eq. pyridine/1 eq. CDCl₃ (v/v). 100 μL of the freshly prepared solution was taken into the NMR tube and vortexed for 1 minute. For acquisition, standard experimental procedure of Bruker Avance 400 MHz NMR spectrometer for ³¹P-NMR analysis was used. The results were collected as 2000 scans and all chemical shifts were reported according to hydrolysis product of phosphorylation reagent peak, which was observed at 121.1 ppm.

2.2.4.8. Thermal Stability Analyses (TGA/DSC) of Lignin

Thermal stability of lignin was determined by thermogravimetric analysis (TGA) method using TA Instruments Q500 TGA device. 5 – 8 mg of samples were weighed and scanned from 25 °C to 900 °C.

Glass transition temperature (T_g) measurements of the samples were performed using TA Instruments Q200 DSC; samples of about 2 – 10 mg were weighed and run

at a heating rate of 20 °C/min from 25 °C to 200 °C. A heating rate of 20 °C/min was used, because the glass transition peaks are sharper at faster heating rates.

2.2.4.9. X-Ray Diffraction (XRD) Analysis

XRDs of cryomilled and non-cryomilled lignin were recorded on X'Pert PRO, PANalytical model X-ray diffractometer with Cu K α radiation. 40 mA current and 45 kV accelerating voltage were applied.

2.2.4.10. Scanning Electron Microscopy (SEM) Analyses

The surface morphology of non-cryomilled and cryomilled lignin samples (5 – 60 minutes) were imaged using Thermo Fisher Scientific Quanta 200F model SEM with an accelerating voltage of 15kV.

2.2.5. Lignin Doping to The Polymers

After extraction of the lignin samples, the samples were cryomilled and then ultrasonicated in order to reduce the particle size and increase the surface area. Ultrasonicated samples have smaller particle size (see section 3.1.1); however, ultrasonication can only be performed in solution and after evaporation of the solvent it is clearly seen that particles can agglomerate in the solid state. Therefore,

thermoplastics (PE, PP, PS, PLA) and elastomers (PDMS) were doped with only cryomilled lignin. Thermoplastics were chosen among the most common engineering polymers currently used in many industries and as an example of an elastomer, PDMS was chosen due to great advantage of forming smooth surface on flat molds upon curing.

2.2.5.1. Lignin Doping to PDMS (Polydimethylsiloxane)

PDMS (Sylgard 184) was prepared by mixing the base and the curing agent in 10:1 ratio and cryomilled lignin (up to 5% w/w) was added by mixing vigorously. After that, the mixture was poured in a petri dish of 1.5 cm height and cured in oven for 4 hours at 60 °C (thickness: 0.2 cm). Then, additional 0.4 cm pure PDMS layer was cured onto lignin-doped PDMS layer in order to handle the samples easily upon electrical measurements. The prepared samples are shown in Figure 17. Cured PDMS-Lignin composite (thickness: 0.6 cm) was cut into 1x1 cm pieces. The smooth surface of lignin-doped PDMS touching with petri dish was used in contact electrification tests. The homogenous 60 minutes cryomilled lignin doped samples were used in all measurements.

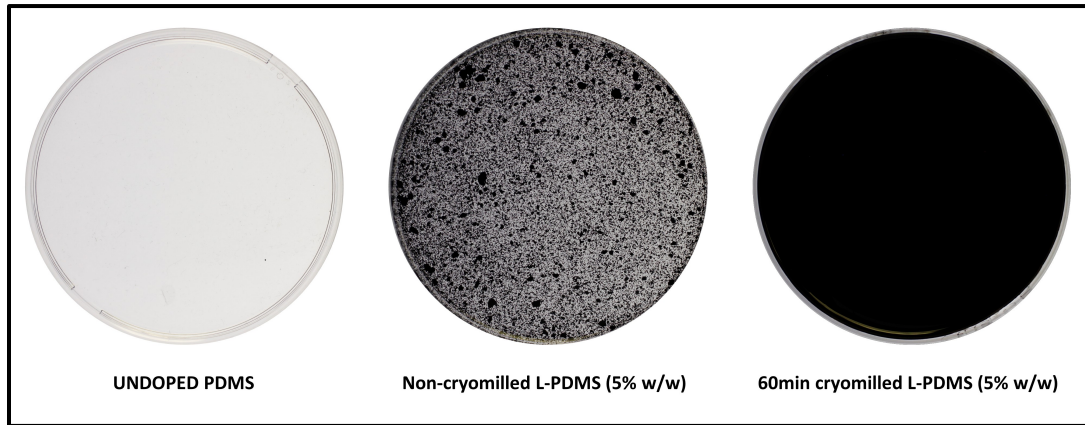


Figure 17. Images of Pure (undoped) PDMS, non-cryomilled lignin doped PDMS and 60 min. cryomilled lignin doped PDMS.

2.2.5.2. Lignin Doping to Thermoplastics (PE, PP, PS, PLA)

All thermoplastics were melted on the hot-plate and pressed with thick Teflon plate in order to achieve a smooth surface. Lignin doping concentration was chosen as 5% (w/w). Polyethylene, polypropylene, polystyrene and polylactic acid were doped with lignin by vigorous mixing of added lignin in melted polymer on aluminum plates. The melt was poured between Teflon plates and was pressed from top. The sample was let to solidify at room temperature. Then, the doped-polymer was taken out from the hot-plate, remained still until the polymer was re-solidified. The same thickness of the doped-polymers was acquired by the aid of Teflon plate and aluminum plates where the polymers melted and doped among them.

The lignin-doped thermoplastics were cut by a laser-cutter into circular pieces of 1.5 cm diameter in order to mount them easily onto the stubs connected to electrodes. These pieces were used in contact electrification measurements without any other alteration.

2.2.6. Preparation of Lignin-Free Wood

Lignin was removed from limba wood (*Terminalia Superba*) by several extraction processes similar to that used in paper industry. In the method, 2.5 M NaOH and 0.4 M Na₂SO₃ solution was prepared by dissolving 50 g of (equal amount of) each substance in 500 mL of distilled water. The solution was stirred until all the substances were dissolved and taken into a flask. Wood pieces (1.5 cm x 10 cm x 1.5 cm) were placed in the solution and the solution was refluxed overnight at 110 °C, by which time a brownish-red solution of lignin forms. This solution was poured off and the wood was washed 3 times with distilled water. Then, wood sample was boiled (bleached) with H₂O₂ solution (500 mL, 9.8 M) for 3 hours in order to remove the lignin and get lignin-free white wood. The white wood sample was washed with distilled water 3 times more and dried under vacuum at 60 °C.

The obtained lignin-free wood can be seen in Figure 47-b. Since the contact electrification experiments give better results (with small standard deviation) with smooth surfaces and the obtained lignin-free wood is rough, in order to have smooth surface of the wood samples, the lignin-free wood was cryomilled for 5 minutes (Figure 47-c) and pressed into a pellet (diameter: 1.4 cm) using hydraulic pellet press (under 5100 bar).

2.2.7. Electrical Measurements

2.2.7.1. Charge Density Measurements

Electrostatic charge on the polymer surfaces were measured by immersing the polymer pieces in a Faraday cup attached to an electrometer (Keithley 6517B). Lignin-doped and undoped PDMS samples were contact charged against Aluminum foil up to 200 touches (Figure 18) to record the maximum charge density that can be obtained on the surfaces. Since it is harder to manipulate hard plastics with tweezers during this process, charging behavior of thermoplastics were monitored using a separate method that utilizes a homemade tapping device attached to an oscilloscope. In this method, surface electrical potential of thermoplastics that increases upon contact charging is recorded as the signal. Samples were placed to the one of the electrodes (base electrode) Aluminum stub were placed to the other electrode (counter electrode) and open circuit voltages were measured and collected from saturated signals (signals that accumulated charges are at their maximum values). 1 Hz tapping frequency were used in all of the measurements (Figure 19). For some samples, due to low propensity for charging on Al), PTFE (Teflon) coated stub surface was also used as counter electrode. All the samples were prepared and measured independently, at least 3 times for calculating standard deviation.

Previously extracted and cryomilled pine bark lignin was mixed with lignin-free wood at 1% to 50% (w/w) ratios by 5 minutes cryomilling. Then all the samples (doped-undoped wood and pure pine bark) were shaped as pellet (as shown in Figure 48), attached to the aluminum stubs with carbon tape. The electric potential acquired on

the samples upon tapping against PTFE (in a setup shown Figure 19) were recorded as V_{oc} .

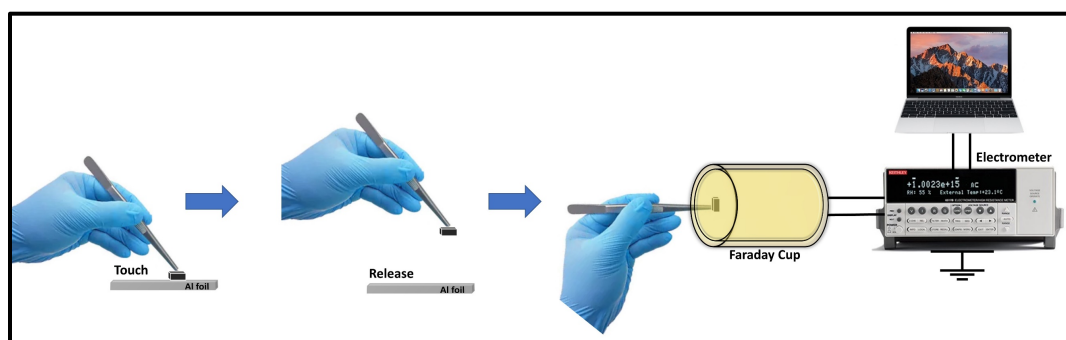


Figure 18. Illustration of Contact Electrification Measurement Setup-1. Determination of maximum net charge density on the polymer surfaces after contact.

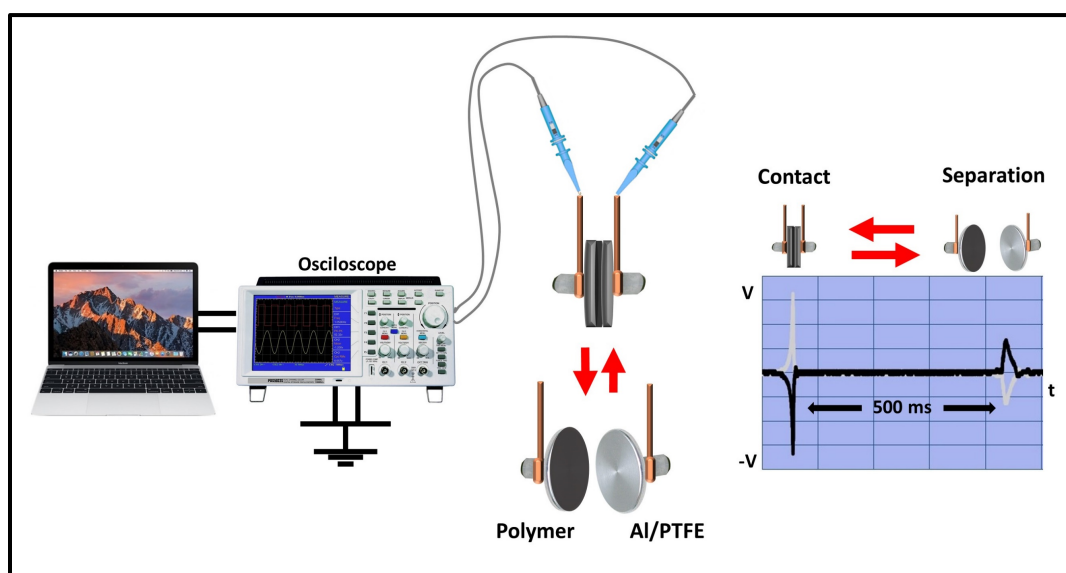


Figure 19. Illustration of Contact Electrification Measurement Setup-2. Determination of surface electric potential upon contact and separation events.

2.2.7.2. Charge Decay Measurements

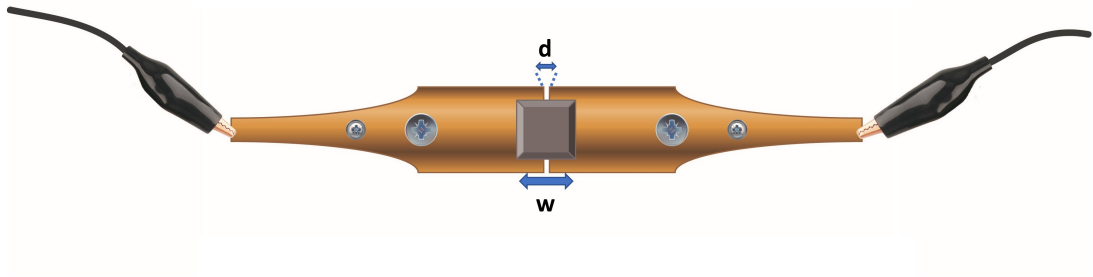
Before charge decay experiments, PDMS pieces were left to discharge for at least 24 hours in isolated container. The electroneutrality of these pieces was confirmed by immersing the pieces in a homemade Faraday cup connected to a high precision

electrometer (Keithley Instruments, model 6517B) that measures electrical charge. Only pieces with net charge densities below the electrometer's detection limit ($\leq \pm 0.005 \text{ nC/cm}^2$) [2] were considered as neutral. Undoped and doped PDMS pieces were charged against aluminium foil several times in order to reach the highest surface charge (charge saturation point). Then, samples were kept immersed in the homemade Faraday cup for 30 minutes. Charge decay rates were calculated using OriginPro2017, by linear equation fitting.

2.2.7.3. Surface Conductance Measurements

In order to investigate whether the fast decay in case of lignin doping is caused by the increase in surface conductivity of doped pieces, surface conductance of PDMS and 5% lignin doped PDMS samples were measured using two probe method connected to electrometer, which acts also as a voltage source upon current measurements (Figure 20-a). Current versus voltage curves of undoped PDMS and 5% lignin doped PDMS was obtained via probe station (with $w = 1 \text{ cm}$ wide samples ($1 \text{ cm} \times 1 \text{ cm}$ square pieces), and the distance between copper electrodes $d = 100 \mu\text{m}$) and the applied voltage was changed from 0 to -100 and 0 to +100 V in steps of 10 V, which gave identical results in terms of surface conductance (Figure 20-b). From the slopes of the I-V curves, the values for surface resistance, R_s were calculated according to equation $R_s = (V/I) \cdot (w/d)$ in Ω . Then, surface resistivities were converted to surface conductance (σ) using the equation $\sigma = 1/R_s$. Standard deviations of the surface conductivities were calculated from at least 3 independent measurements.

a)



Distance between electrodes: $d = 100 \mu\text{m}$
Sample width: $w = 1 \text{ cm}$

b)

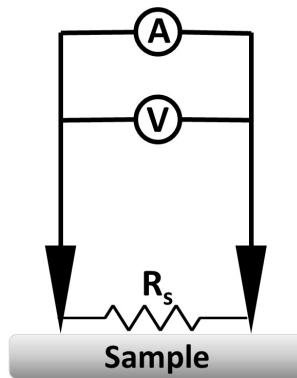


Figure 20. (a) Illustration of surface conductance measurement setup. (b) Electrical circuit scheme of the two probe method.

CHAPTER 3

3. RESULTS & DISCUSSION

3.1. Characterization of Extracted, Cryomilled and Acylated Lignin

We successfully extracted the lignin from various natural sources such as nutshell, hardwood barks (maple, pine and birch tree). The obtained lignins were subjected to mechanochemical treatment (cryomilling) for different milling times (5 to 60 min) to investigate the effect of milling time on the particle size and the number of radicals generated upon milling. Functional groups in the obtained lignin were analyzed by FTIR spectroscopy, ^{13}C -CP/MAS-NMR, and ^{31}P -NMR spectroscopy, total phenol content (TPC) determination by Prussian blue method, mechanoradical content determination by DPPH test. For the obtained lignin samples, molecular weight was determined by GPC, thermal stability was probed by TGA/DSC, and surface morphology is analyzed by SEM.

3.1.1. Particle Size Measurement Results

In order to have a homogeneous distribution of lignin particles in a sample, particle size of lignin reduced by cryomilling, which offers milling of samples at cryoconditions. For example, for nutshell lignin, the particle size is reduced from approximately 50 μm to 1324 ± 173.4 , 892.3 ± 17.8 , 913.8 ± 27.4 , and 756.8 ± 11.3 nm for 5, 10, 30, and 60 min cryomilling, respectively (Figure 21). Therefore, it can be said that cryomilling is a proper mechanochemical treatment method to reduce the particle sizes of the lignin samples.

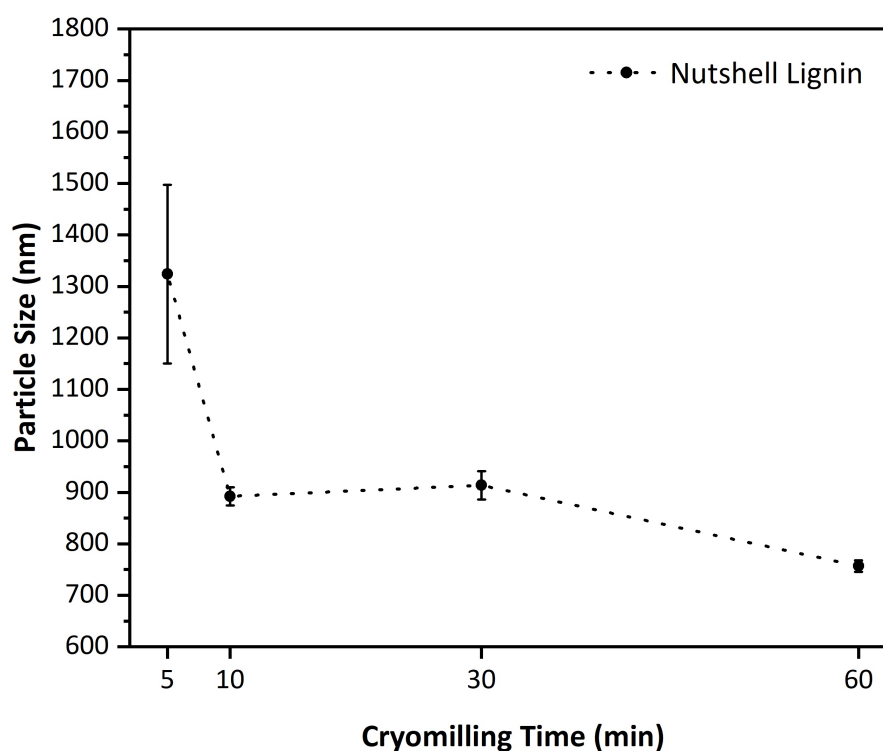


Figure 21. Particle size vs cryomilling time of cryomilled nutshell lignin. Error bars were calculated from 3 independent measurements of each sample.

For further reduction of particle size, ultrasonication was also performed. It is found out that lignin samples from different sources show different behaviour upon ultrasonication (Figure 22). Maple and birch lignin exhibited continuous decrease in particle size along with ultrasonication time; however, 4 minutes of ultrasonication time was enough for nutshell lignin. Agglomeration of the particles in the suspension started for pine and nutshell lignin upon prolonged ultrasonication.

Although ultrasonication of the lignin samples let us get smaller (down to 200 nm) particle sizes of lignin samples, the lignin obtained is in the form of a 1,4-dioxane suspension. In order to dope the lignin into the polymers, solvent must be evaporated. This evaporation causes instantaneous agglomeration, followed by an increase in the particle sizes. Therefore, we avoided the ultrasonication step for the rest of the samples we prepared and used only cryomilling (for 60 min) to reduce their particle size.

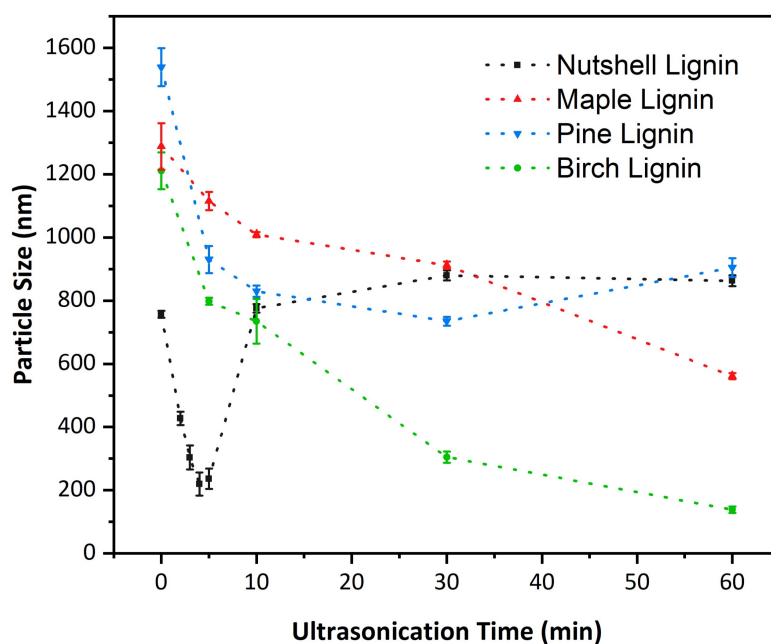


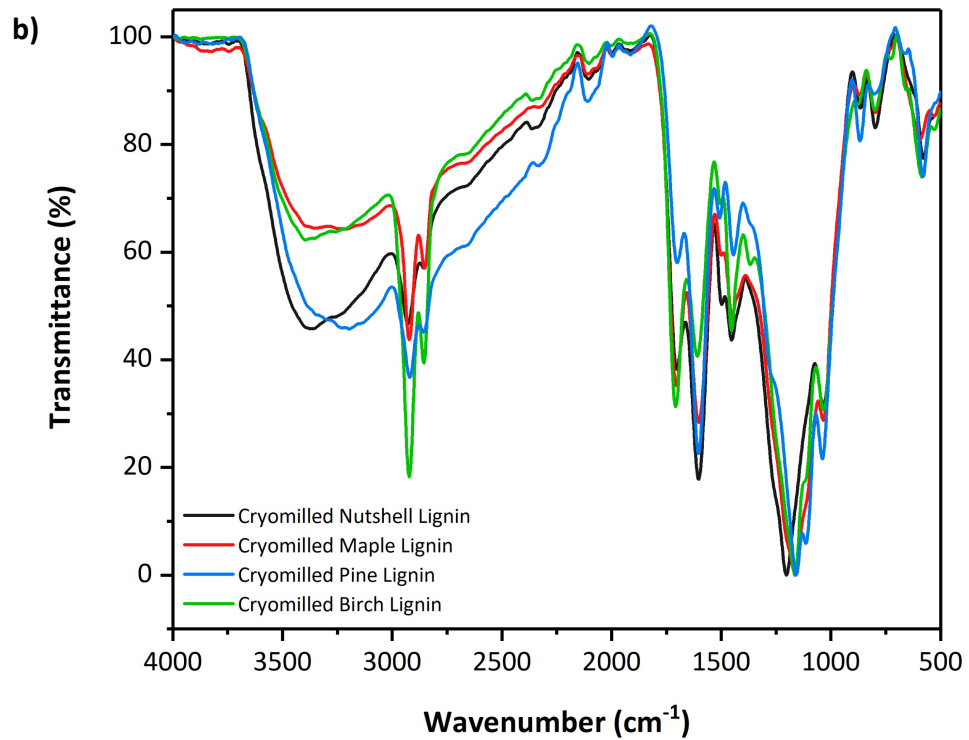
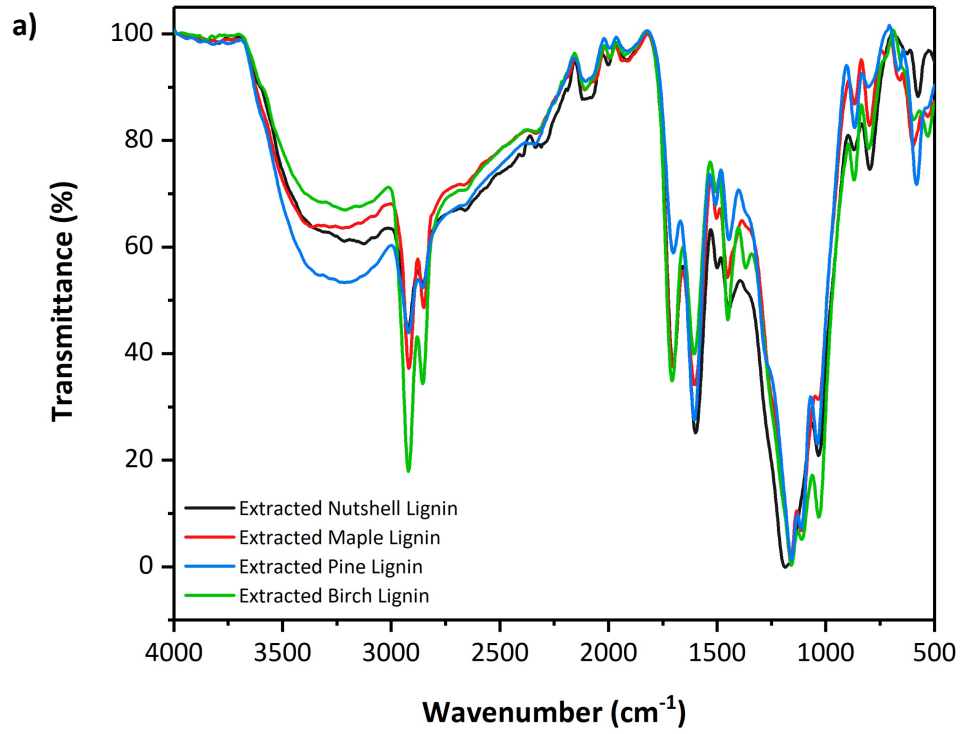
Figure 22. Particle size vs. ultrasonication time for lignin samples from different sources, namely nutshell, maple, pine, and birch. 0 min sonication refers to previously 60 min. cryomilled lignin. Error bars were calculated using 3 independent measurements of each sample.

3.1.2. Structural Analyses of Lignin by FTIR Spectroscopy

It is shown that there is no change on the characteristic peaks of the lignin samples (aromatic skeleton vibrations at 1600 cm^{-1} , 1510 cm^{-1} and 1450 cm^{-1}), and (sp^2 and sp^3 vibrations of methylene and methyl groups at 2925 cm^{-1} and 2852 cm^{-1} , respectively) by mechanical treatment (cryomilling); however, -OH peak at 3400 cm^{-1} tends to shift towards 3500 cm^{-1} via cryomilling due to hydrogen bonding breakage of phenolic units on the polymer backbone (Figure 23a-b).

Cryomilling time has a visible effect on OH-group intensities, however, there is no continuous trend (e.g. constant increase or decrease). Nevertheless, it is clearly seen that the peaks tend to shift to higher wavenumbers, which is an indication of hydrogen bond breakages and generation of more free-OH groups (Figure 23-c).

FTIR spectra of acylated lignin samples (Figure 23-d) proved that the reaction occurs on the phenolic OH groups, i.e. by attaching acetoxy unit to phenol ring shows significant decrease at the OH peak at 3400 cm^{-1} and enhancement on C-O-C aromatic acyl groups at 1200 cm^{-1} . Carbonyl peak on aromatic structures at 1708 cm^{-1} was also increased and shifted to 1728 cm^{-1} due to esterification reaction [64,65].



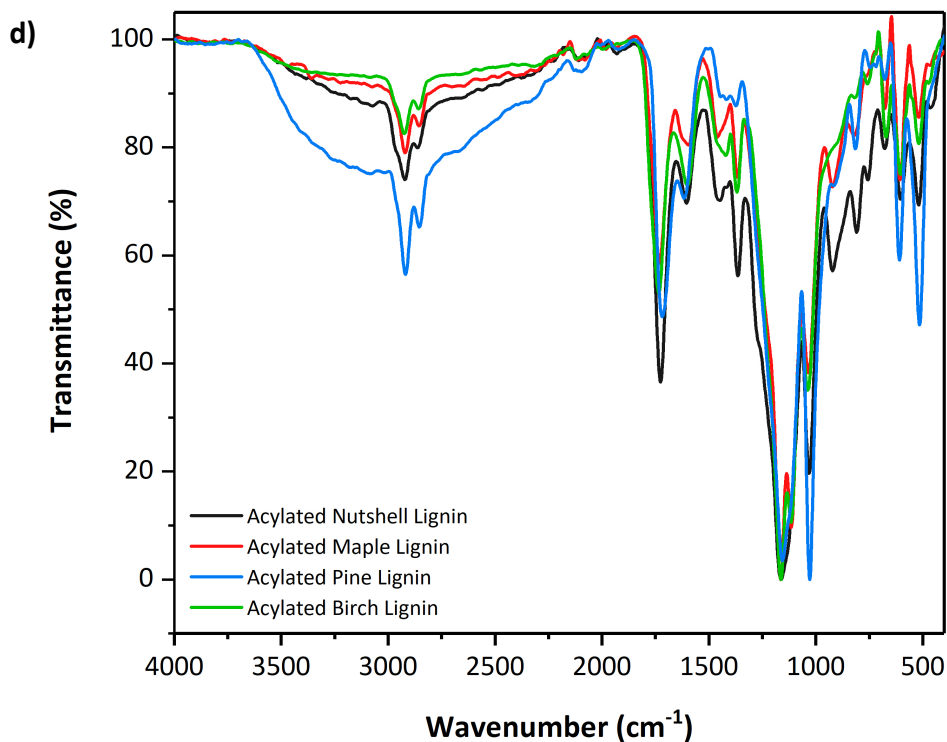
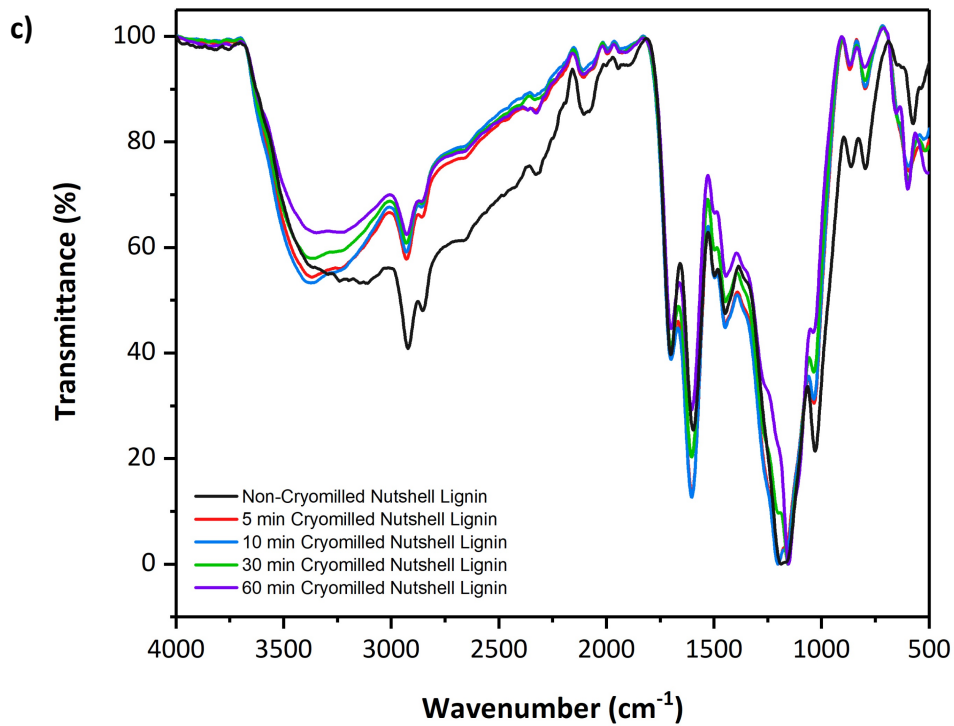
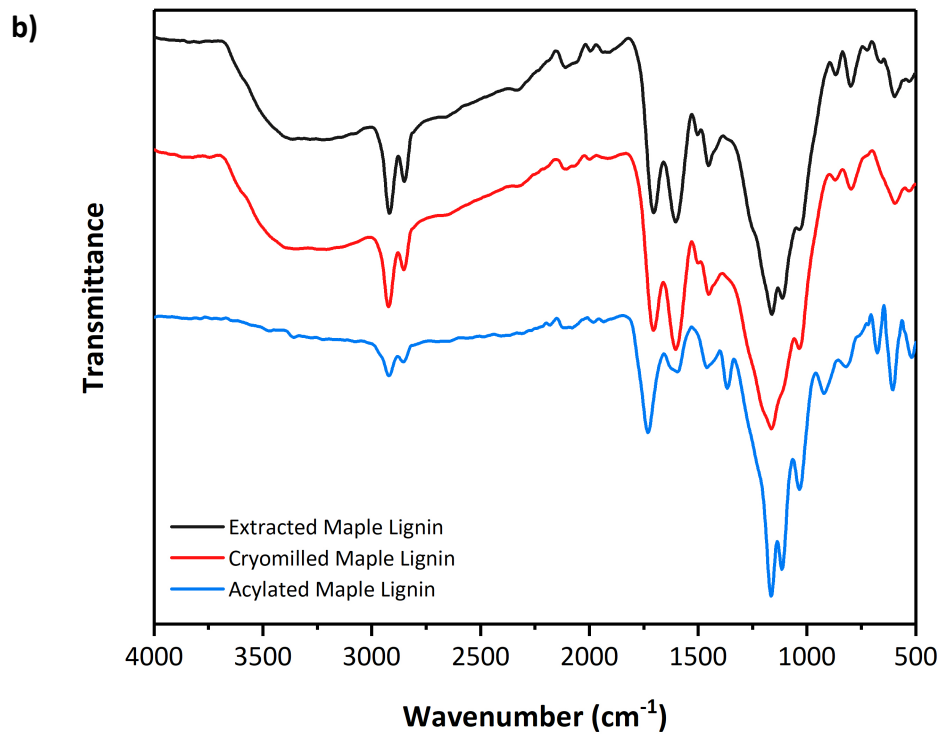
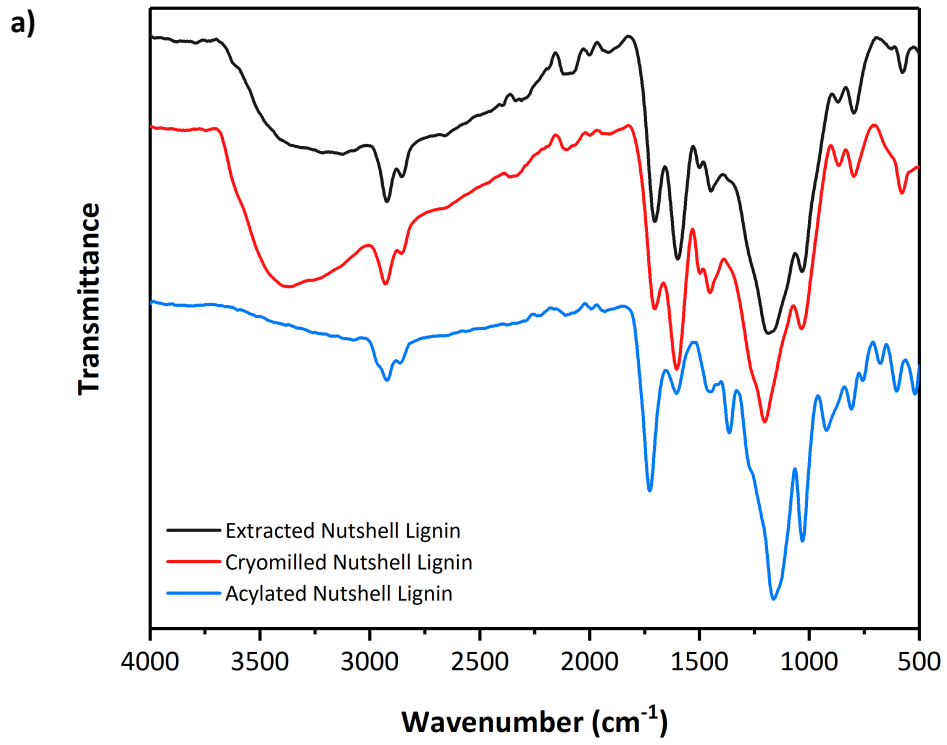


Figure 23. FTIR spectra of lignin (nutshell, maple bark, pine bark and birch bark). All spectra were given as normalized transmittance percentage vs wavenumber. (a) Extracted lignin, (b) 60 min cryomilled lignin, (c) 5-10-30-60 min. cryomilled nutshell lignin, (d) acylated lignin.



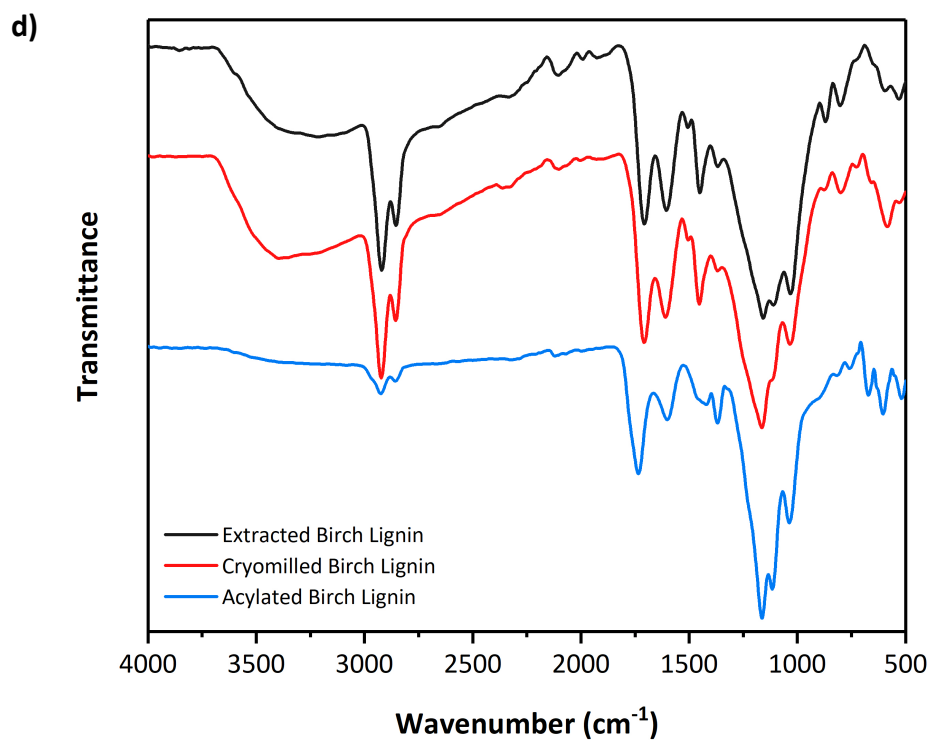
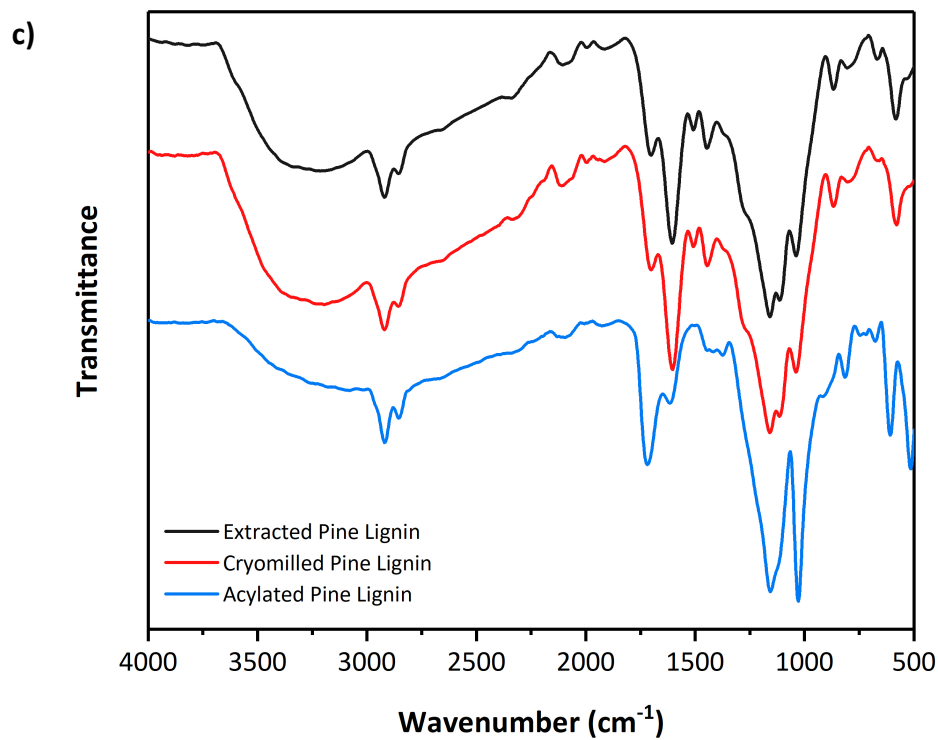


Figure 24. Stacked spectra (shifted on the vertical axis for clarity) of extracted-cryomilled (60 min)-acylated lignin samples. (a) Nutshell lignin, (b) maple lignin, (c) pine lignin, and (d) birch lignin.

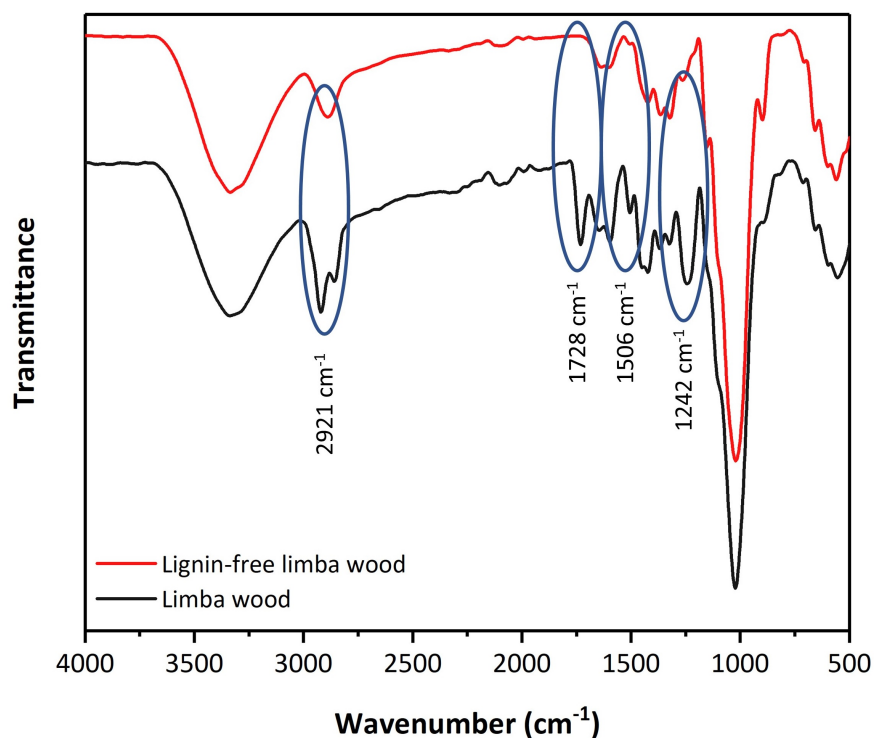


Figure 25. FTIR spectrum of lignin removal from limba wood.

Lignin-free limba wood has a lack of peaks at 2921 cm⁻¹, 1728 cm⁻¹, 1506 cm⁻¹ and 1242 cm⁻¹ for aromatic C-H stretch, carbonyl (C=O) stretch, guaiacyl and syringyl aromatic skeletal vibrations and guaiacyl ring plus C=O stretch, respectively. It is shown that lignin removal from the wood kept the OH band at 3400 cm⁻¹ due to OH groups on cellulose and hemicellulose structures in lignin-free wood while, peaks originating from aromatic groups (aromatic skeleton vibrations, C-H stretches, guaiacyl (G), and syringyl (S) unit vibrations) disappeared (see Figure 25).

3.1.3. Total Phenol Content (TPC) Determination

Total phenol content (TPC) is a simple method to investigate the amount of phenolic moieties in plant materials and natural extracts, and is especially used in the determination of polyphenols [66].

The polyphenol (PP) (in this case lignin) reacts with the ferricyanide ion $(\text{Fe}(\text{CN})_6)^{-3}$ and is oxidized during reduction of the $(\text{Fe}(\text{CN})_6)^{-3}$ to the ferrocyanide ion $(\text{Fe}(\text{CN})_6)^{-4}$. Then, $(\text{Fe}(\text{CN})_6)^{-4}$ reacts with the ferric ion (Fe^{+3}) (FeCl_3 ionization) to form ferric ferrocyanide $(\text{Fe}_4[\text{Fe}(\text{CN})_6]_3)$, called Prussian blue, which has a distinct absorption centred around 700 nm with an absorptivity of $5770 \text{ L}\cdot\text{mol}^{-1}\cdot\text{cm}^{-1}$. The oxidation-reduction reaction can be demonstrated as follows:

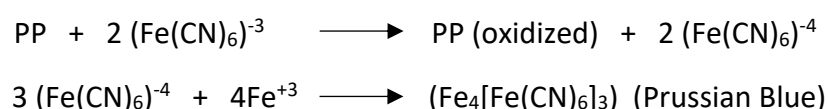


Figure 26. "Prussian Blue test" reactions of polyphenols (PP).

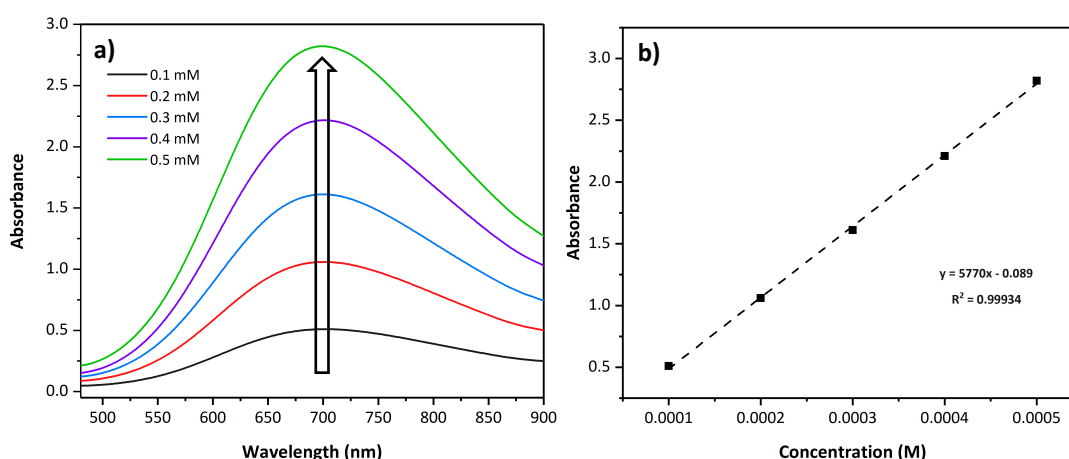


Figure 27. (a) UV-Vis spectra of Methyl Gallate standard solutions with concentrations 0.1 mM-0.5 mM used in Prussian Blue test for polyphenols showing an increase of the absorption band at 700 nm (the absorption maximum for Prussian blue that forms upon oxidation of polyphenols) and (b) the generated calibration curve. For details of the solution preparations and the test, see section 2.2.4.2.

Calibration curve for Prussian Blue total phenol content test of lignins was generated by using the absorbance maximum values of 700 nm band obtained (Figure 27-a) by the methyl gallate standard solutions (0.1 mM to 0.5 mM). (Figure 27-b). Then all the lignin samples were reacted using the same procedure, their UV-Vis spectra were recorded, and the total phenol contents were obtained from the spectra as shown in (Figure 28).

Lignin-free blank sample, too, has a slight absorbance at 700 nm, resulting from self-reduction of ferricyanide ion in time. We subtracted this change in absorbance from the absorbance of lignin samples to obtain the net absorbance change due to reaction of the lignins (Figure 29-b).

TPC (%) values of lignin samples were found to be 67.9 ± 4.6 , 74.7 ± 7.6 , 63.3 ± 5.9 , and 61.4 ± 5.1 for nutshell, maple, pine and birch lignin as methyl gallate equivalent (MGE), respectively (Table 2). The colour change during the reaction is demonstrated in Figure 30.

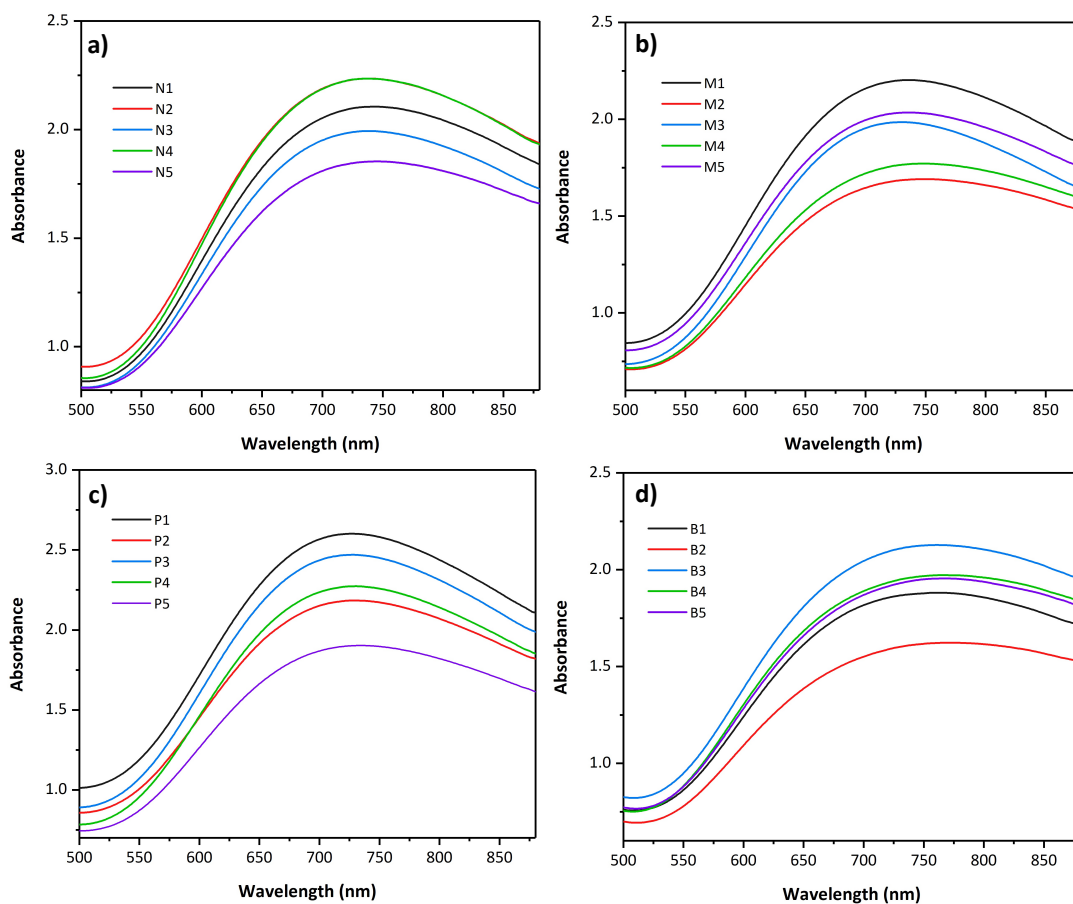


Figure 28. UV-Vis spectra recorded during Prussian blue test: Nutshell (a), maple (b), pine (c), and birch lignin (d). N(1-5), M(1-5), P(1-5), and B(1-5) indicate each of 5 identical experiments performed in order to calculate standard deviations for nutshell, maple, pine, and birch lignin respectively.

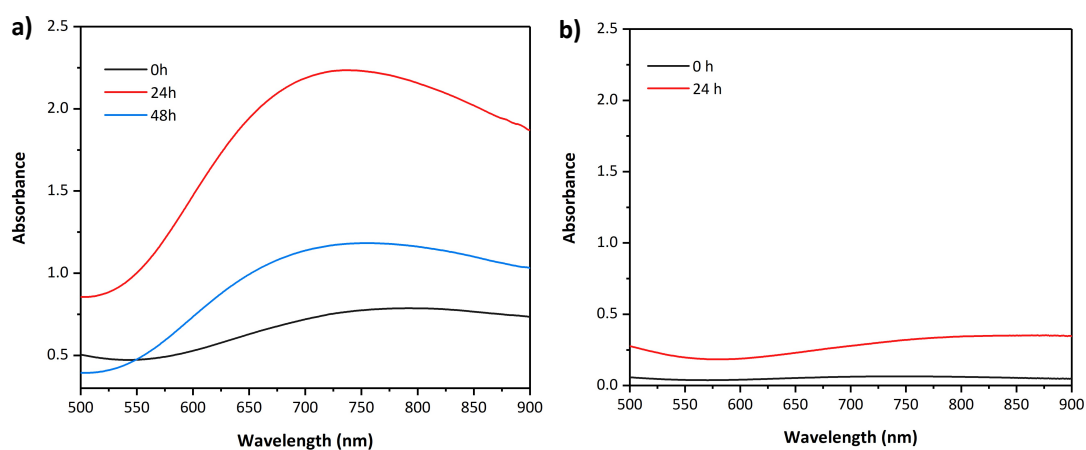


Figure 29. UV absorption changes of Prussian Blue reaction of (a) lignin and (b) blank control sample (lignin-free) solution initial and after 24 hours.

Table 2. Total phenol content determination of the lignin samples. Standard deviations and mean values were calculated using the data from 5 different samples prepared by using identical procedure^(a). Methyl gallate standard^(b).

Sample	Absorbance Mean at (700 nm)	M.G. ^b Equivalent Mean (mg)	MG Equivalent Mean (%)
Nutshell Lignin	2.04 ± 0.14 ^a	3.39 ± 0.23 ^a	67.9 ± 4.6
Pine Lignin	2.25 ± 0.24	3.74 ± 0.38	74.7 ± 7.6
Maple Lignin	1.90 ± 0.18	3.17 ± 0.29	63.3 ± 5.9
Birch Lignin	1.83 ± 0.16	3.07 ± 0.25	61.4 ± 5.1

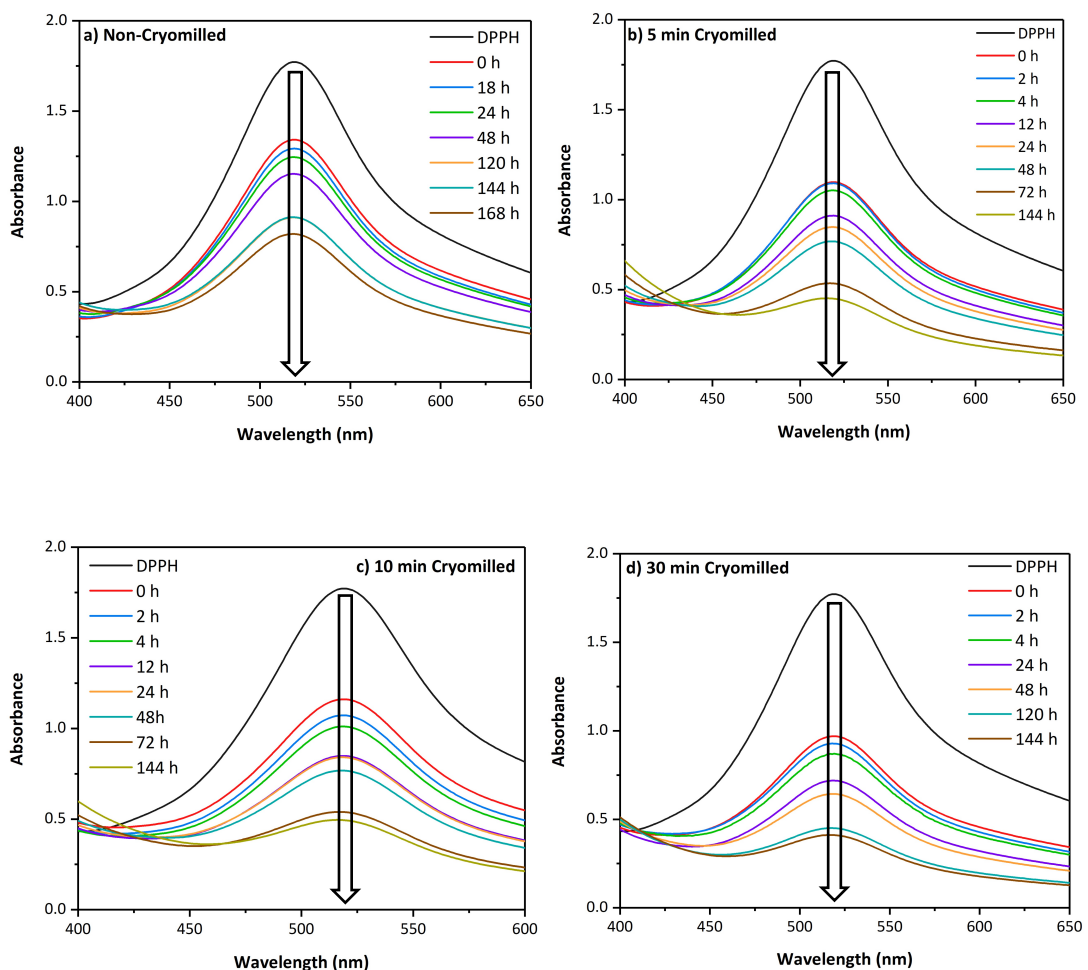


Figure 30. Prussian blue reaction. Visual comparison of the blank sample (without lignin) and lignin contained sample (polyphenol) after 24 hours .

3.1.4. Mechanoradical Content Determination

Mechanoradical content of the lignin samples were determined using DPPH test. Non-cryomilled, 5 to 60 min cryomilled nutshell lignin samples were reacted with DPPH and reacted number of radicals in each sample was tracked by the absorbance decrease in the absorbance max of DPPH absorption at 517 nm, using UV-Vis spectroscopy (Figure 31). For all DPPH/lignin solutions, with prolonged waiting times the absorbance decreases. This decrease is not caused by the instability of the DPPH solutions or their reaction with air, etc., as we tested for a control sample having no

lignin but just the DPPH in the solvent (see Figure 31-f). This decrease is presumably the time needed for the DPPH solution into the closed structure of lignin and react with all radicals “buried”. Nevertheless, the data shows that the reacted number of radicals in lignin samples increased together with reaction time and cryomilling duration. 30 and 60 minutes cryomilled lignin produced the highest reacted number of radicals at the “initial time” and after 144 hours of waiting (Figure 32). It is reported that non-cryomilled lignin (native lignin) also possess radicals and therefore even with no cryomilling, lignin has $2.5 \times 10^{21} \pm 1.8 \times 10^{19} \text{ g}^{-1}$ radicals.



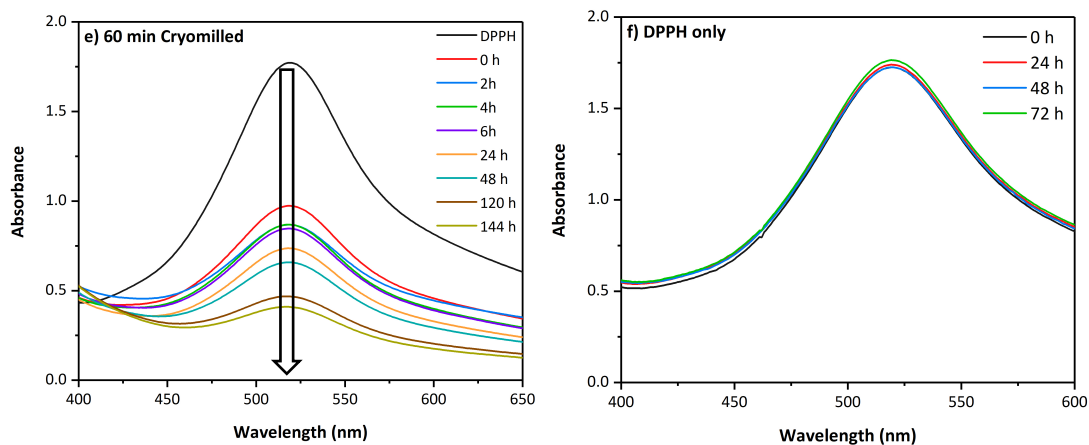


Figure 31. UV-Vis spectrum of DPPH-lignin mixtures at given reaction times. (a) Non-cryomilled, (b) 5 minutes, (c) 10 minutes, (d) 30 minutes, and (e) 60 minutes cryomilled samples, (f) control sample having no lignin but only DPPH.

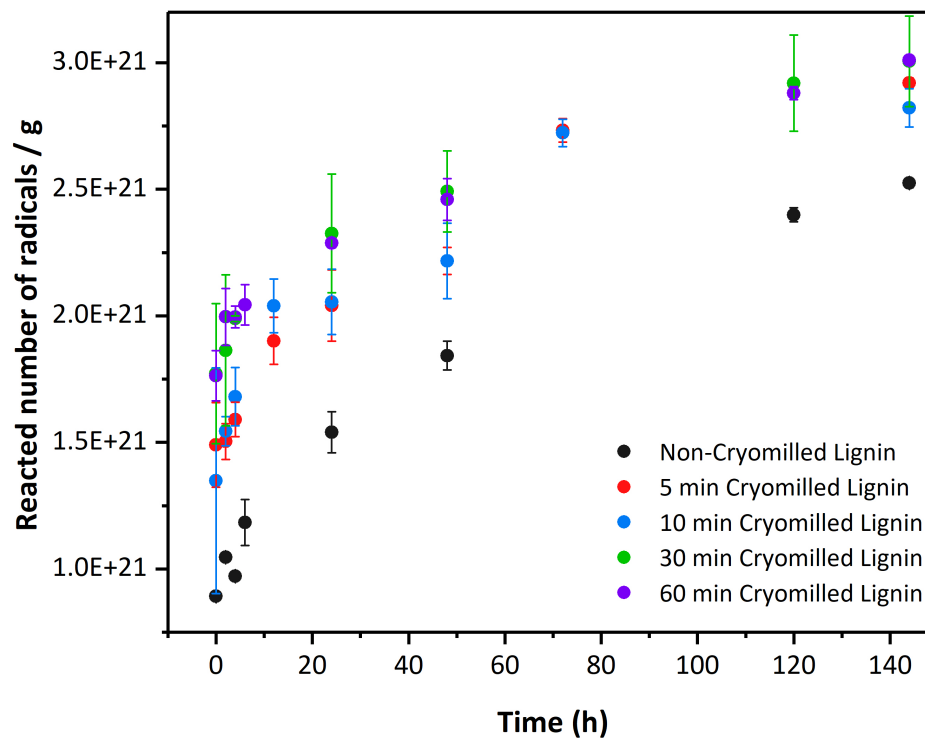


Figure 32. The reacted number of radicals per gram of lignin sample cryomilled for the given milling times at the given reaction times. The reaction between DPPH radical scavenger and the lignins continue at even prolonged times.

3.1.5. Molecular Weight Determination of Acylated Lignins

Molecular weight values of acylated lignins (nutshell, pine, maple, and birch tree) were determined by GPC and found to be around 1000 g/mol as summarized below in Table 3. Low molecular weights correspond to the decreased particle size of the samples upon the previous mechanochemical treatment. Also, the THF suspensions of lignins must be filtered before GPC analysis (GPC measurements require 0.45 μm filtering) and only particles with particle sizes less than 0.45 μm could be analysed by GPC. Although acylation enhances the solubility in lignin in common organic solvents, even acylated lignin is not completely soluble in any of the common organic solvents.

Table 3. Molecular weights of acylated polymers. *Polydispersity index

Lignin	M_w (g/mol)	M_n (g/mol)	M_z (g/mol)	PDI*
Ac-Nutshell	1110	746	1562	1.48
Ac-Pine	1121	848	1425	1.32
Ac-Maple	1127	846	1448	1.33
Ac-Birch	988	680	1401	1.45

3.1.6. ^{13}C -CP/MAS NMR Results

Lignin solubility is a main drawback to analyse the material in a solution as mentioned previously, so solid-state ^{13}C -NMR spectroscopy was performed in order to understand the chemical structure of the lignin in detail. The chemical shifts of the aromatic and aliphatic peaks of obtained from the lignin samples subjected to solid state carbon NMR (showed in Figure 33) were found to be in a compliance with

previous reports [67–69]. It can be concluded that different lignin sources contain different amount of linkage type of each syringyl (S), guaiacyl (G) and p-hydroxyphenyl (H) sub-units.

^{13}C -NMR peaks were found and listed below:

Nutshell Lignin: ^{13}C NMR (75 MHz, CDCl_3) δ 171.9, 143.9, 124.4, 109.0, 57.1, 52.4, 26.2, 10.5 ppm.

Maple Lignin: ^{13}C NMR (75 MHz, CDCl_3) δ 171.9, 143.9, 124.8, 112.7, 57.5, 53.0, 27.1, 11.7 ppm.

Pine Lignin: ^{13}C NMR (75 MHz, CDCl_3) δ 171.5, 148.4, 141.7, 123.1, 110.6, 68.1, 52.0, 31.9, 25.9 ppm.

Birch Lignin: ^{13}C NMR (75 MHz, CDCl_3) δ 170.1, 142.7, 126.3, 109.2, 84.7, 68.6, 52.9, 38.4, 27.1, 12.9 ppm.

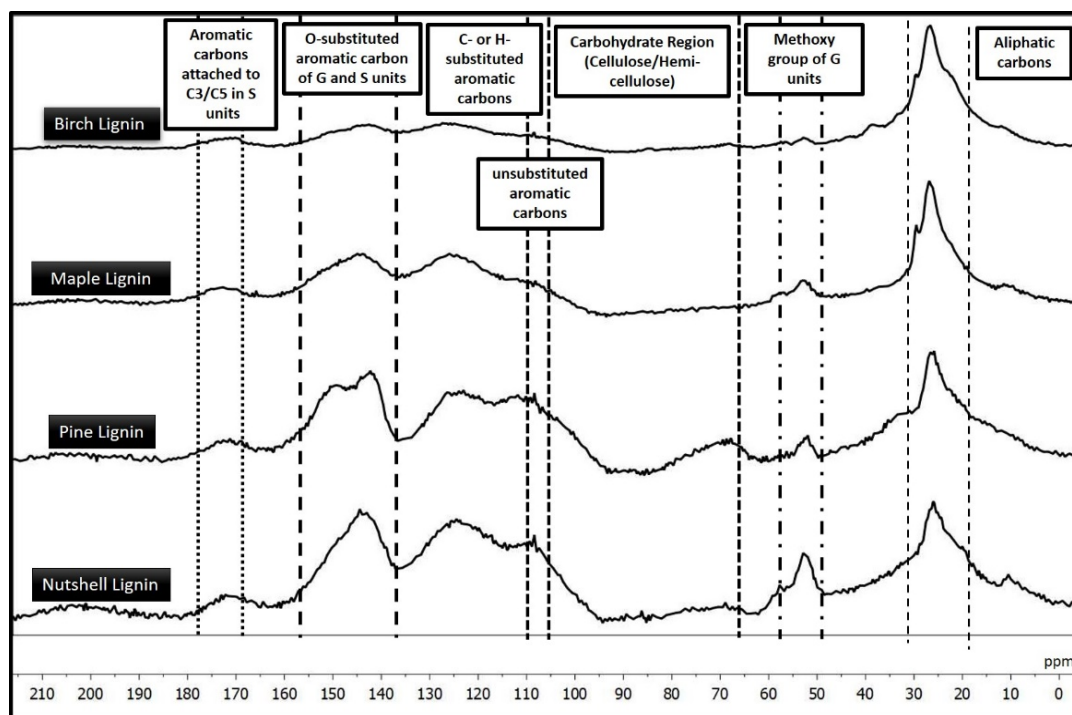


Figure 33. ^{13}C -CP/MAS NMR spectra of 60 minutes cryomilled lignins.

3.1.7. ³¹P-NMR Results

The -OH groups in lignin were labelled by phosphorylation reaction as shown below for ³¹P-NMR analyses. All the chemical shifts reported are referenced by hydrolysis product of 2-Chloro-1,3,2-dioxaphospholane at 121.1 ppm and cholesterol internal standard observed at 134.6 ppm [70–72].

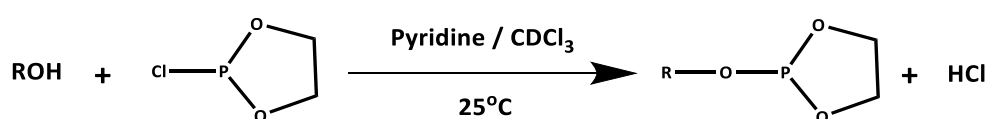


Figure 34. The reaction of 2-Chloro-1,3,2-dioxaphospholane with active hydroxyl groups. R = phenol residues, alcohols, aldehydes and carboxylic acids.

Nutshell lignin was used as an example of lignin resource, ³¹P-NMR spectrum (Figure 35) clearly shows the carboxylic acid derivatives at 127.1 ppm, p-hydroxyphenyl (H) units at 128.1 ppm and guaiacyl-OH groups around 130 ppm [71,73]. Aliphatic-OH units cannot be labelled as efficiently as aromatic OHs, however, the peaks at 133.3 can be assigned to aliphatic-OH units [72]. Erythro and threo isomers of OH groups attached to α -carbon in β -O-4 linkages were observed at 135 ppm and 134 ppm, respectively.

³¹P-NMR spectrum showed the existence of different -OH species at different subunits in the nutshell lignin example. The area under the peaks of carboxylic acid derivatives, p-hydroxyphenyl derivatives and guaiacyl-OH units were compared and found as 3%, 54%, and 43%, respectively.

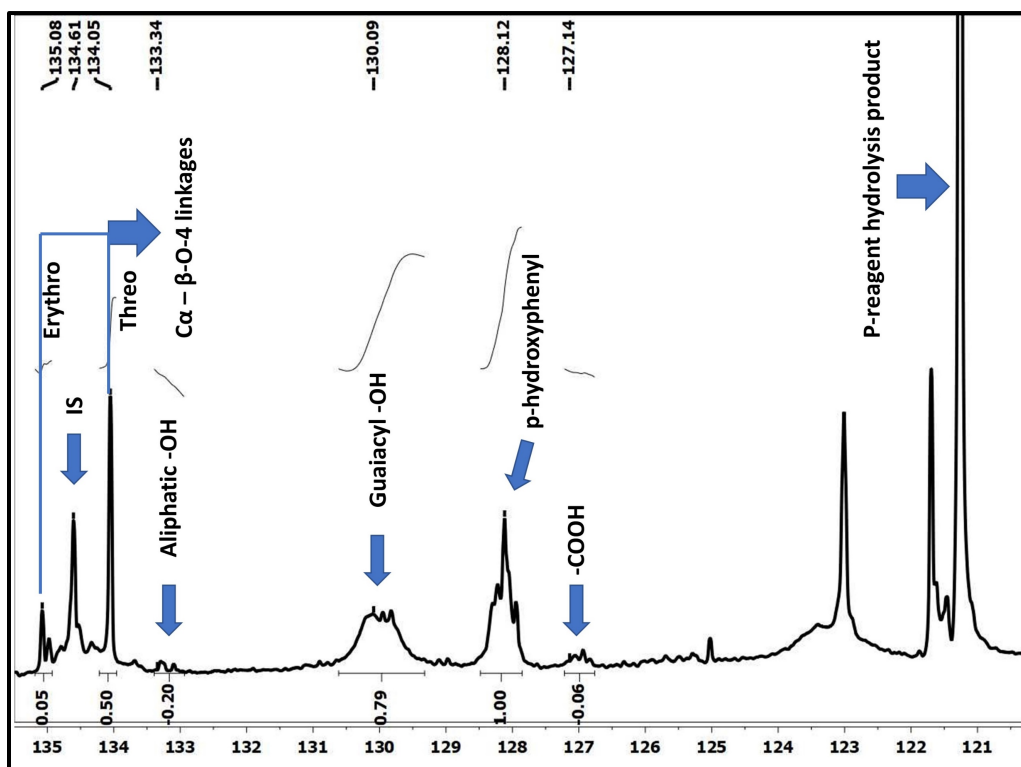


Figure 35. ^{31}P -NMR spectrum of the phosphorylated nutshell lignin.

3.1.8. Thermal Stability Results

The weight loss (Figure 36-a) and decomposition rate were plotted (calculated as derivative of weight) against temperature (Figure 36-b). Decomposition started over 200 °C, the rate maxima of all lignin were found at 450 °C, except for pine lignin, which was at 400 °C. The highest decomposition rate was observed for birch lignin and the lowest rate was observed for pine lignin. Nutshell lignin showed the best stability among the four different lignin sources, i.e. less decomposition around 250 °C and low rate over 400 °C.

Glass transition temperature (T_g) values were found as in the range of 51.65 - 87.14°C, 51.15 – 89.78°C, 52.28 – 84.30°C, and 64.31 – 92.87°C for nutshell, maple, pine and birch lignin, respectively. The decomposition curve and maximum of

the lignin were found in accordance with the literature [51], on the other hand T_g values were found to be lower than any lignin source due to devastation of intermolecular hydrogen bonds and condensed structure.

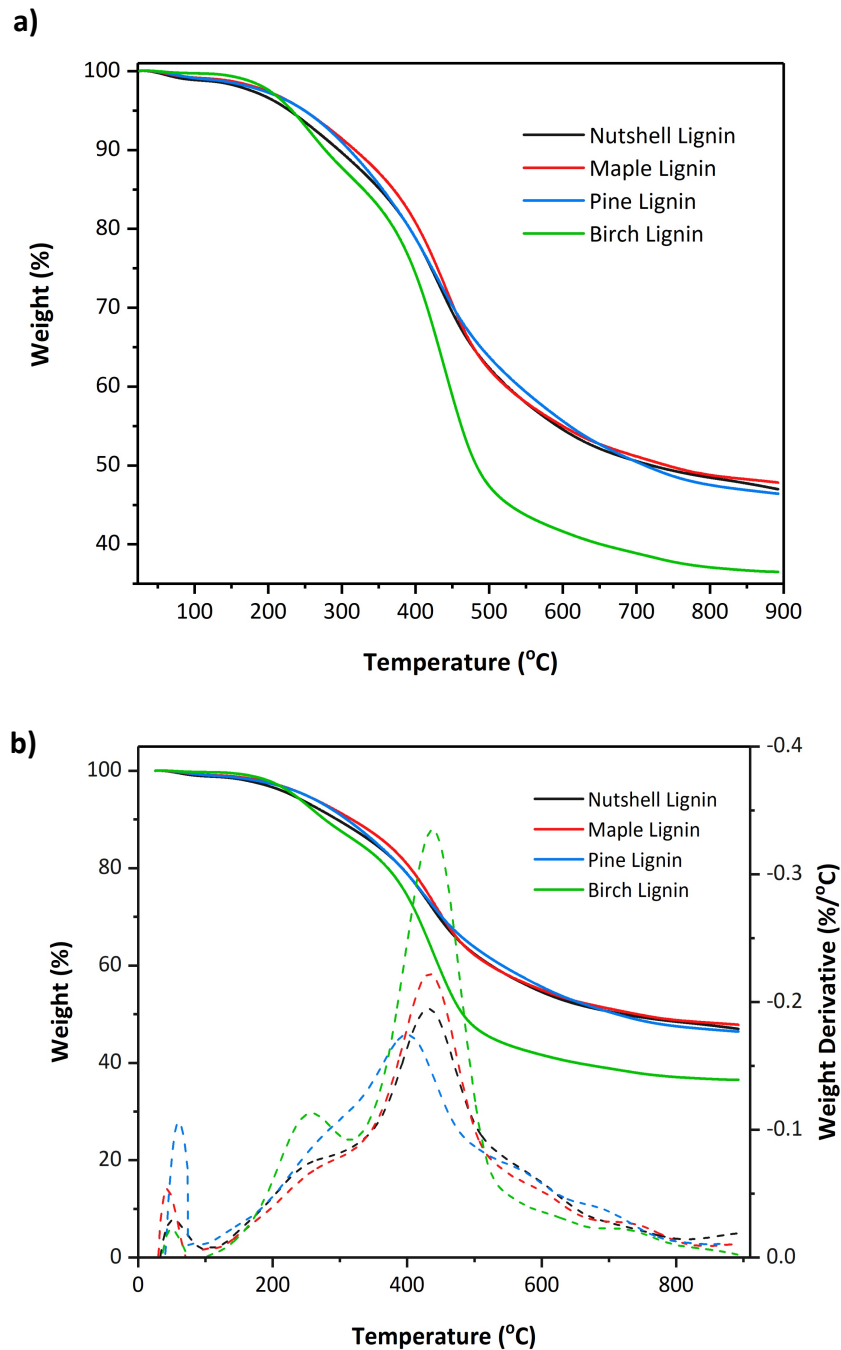


Figure 36. (a) Thermogravimetric Analysis (TGA) curve of all lignin samples. (b) TGA/DTG curve shows the decomposition rate of the samples.

3.1.9. XRD Analysis of Lignin

Nutshell Lignin XRD diffractogram was recorded as shown in Figure 37. This XRD pattern obtained shows that the obtained lignin was successfully extracted from cellulose (See red pattern of cellulose obtained from cotton in Figure 37 for comparison).

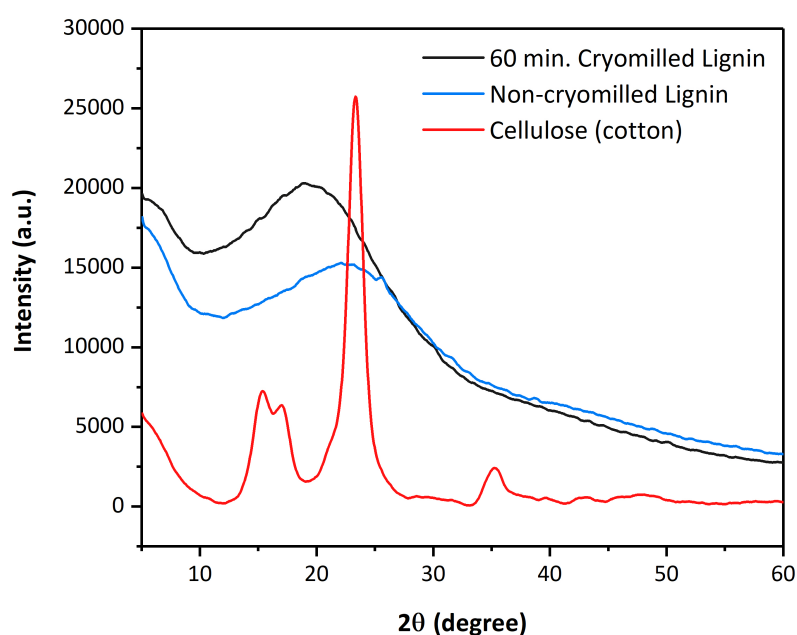


Figure 37. XRD diffractogram of cryomilled nutshell lignin and cellulose (cotton).

3.1.10. Surface Morphology Analysis of Cryomilled Lignin

Scanning Electron Microscopy (SEM) was used to image morphology of the non-cryomilled and cryomilled lignin samples (Figure 38). The SEM micrographs show vivid picture of the amorphous lignin polymer. It is shown that increasing cryomilled duration, decreases the particle size of the lignin. Mechanical treatment can reduce

the size as well as change the particle shapes – the edges sharpen during the treatment.

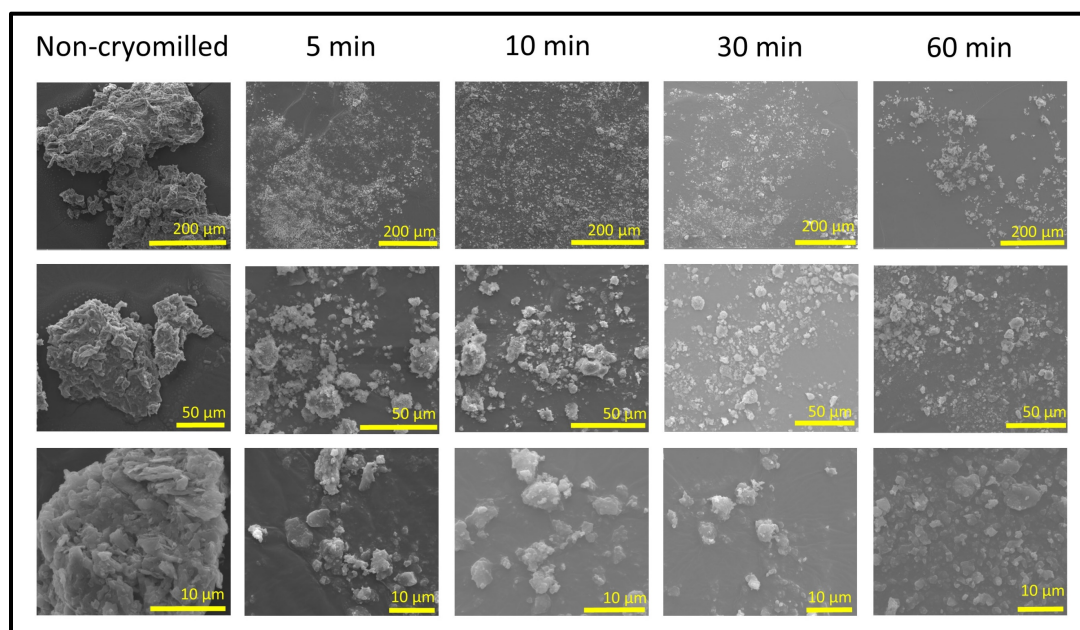


Figure 38. SEM images of non-cryomilled and 5 to 60 minutes cryomilled lignins.

3.2. Contact Charge Density and Charge Decay Measurements

3.2.1. Contact Charge Density of Thermoplastics and the Effect of Lignin

Doping

The common way that the charge measurements are pursued for soft elastomeric polymers do not work practically for the hard thermoplastics. The method suffers from the problems encountered in manipulation of the pieces into the Faraday cup with tweezers during many contact events, such as the sliding of the piece from the tweezers (see section 2.2.7). Therefore, we adopted another reliable method for measurements of surface charging for polymers using a tapping device. This time the surface electric potential is followed as the signal for charging. Indeed, this method

is beneficial over the charge measurements, especially when temporal resolution of the contact charging event is sought. It was previously shown in our group that contact and separation events can be resolved and can be separately monitored using this technique [74]. Briefly, the polymer and the metal are mounted on the two metal stubs connected to two electrobe probes of the oscilloscope. The instrument is set to measure the electric potential of the stubs (or the two materials attached to it) with respect to the ground. The two surfaces (polymer and metal) are let to tap each other at a moderate (1 Hz) frequency. When the surfaces start accumulating charges, they either pull or push electrons from/to the electrodes developing a positive or negative potential, which decays with time; all these potential signals (both their generation and their time decay) can be monitored and recorded with respect to time. As an example, contact and separation events taking place between a doped (or undoped) PS piece and PTFE piece during such a tapping event, which is recorded as the open circuit voltage is shown in (Figure 39a - b). The maximum open surface voltages observed upon contact and separation for polypropylene (PP), polylactic acid (PLA), polyethylene (PE), and polystyrene (PS), doped with 5% lignin, as shown in Table 4. These values listed in Table 4 correspond to a successful mitigation of the surface charges on thermoplastic polymers of 55.5%, 77.3%, 54%, and 78.5% for L-PP, L-PLA, L-PE, and L-PS, respectively (Figure 40).

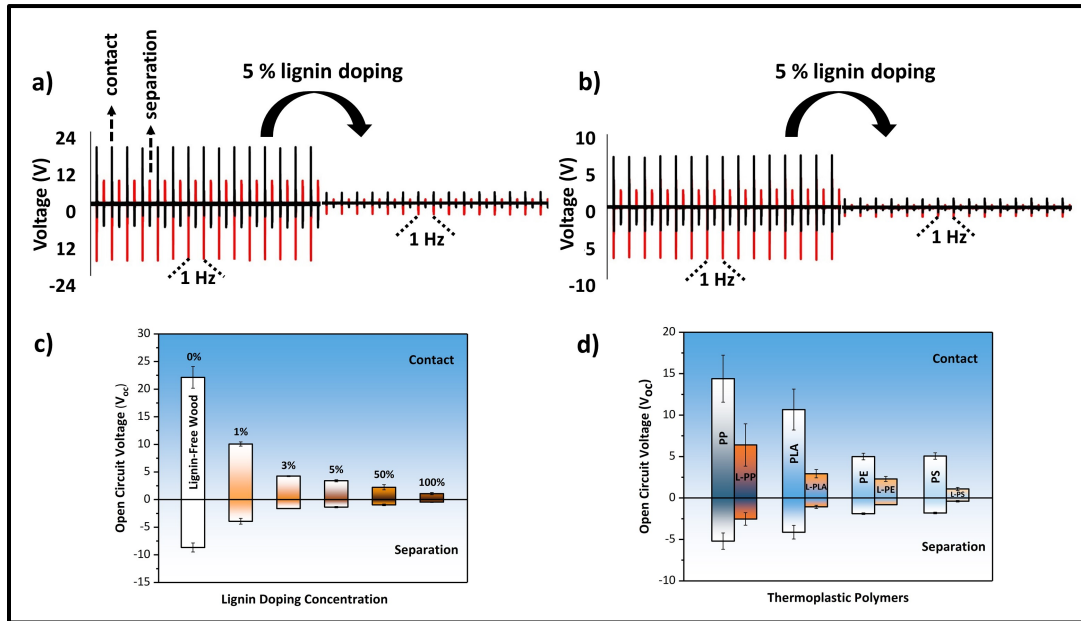


Figure 39. a) The signals of lignin-free and lignin-doped wood, b) the voltage signals of undoped and doped PS against PTFE, collected from the homemade tapping device. c-d) Surface charges of wood and thermoplastics.

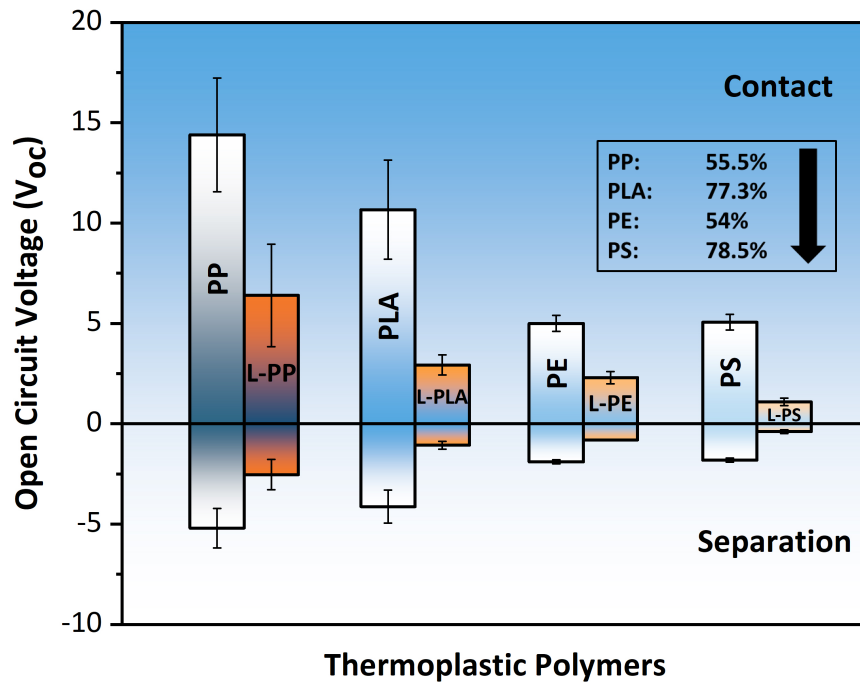


Figure 40. Open circuit voltages obtained as a result of tapping and contact-charging of the samples of selected undoped and doped with 5% (w/w) thermoplastic polymers. Lignin was 60 min cryomilled before doping. PP, PLA, PE and PS refer to pure polymers and L-PP, L-PLA, L-PE and L-PS refer to polymers doped with lignin.

All in all, it is shown that lignin is a promising material to dissipate the surface charges on both elastomers (PDMS) (see section 3.2.2) and thermoplastics (PP, PLA, PE and PS) upon doping.

Table 4. Contact Electrification results of lignin doping to wood and thermoplastics

	Samples	Contact (V_{oc})	Separation (V_{oc})
WOOD SAMPLES	Lignin - Free Wood (LFW)	22.13 ± 1.97	-8.67 ± 0.82
	1 % doped LFW	10.07 ± 0.38	-3.93 ± 0.52
	3 % doped LFW	4.26 ± 0.09	-1.63 ± 0.04
	5 % doped LFW	3.41 ± 0.2	-1.36 ± 0.13
	50 % doped LFW	2.23 ± 0.47	-0.96 ± 0.16
	Lignin	1.08 ± 0.2	-0.46 ± 0.07
THERMOPLASTICS	Polypropylene (PP)	14.4 ± 2.83	5.2 ± 0.98
	Lignin doped PP (L-PP)	6.4 ± 2.55	2.53 ± 0.75
	Polylactic acid (PLA)	10.67 ± 2.47	4.13 ± 0.82
	Lignin doped PLA (L-PLA)	2.93 ± 0.5	1.07 ± 0.19
	Polyethylene (PE)	5.0 ± 0.4	1.9 ± 0.1
	Lignin doped PE (L-PE)	2.3 ± 0.3	-0.8
	Polystyrene (PS)	5.06 ± 0.39	1.81 ± 0.1
	Lignin doped PS (L-PS)	1.09 ± 0.19	0.39 ± 0.09

3.2.2 Contact Charge Density of PDMS and The Effect of Lignin Doping

3.2.2.1. The Effect of Milling Time of Lignin on Contact Charging of PDMS

Although tapping device is advantageous because it offers a high temporal resolution and separate monitoring of contact and separation events, which provides valuable information about the mechanism of charging and discharging, it is not useful in the monitoring of CE of the PDMS samples, which have a high inherent adhesion.

Therefore, the conventional method is taken to follow its contact charging of lignin- doped and undoped PDMS samples. In this method, electrically neutral PDMS pieces held by metal tweezers are contact charged by gently touching against an aluminum foil (see section 2.2.7) up to 200 touches to acquire maximum charge density on the surfaces. The pieces are then immersed into a homemade Faraday cup connected to an electrometer that directly measures the charges induced into the Faraday cup by the charged piece immersed in it. The number of touching events and the net charge density obtained on the piece after these events are plotted (see Figure 41).

Firstly, the effect of cryomilling time of lignin on the acquired contact charges on the lignin doped PDMS pieces is investigated (Figure 42). 5 to 60 minutes cryomilled nutshell lignin was doped into PDMS to obtain 5% (w/w) lignin-doped PDMS (L- PDMS) pieces. It is shown that, as the cryomilling duration of lignin increases the surface charge density of PDMS diminishes: The maximum charges that can be obtained were found as -1.18 ± 0.20 , -1.17 ± 0.18 , -1.10 ± 0.16 and -0.84 ± 0.15 nC/cm², for 5, 10, 30, and 60 minutes, respectively, after 200 touches to aluminium foil. With 60 min cryomilled lignin, a charge mitigation of about 62% is obtained (-2.2 ± 0.20 nC/cm² (undoped) to -0.84 ± 0.15 nC/cm² (60 min cryomilled)). 60 minutes cryomilled lignin exhibits maximum impact on the charge magnitudes as less charge accumulation from even at the very first touches.

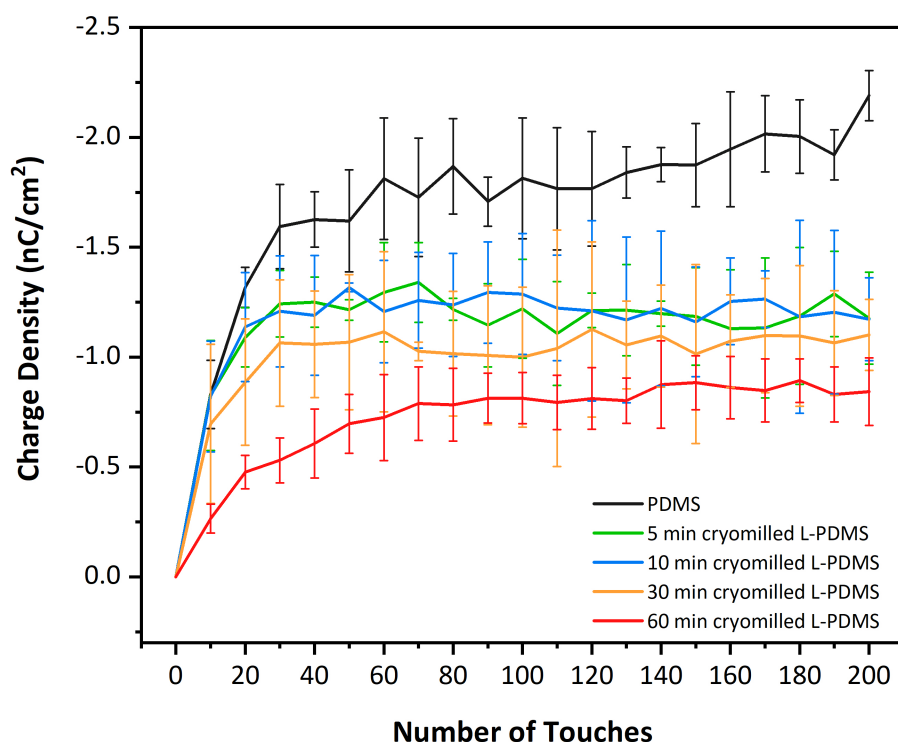


Figure 41. Contact Electrification results of 5 % lignin-doped PDMS. Undoped PDMS vs 5-10-30-60 min cryomilled doped PDMS.

Such an increase in the extent of contact charge mitigation by lignin-doping in PDMS by the increase in milling time of lignin can be attributed several factors: 1) the increase in the reacted number of radicals that are generated upon prolonged milling time, 2) the decrease in the particle size of lignin upon longer milling, which gives a higher surface area of lignin for the contact charges (mechanoions) and mechanoradicals to interact with.

Table 5 indicates that there is a continuous increase in reacted number of radicals of nutshell lignin as the cryomilling duration increases (as determined by the DPPH test, for details of this test, see Experimental part). In Table 5, it is shown that cryomilling encourages the formation of mechanoradicals, there is a ca. 20% increase in the reacted number of radicals in lignin upon milling.

Table 5. Comparison of the effects of cryomilling time on particle size, reacted number of radicals in lignin and charge density of PDMS. Reacted number of radicals were calculated after the complete reaction of lignin radicals with DPPH radicals (144 hours).

CRYOMILLING TIME (min)	PARTICLE SIZE (nm)	CHARGE DENSITY (nC/cm ²)	REACTED NUMBER OF RADICALS / g
0	-	-	$2.5 \times 10^{21} \pm 1.8 \times 10^{19}$
5	1324 ± 173.4	-1.18 ± 0.20	$2.9 \times 10^{21} \pm 1.9 \times 10^{19}$
10	892.3 ± 17.8	-1.17 ± 0.18	$2.8 \times 10^{21} \pm 7.5 \times 10^{19}$
30	913.8 ± 27.4	-1.10 ± 0.16	$3.0 \times 10^{21} \pm 1.7 \times 10^{20}$
60	756.8 ± 11.3	-0.84 ± 0.15	$3.0 \times 10^{21} \pm 1.0 \times 10^{19}$

On the other hand, surface area of the particles grows with milling time, as evident from the SEM micrographs, thanks to reduction of the particle sizes. Figure 42 and Table 5 show the inverse relation between the particle size and cryomilling time.

All in all, it is displayed that mechanical treatment of extracted lignin helps to create more radical units, as well as larger surface area of the dopant, and therefore, results in an efficient charge mitigation on PDMS surface (see Figure 42).

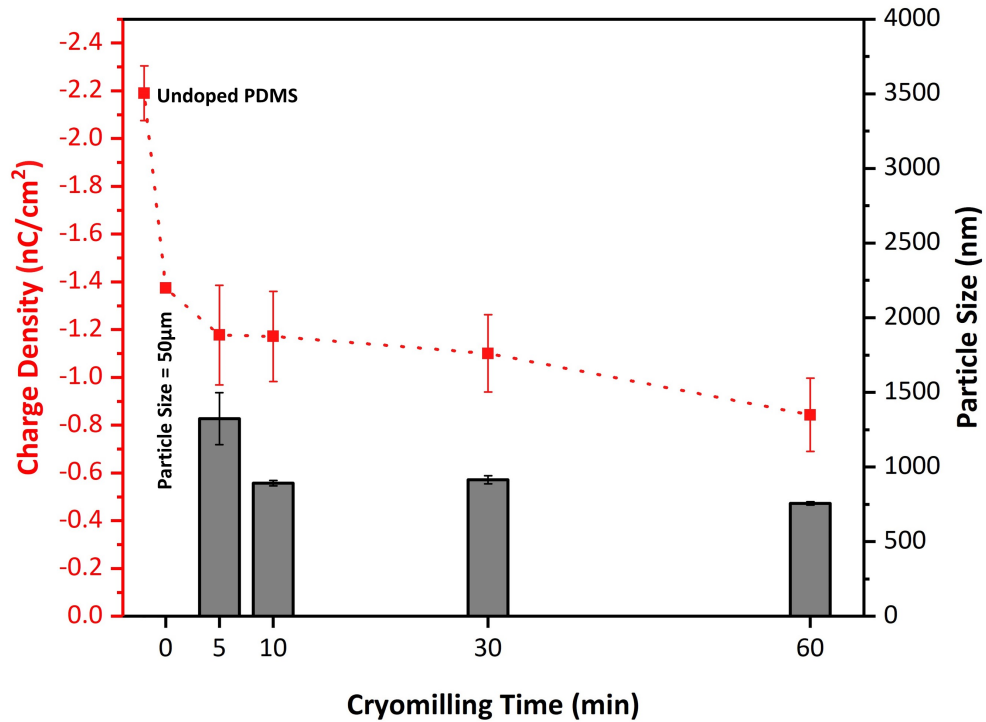


Figure 42. Charge density of PDMS and particle size of lignin as a function of cryomilling time.

3.2.2.2. The Effect of Lignin Sources on Contact Charging of PDMS

The charge mitigation effect of doping of polymers with lignin extracted from different lignin sources extracted from maple, pine, and birch barks were also investigated to understand any variations stemming from the extraction source. Lignin samples extracted from these sources were cryomilled for 60 minutes and doped into PDMS as 1% and 5% (w/w). As it is shown that in Figure 43, lignin doping reduces the surface charges of PDMS even upon 1 % doping.

The maximum charge density obtained on the lignin-doped PDMS are found as: -1.05 ± 0.12 (1%) and -0.84 ± 0.15 (5%), -1.17 ± 0.12 (1%) and -0.89 ± 0.16 (5%), -1.05 ± 0.14 (1%) and -0.93 ± 0.13 (5%), -1.23 ± 0.28 (1%) and -1.06 ± 0.28 nC/cm² (5%) for

nutshell, maple, pine and birch lignin, respectively. The nutshell lignin doped PDMS can be charged up to -1.05 ± 0.12 (1%) and -0.84 ± 0.15 (5%), while pure PDMS (undoped) charged up to -2.19 ± 0.11 nC/cm². These numbers correspond to a charge mitigation of about 52-62% upon 1 – 5% doping with lignin.

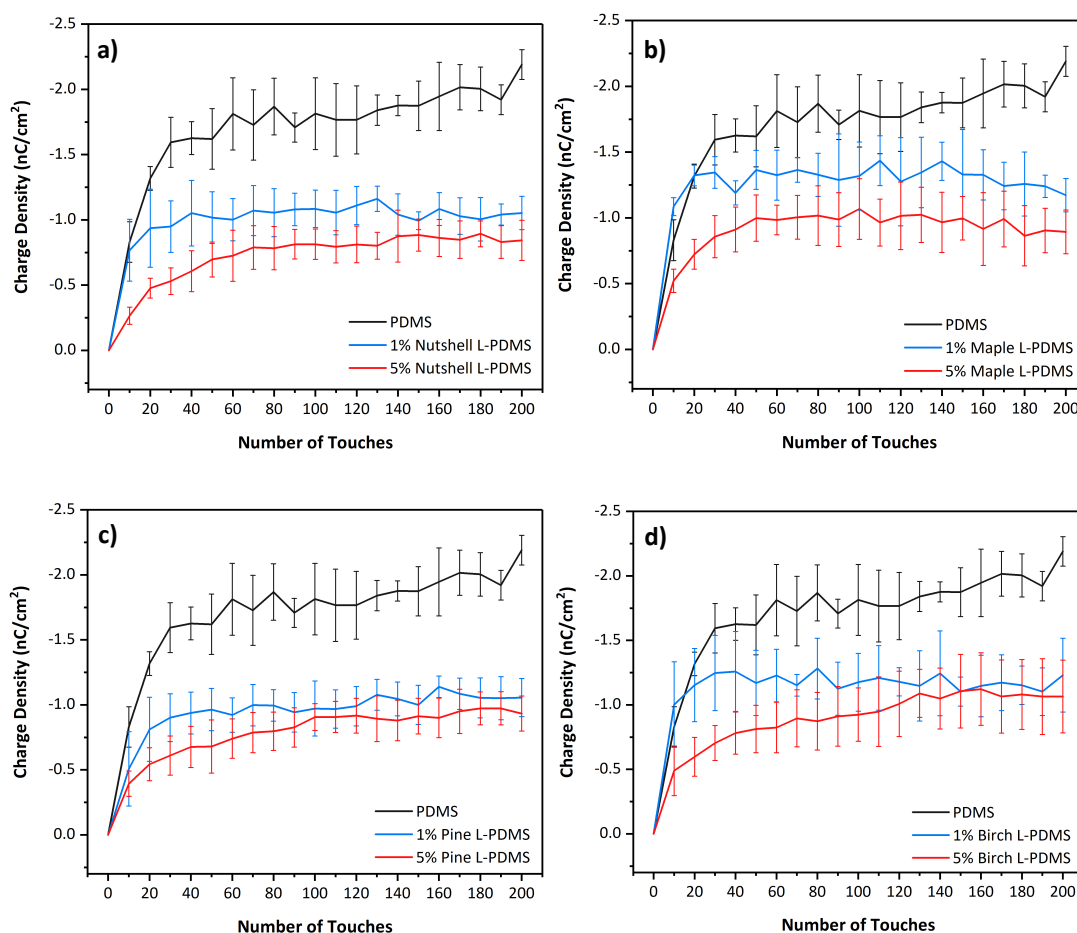


Figure 43. Charge density vs number of touches on the surface of PDMS and L-PDMS (1% and 5% doping) samples prepared with lignin extracted from nutshell, maple, pine, and birch. All samples extracted from the sources are cryomilled for 60 min before doping.

3.2.2.3. The Effect of Total Phenol Content of Lignin on Contact Charging of PDMS

The total phenol contents (TPC) of lignin samples extracted from the lignin sources listed above were calculated and listed in Table 6. In Figure 44, the charge densities obtained by touching PDMS and L-PDMS samples to aluminium foil are shown and the pieces' MGE (Methyl gallate equivalent) TPC values are given. All samples have TPCs between 61 – 75% MGE and they have a charge mitigation percentage of 52 –62%. Here, we deduce that TPC value of at least 61% MGE (birch) is sufficient to have a 52% charge mitigation in the sample.

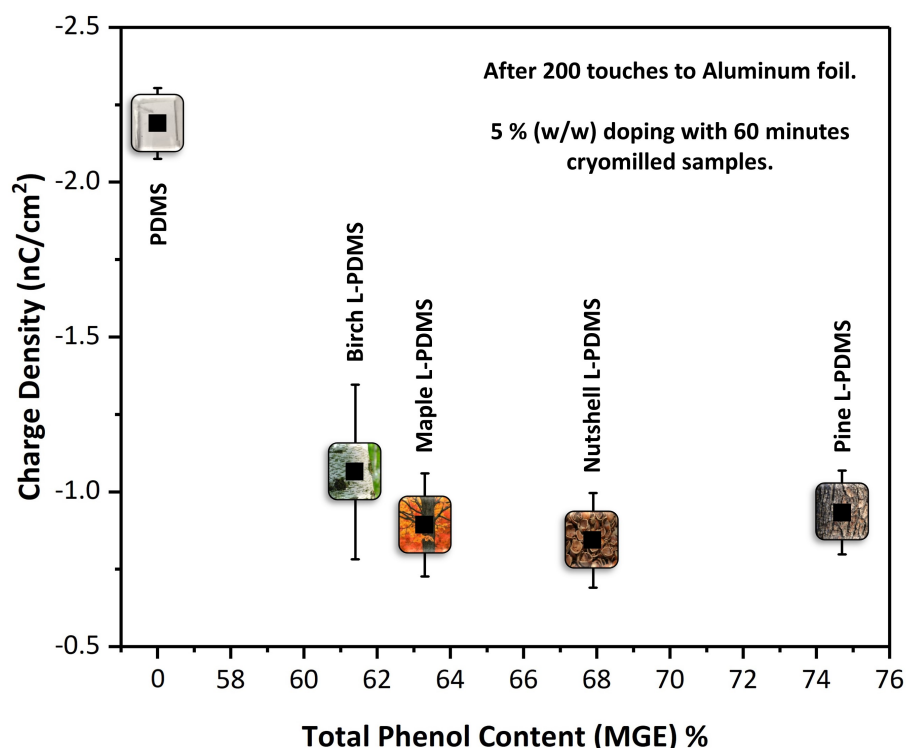


Figure 44. Charge density of undoped and doped PDMS versus total phenol content of lignin.

Table 6. Comparison of lignin total phenol content and charge density of lignin doped PDMS.

Lignin	Total Phenol Content (MGE) %	Charge Density (nC/cm ²)
PDMS	-	-2.19 ± 0.11
Birch	61.4 ± 5.1	-1.06 ± 0.28
Maple	63.3 ± 5.9	-0.89 ± 0.16
Nutshell	67.9 ± 4.6	-0.84 ± 0.15
Pine	74.7 ± 7.6	-0.93 ± 0.13

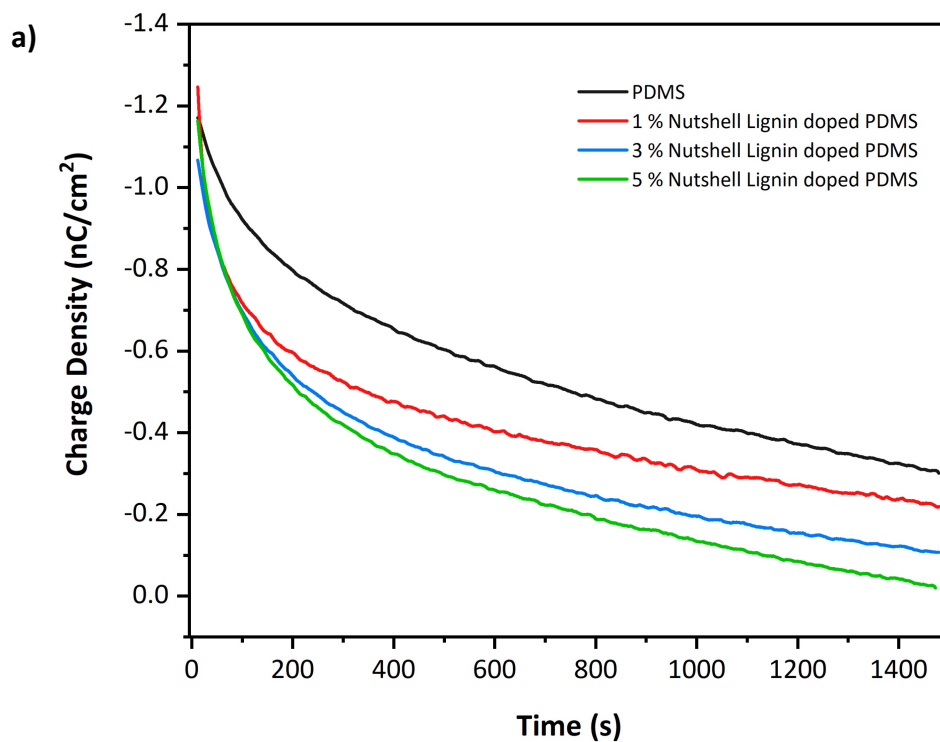
3.2.3. Contact Charge Decay on PDMS and the Effect of Lignin Doping

The comparison of the charge decay profiles of the doped and undoped polymer pieces gives information about the stability of the charges on the surfaces: whether 1) the mitigation is because less charges are produced on the surfaces upon doping or 2) there is the same amount of charges forming on the surface, however the species are now less stable because of doping. The profiles can also give information about the number of species involved in the decay process. It is reported that a contact charge decay on an undoped surfaces is first order (only one species, the mechanoions that react, migrate, etc. are involved) [20]. An involvement of a second species (e.g. dopant) can also be observed as a deviation from the first order decay [75]. Therefore, decay profiles of lignin doped and undoped PDMS pieces were recorded by letting the pieces immersed in the homemade Faraday cup for 30 minutes.

The decay rate constants were determined from the slopes of $\ln Q$ vs time plots assuming a first order decay initially. These values are found as $7.81 \times 10^{-4} \text{ s}^{-1}$, $8.22 \times 10^{-4} \text{ s}^{-1}$, $1.29 \times 10^{-3} \text{ s}^{-1}$, and $2.02 \times 10^{-3} \text{ s}^{-1}$ for undoped, 1% doped, 3% doped, and

5% doped PDMS, respectively (Figure 45-b). 5% lignin doped PDMS shows 2.6 times faster decay than undoped PDMS. It is also revealed that, increasing doping concentration from 1% to 5% accelerates the dissipation of the charges from the polymer surface.

The decay profiles show, although lignin doped PDMS can be contact charged up to a similar charge density as the undoped PDMS, however, the charges are less stable on the former and decay faster. The deviations from linearity at the $\ln Q$ vs time plots upon doping with lignin shows that the dopant has a major role in dissipation of charges.



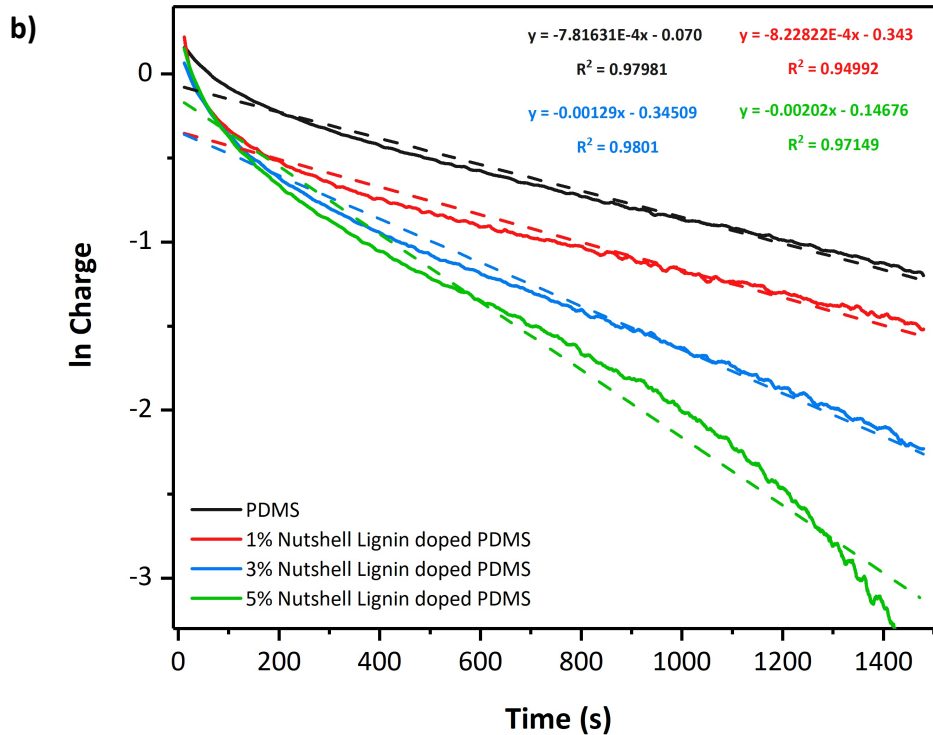


Figure 45. Charge decay plot of undoped and doped PDMS samples (a). The solid lines represent the average of at least 3 measurements. Semi-logarithmic plots of charge vs time (b).

3.2.4. Why Does Wood Not Get Charged? Does Lignin Have Any Effect?

The standpoint of the thesis idea was that lignin is the main material responsible for the wood's reluctant behaviour towards contact charging. Although many other materials' positions are debated in the triboelectric series, the position of wood in the triboelectric series does not change – it is always in the middle of the series.

To experimentally assess whether the antistatic nature of wood can be attributed to the presence of lignin, first wood's neutrality was verified by an initial experiment: Wood (pine bark) and PDMS pieces of surface area 1.5 cm² are contacted against aluminium foil under identical conditions, and any charge accumulated on the pieces are recorded vs the number of touches to Al sheet. The results show that wood does

not get charged while PDMS can be contact charged up to $-2.19 \pm 0.11 \text{ nC/cm}^2$ after 200 touches (Figure 46).

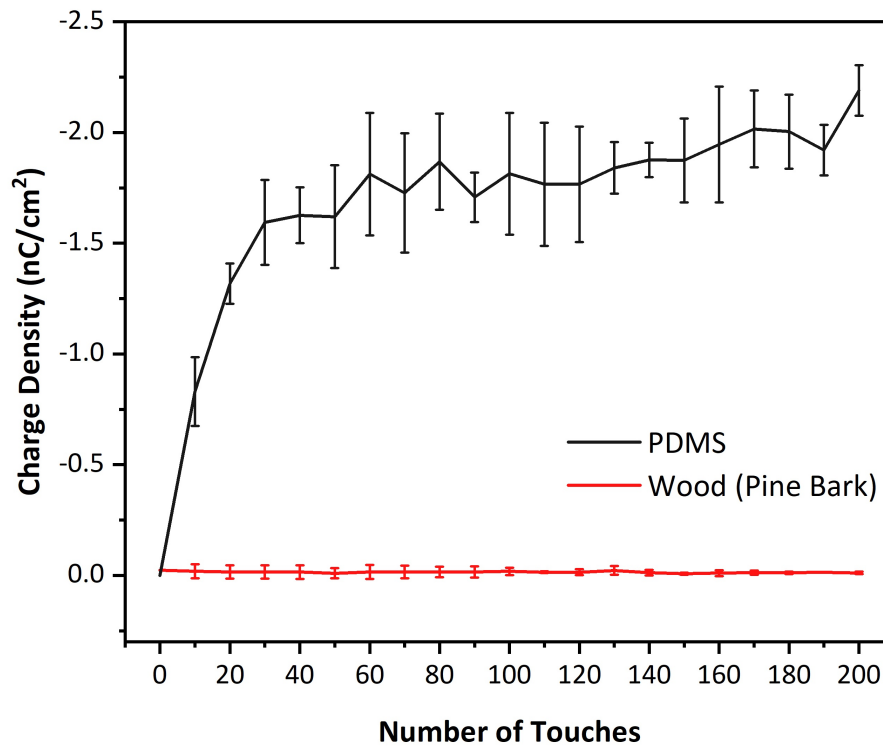


Figure 46. Charge density vs number of touches on the surface of PDMS and Pine bark wood against aluminum foil.

In a second experiment, we tried to extract lignin from wood, without changing the morphology of the wood by a previously reported method [76]. Lignin is the material that gives strength and colour to the wood; without it, wood is soft, fragile and fibrous substance. Limba wood is especially appropriate for this purpose since the cellulosic structure does not disintegrate even after the chemical removal of lignin. Lignin-free wood is a white, cellulose-like material as shown in (Figure 47-b). After complete removal of lignin, lignin-free wood was treated with cryomill, and then doped with previously extracted lignin (1, 3, 5, 50% w/w) and the final powder

material was pressed into pellets to obtain smooth surface ideal for contact charging measurements (Figure 48).



Figure 47. Lignin extraction and wood bleaching (a-b), lignin-free wood after 5 min cryomilling and lignin doping of wood by cryomilling (c-d).

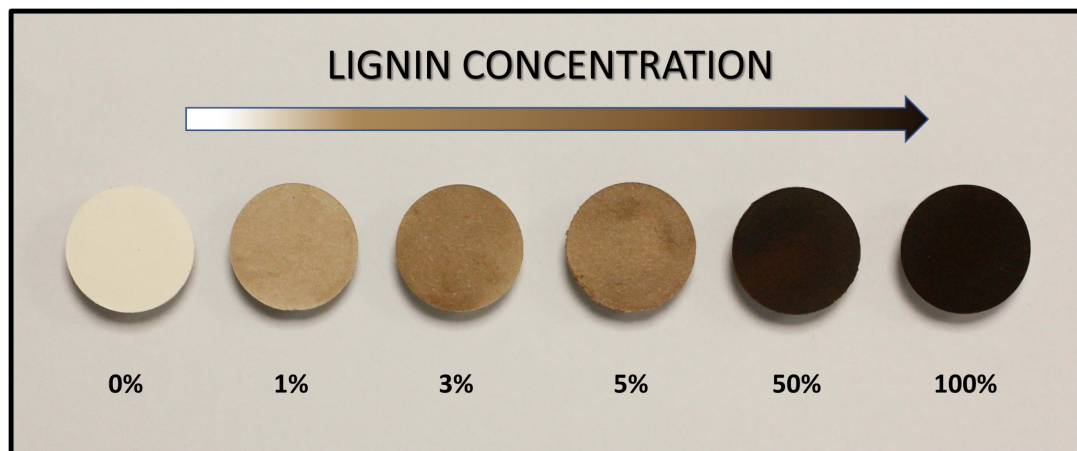


Figure 48. Lignin (pine bark) doping to lignin-free wood from 1% to 50% (w/w) by cryomilling. The samples were doped with lignin by 5 minutes of cryomilling.

Wood samples, doped with lignin and undoped, were then contact charged against PTFE and the electric potential of the surfaces created upon tapping is recorded. Contact and separation voltages were separately assigned after saturation of the oscilloscope signal (Figure 49). After the lignin extraction, lignin-free wood showed

up to 22.13 ± 1.97 V (V_{contact}) while, 1 %, 3 %, 5% and 50 % doped wood charged 10.07 ± 0.38 , 4.26 ± 0.09 , 3.41 ± 0.2 and 2.23 ± 0.47 V (V_{contact}), respectively. It can be seen that increasing lignin doping ratio inhibits the charging on the wood samples.

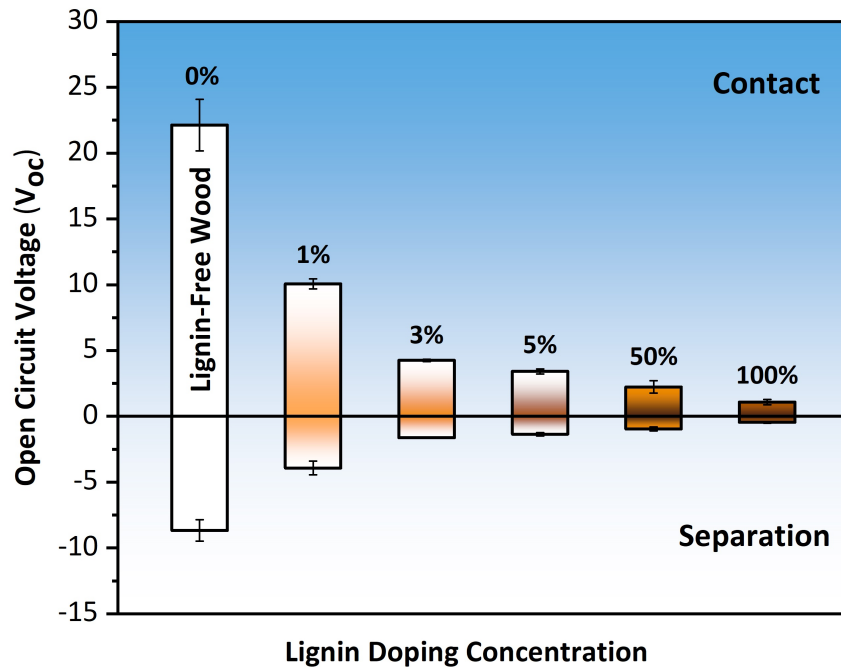


Figure 49. Contact Electrification of lignin-free wood and lignin doping concentration to wood by 1-3-5-50% (w/w). 100% doping concentration refers to pure lignin.

3.2.5. The Effect of Lignin Doping on The Surface Conductance of PDMS

One of the traditional mechanisms by which a dopant can render a polymer antistatic is the increase in surface conductance. Metals, carbon, conductive polymers or humidity enhancers can increase the surface conductance of the polymers by causing a direction percolation (metals, carbon, conductive polymers) or a quench the charges by conducting them on a continuous layer of water. Some organic molecules can also be doped into polymers to increase the surface conductance above the antistatic threshold. In order to find out whether lignin doping increases the surface

conductance, we performed two-probe surface conductance measurements on the samples. From the results of these measurements, it can be claimed that surface conductance of PDMS does not change (or changes in negligible amount) after doping with 5% (w/w) of lignin. Surface conductance was found to be independent from both lignin doping and the origin of lignin.

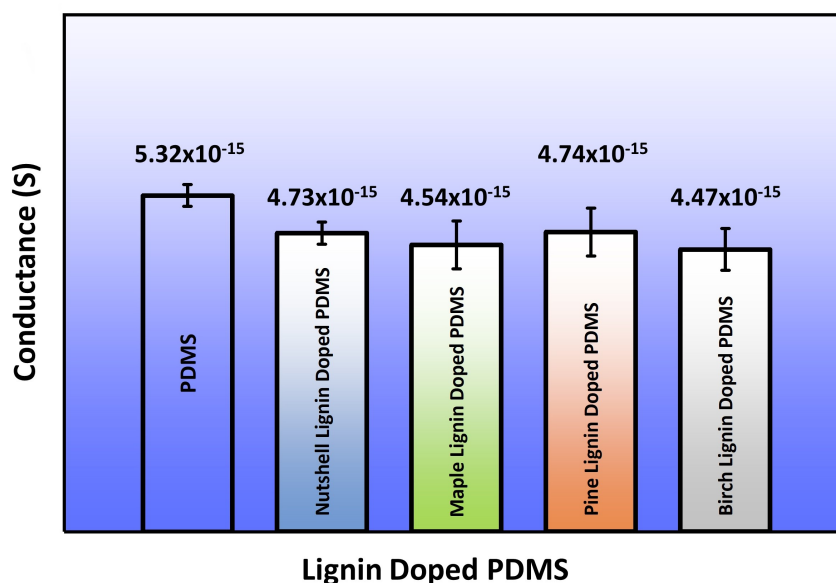


Figure 50. Surface conductance results of PDMS and 5% lignin doped PDMS samples. Conductance of the samples were calculated from surface resistivities measured via two-probe method. For experimental details see section 2.2.7.3.

3.3. Mechanism of Charge Dissipation by Radical Scavenging

The charges on contact charged polymers can be stable up to weeks and even to months. If there is no antistatic additive present in the polymer, the contact charges are proposed to decay through mechanisms that involve reactions with gases in the air, or through migration into the polymer bulk. There are several methods described in the literature in order to eliminate or decrease the surface charges on contact-charged polymers by additives increasing the rate of decay through creation of other

pathways in the decay mechanism. All the traditional methods of contact charge dissipation involve a conductance increase upon doping the dielectric materials with metals, carbon powder, and conductive polymers. The surface conductance can also be enhanced indirectly by attracting water from atmosphere on the polymer surfaces by doping the polymers with surface humidity enhancers such as ionic polymers. As explained in detail below, a new method was proposed recently to involve another pathway, including removal of mechanoradicals on surfaces, which does not increase surface conductance.

Herein, we have verified that, lignin, can also be used as an antistatic additive, addition of which decreases the accumulation of surface charges acquired on contact charged polymers. Its presence in low amounts (1-5%) in polymeric materials also increases the discharge rates of the charge on the surfaces. Initially lignin was chosen as a possible antistatic polymer additive depending on its radical scavenging ability. However, the mechanism of charge dissipation must be clarified before the next steps are taken; to understand whether the mechanism 1) includes an increase in conductance, 2) includes an action of mechanoradicals or 3) involves participation of other functional groups present in the structure of lignin. Since there exists no direct spectroscopic or chemical tool to assess the mechanism that is taking place at the very surface of the polymer, the clues obtained from several observations helped us to understand some facts about the mechanism as follows.

First of all, we rule out the conventional mechanism of conductance increase since the surface conductance did not increase upon lignin doping at the doping concentrations we used in the experiments (section 3.2.5).

Secondly, we analysed the hints from the “radical scavenging mechanism” that involves mechanoradicals. In Figure 51, the mechanoradicals ($\text{ROO}\cdot$) created upon contact and separation on polymer surfaces due to bond-breakages are shown together with charges, which are mechanoions. On the right in Figure 51, stabilization of the co-formed surface charges by mechanoradicals is pictured: The strong orbital interactions between anion/cation orbitals with SOMO of radical orbitals, which is confirmed by a later computational study, is the reason for this stabilization [2,24,25]. Upon doping with lignin, radicals that are known to exist in native lignin may also play a role in the mechanism: They can react with mechanoradicals and remove them from the surface. Therefore, the surface charges are no longer stabilized and dissipate faster inevitably (Figure 52). For this mechanism to take place, native (extracted) lignin has already a reacted number of radicals (ca. $2.5 \times 10^{21}/\text{g}$, section 3.1.4.). However, we also found that the cryomilling time of 60 minutes increases the (chemically accessible) radicalic content by only 20%; however, this causes an increase in charge dissipation of more than 60% (compared to an undoped state). Therefore, charge dissipation by the native lignin radicals (even when the number of lignin radicals are increased upon milling) cannot be the sole mechanism.

Therefore, we surmise the mechanism should involve stable radical (phenoxy-type) formation by H-transfer from the phenol groups of lignin (the most acidic positions) to the mechanoradicals. This reaction, too, results in the scavenging of mechanoradicals and destabilizes the charges, yielding an apparently faster decay of them. This mechanism is supported by the fact that 1) lignin has enough phenolic-OH content in the polymer backbone (in the same order with common molecular radical

scavengers), which is evident from the total phenol content analysis (section 3.1.3) and 2) by the fact that alkali lignin cannot provide the same level of an antioxidant activity upon doping. By using lignin extracted from different sources that have slight differences between the ratio of different monomeric units (differently substituted phenyls), we also tried to assess which of these monomeric units might be more active in this reaction. However, as the solid-state NMR studies show, the similar ratio of the monomeric units in the examples of lignin sources we chose to use, does not allow for such a comparison.

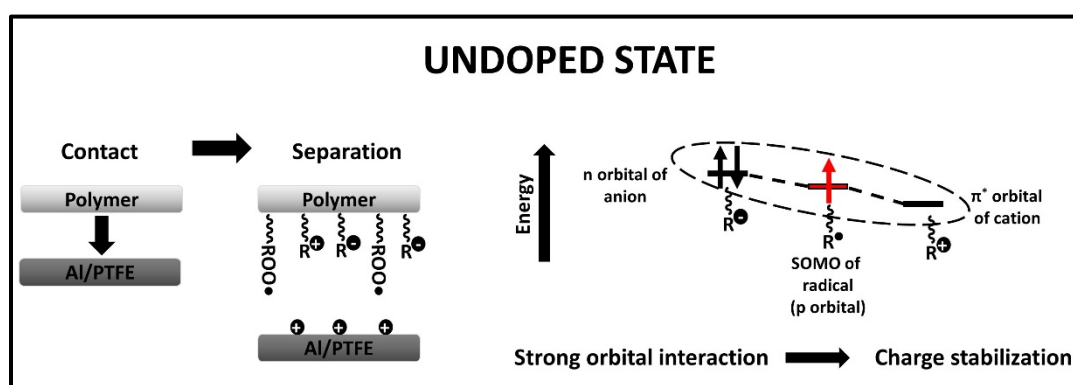


Figure 51. The mechanism of contact charge formation and stabilization on polymer surface of an undoped polymer.

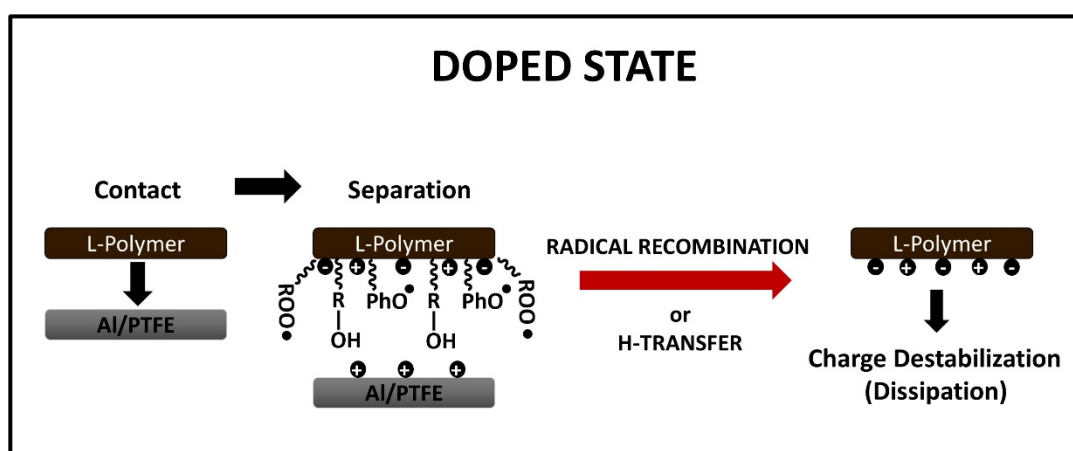


Figure 52. The mechanism of contact charge dissipation by removal of mechanoradicals by radical (re)combination or H-transfer via lignin doping.

CHAPTER 4

4. CONCLUSION

In this thesis, lignin was successfully extracted from available natural sources: nutshell, and maple, pine, birch tree barks were used to display the lignin's antistatic action upon doping it to common polymers and to investigate the mechanism of this action. It was found out that, up to 5% lignin doping caused 60-80% decrease in accumulated charge on the polymer surfaces studied. The doping also caused a faster decay (ca. 3 times faster than undoped) of charge on the surfaces. Unlike common molecular radical scavengers, which were shown to provide an antistatic activity through a mechanoradical removal, due to lignin's complicated structure, several other mechanisms might be involved in its antistatic action. Primarily, we ruled out the increase in surface conductance by doping through surface conductance measurements. Through total phenol content and quantitative radical analyses, we show that the mechanism should involve an H-transfer from the phenolic groups in lignin to the mechanoradicals formed, resulting in (more) stable radicals and removal of the mechanoradicals that are responsible for charge stability. The antistatic action could also be assisted by radicals that are present in native lignin, which might

combine with mechanoradicals, remove them, and cause a destabilization of charges. The results are demonstrated that lignin, a naturally available, low-cost material is a good candidate to be used as an antistatic additive for common polymers even with low concentrations of doping to get rid of charge accumulation-based hazards in industry, particularly, space, pharmaceuticals, electronics, packaging, and plastics manufacturing. We hope that the explanation we provided on the antistatic action of lignin in contact-charged polymers will be helpful in this technological endeavor as well as in understanding the long-debated molecular mechanism of contact-charging and its dissipation on common polymers.

5. REFERENCES

1. Baytekin, H.T.; Patashinski, A.Z.; Branicki, M.; Baytekin, B.; Soh, S.; Grzybowski, B.A. The Mosaic of Surface Charge in Contact Electrification. *Science* **2011**, *333*, 308–312.
2. Baytekin, H.T.; Baytekin, B.; Hermans, T.M.; Kowalczyk, B.; Grzybowski, B.A. Control of Surface Charges by Radicals as a Principle of Antistatic Polymers Protecting Electronic Circuitry. *Science* **2013**, *341*, 1368–1371.
3. Zou, H.; Zhang, Y.; Guo, L.; Wang, P.; He, X.; Dai, G.; Zheng, H.; Chen, C.; Wang, A.C.; Xu, C.; et al. Quantifying the triboelectric series. *Nat. Commun.* **2019**, *10*, 1427.
4. Zhang, X.; Huang, X.; Kwok, S.W.; Soh, S. Designing Non-charging Surfaces from Non-conductive Polymers. *Adv. Mater.* **2016**, *28*, 3024–3029.
5. Greason, W.D. Review of the Effect of Electrostatic Discharge and Protection Techniques for Electronic Systems. *IEEE Trans. Ind. Appl.* **1987**, *IA-23*, 205–216.
6. Gibson, N. Static electricity — an industrial hazard under control? *J. Electrostat.* **1997**, *40–41*, 21–30.
7. Lai, S.T. *Spacecraft Charging*; Amer Inst of Aeronautics & Reston, VA, 2011; ISBN 978-1-60086-836-8.

8. Angelopoulos, M. Conducting Polymers in Microelectronics. *IBM J Res Dev* **2001**, *45*, 57–75.
9. Matsusaka, S.; Maruyama, H.; Matsuyama, T.; Ghadiri, M. Triboelectric charging of powders: A review. *Chem. Eng. Sci.* **2010**, *65*, 5781–5807.
10. Chen, L.; Shi, Q.; Sun, Y.; Nguyen, T.; Lee, C.; Soh, S. Controlling Surface Charge Generated by Contact Electrification: Strategies and Applications. *Adv. Mater.* **2018**, *30*, 1802405.
11. Grzybowski, B.A.; Winkleman, A.; Wiles, J.A.; Brumer, Y.; Whitesides, G.M. Electrostatic self-assembly of macroscopic crystals using contact electrification. *Nat. Mater.* **2003**, *2*, 241.
12. McCarty, L.S.; Winkleman, A.; Whitesides, G.M. Electrostatic Self-Assembly of Polystyrene Microspheres by Using Chemically Directed Contact Electrification. *Angew. Chem. Int. Ed.* **2007**, *46*, 206–209.
13. Fan, F.-R.; Tian, Z.-Q.; Lin Wang, Z. Flexible triboelectric generator. *Nano Energy* **2012**, *1*, 328–334.
14. Wang, Z.; Lin, L.; Chen, J.; Niu, S.; Zi, Y. *Triboelectric Nanogenerators; Green Energy and Technology*; Springer International Publishing, 2016; ISBN 978-3-319-40038-9.
15. Wu, C.; Wang, A.C.; Ding, W.; Guo, H.; Wang, Z.L. Triboelectric Nanogenerator: A Foundation of the Energy for the New Era. *Adv. Energy Mater.* **2019**, *9*.
16. McCarty, L.S.; Winkleman, A.; Whitesides, G.M. Ionic Electrets: Electrostatic Charging of Surfaces by Transferring Mobile Ions upon Contact. *J. Am. Chem. Soc.* **2007**, *129*, 4075–4088.

17. McCarty, L.S.; Whitesides, G.M. Electrostatic Charging Due to Separation of Ions at Interfaces: Contact Electrification of Ionic Electrets. *Angew. Chem. Int. Ed.* **2008**, *47*, 2188–2207.
18. Baytekin, B.; Baytekin, H.T.; Grzybowski, B.A. What Really Drives Chemical Reactions on Contact Charged Surfaces? *J. Am. Chem. Soc.* **2012**, *134*, 7223–7226.
19. Baytekin, H.T.; Baytekin, B.; Incorvati, J.T.; Grzybowski, B.A. Material Transfer and Polarity Reversal in Contact Charging. *Angew. Chem. Int. Ed.* **2012**, *51*, 4843–4847.
20. Baytekin, H.T.; Baytekin, B.; Soh, S.; Grzybowski, B.A. Is Water Necessary for Contact Electrification? *Angew. Chem. Int. Ed.* **2011**, *50*, 6766–6770.
21. Li, C.; Liang, T.; Lu, W.; Tang, C.; Hu, X.; Cao, M.; Liang, J. Improving the antistatic ability of polypropylene fibers by inner antistatic agent filled with carbon nanotubes. *Compos. Sci. Technol.* **2004**, *64*, 2089–2096.
22. Tolinski, M. Trends in Polyolefin and Additive Use. In *Additives for Polyolefins*; Elsevier, 2009; pp. 9–21 ISBN 978-0-8155-2051-1.
23. Orlando, J.J.; Tyndall, G.S. Laboratory studies of organic peroxy radical chemistry: an overview with emphasis on recent issues of atmospheric significance. *Chem. Soc. Rev.* **2012**, *41*, 6294.
24. Mazur, T.; Grzybowski, B.A. Theoretical basis for the stabilization of charges by radicals on electrified polymers. *Chem. Sci.* **2017**, *8*, 2025–2032.
25. Baytekin, H.T.; Baytekin, B.; Grzybowski, B.A. Mechanoradicals Created in “Polymeric Sponges” Drive Reactions in Aqueous Media. *Angew. Chem. Int. Ed.* **2012**, *51*, 3596–3600.

26. Fang, Y.; Gonuguntla, S.; Soh, S. Universal Nature-Inspired Coatings for Preparing Noncharging Surfaces. *ACS Appl. Mater. Interfaces* **2017**, *9*, 32220–32226.
27. Lacks, D.J.; Mohan Sankaran, R. Contact electrification of insulating materials. *J. Phys. Appl. Phys.* **2011**, *44*, 453001.
28. Coehn, A. Ueber ein Gesetz der Electricitätserregung. *Ann. Phys.* **1898**, *300*, 217–232.
29. Hersh, S.P.; Montgomery, D.J. Static Electrification of Filaments: Experimental Techniques and Results. *Text. Res. J.* **1955**, *25*, 279–295.
30. Henniker, J. Triboelectricity in Polymers. *Nature* **1962**, *196*, 474.
31. Adams, C.K. *Nature's Electricity*; 1 edition.; Tab Books: Blue Ridge Summit, PA, 1987; ISBN 978-0-8306-2769-1.
32. Diaz, A.F.; Felix-Navarro, R.M. A semi-quantitative tribo-electric series for polymeric materials: the influence of chemical structure and properties. *J. Electrostat.* **2004**, *62*, 277–290.
33. Harper, W.R. *Contact and frictional electrification*; Laplacian Press: Morgan Hill, Calif, 1998; ISBN 978-1-885540-06-5.
34. Apodaca, M.M.; Wesson, P.J.; Bishop, K.J.M.; Ratner, M.A.; Grzybowski, B.A. Contact Electrification between Identical Materials. *Angew. Chem. Int. Ed.* **2010**, *49*, 946–949.
35. Faustino, H.; Gil, N.; Baptista, C.; Duarte, A.P. Antioxidant Activity of Lignin Phenolic Compounds Extracted from Kraft and Sulphite Black Liquors. *Molecules* **2010**, *15*, 9308–9322.

36. Ponomarenko, J.; Lauberts, M.; Dizhbite, T.; Lauberte, L.; Jurkjane, V.; Telysheva, G. Antioxidant activity of various lignins and lignin-related phenylpropanoid units with high and low molecular weight. *Holzforschung* **2015**, *69*.
37. Mahmood, Z.; Yameen, M.; Jahangeer, M.; Riaz, M.; Ghaffar, A.; Javid, I. Lignin as Natural Antioxidant Capacity. *Lignin - Trends Appl.* **2018**.
38. Lu, F.J.; Chu, L.H.; Gau, R.J. Free radical-scavenging properties of lignin. *Nutr. Cancer* **1998**, *30*, 31–38.
39. Gregorova, A.; Košíková, B.; Staško, A. Radical scavenging capacity of lignin and its effect on processing stabilization of virgin and recycled polypropylene. *J. Appl. Polym. Sci.* **2007**, *106*, 1626–1631.
40. Nsimba, R.Y.; West, N.; Boateng, A.A. Structure and Radical Scavenging Activity Relationships of Pyrolytic Lignins. *J. Agric. Food Chem.* **2012**, *60*, 12525–12530.
41. García, A.; González Alriols, M.; Spigno, G.; Labidi, J. Lignin as natural radical scavenger. Effect of the obtaining and purification processes on the antioxidant behaviour of lignin. *Biochem. Eng. J.* **2012**, *67*, 173–185.
42. McCarthy, J.L.; Islam, A. Lignin Chemistry, Technology, and Utilization: A Brief History. In *Lignin: Historical, Biological, and Materials Perspectives*; Glasser, W.G., Northey, R.A., Schultz, T.P., Eds.; American Chemical Society: Washington, DC, 1999; Vol. 742, pp. 2–99 ISBN 978-0-8412-3611-0.
43. Sakakibara, A. A structural model of softwood lignin. *Wood Sci. Technol.* **1980**, *14*, 89–100.
44. Zakzeski, J.; Bruijnincx, P.C.A.; Jongerius, A.L.; Weckhuysen, B.M. The Catalytic Valorization of Lignin for the Production of Renewable Chemicals. *Chem. Rev.* **2010**, *110*, 3552–3599.

45. Upton, B.M.; Kasko, A.M. Strategies for the Conversion of Lignin to High-Value Polymeric Materials: Review and Perspective. *Chem. Rev.* **2016**, *116*, 2275–2306.
46. Schutyser, W.; Renders, T.; Van den Bosch, S.; Koelewijn, S.-F.; Beckham, G.T.; Sels, B.F. Chemicals from lignin: an interplay of lignocellulose fractionation, depolymerisation, and upgrading. *Chem. Soc. Rev.* **2018**, *47*, 852–908.
47. Achyuthan, K.E.; Achyuthan, A.M.; Adams, P.D.; Dirk, S.M.; Harper, J.C.; Simmons, B.A.; Singh, A.K. Supramolecular Self-Assembled Chaos: Polyphenolic Lignin's Barrier to Cost-Effective Lignocellulosic Biofuels. *Molecules* **2010**, *15*, 8641–8688.
48. Duval, A.; Lawoko, M. A review on lignin-based polymeric, micro- and nano-structured materials. *React. Funct. Polym.* **2014**, *85*, 78–96.
49. Ponnusamy, V.K.; Nguyen, D.D.; Dharmaraja, J.; Shobana, S.; Banu, J.R.; Saratale, R.G.; Chang, S.W.; Kumar, G. A review on lignin structure, pretreatments, fermentation reactions and biorefinery potential. *Bioresour. Technol.* **2019**, *271*, 462–472.
50. Thakur, V.K.; Thakur, M.K.; Raghavan, P.; Kessler, M.R. Progress in Green Polymer Composites from Lignin for Multifunctional Applications: A Review. *ACS Sustain. Chem. Eng.* **2014**, *2*, 1072–1092.
51. Sen, S.; Patil, S.; Argyropoulos, D.S. Thermal properties of lignin in copolymers, blends, and composites: a review. *Green Chem.* **2015**, *17*, 4862–4887.
52. Patil, S.V.; Argyropoulos, D.S. Stable Organic Radicals in Lignin: A Review. *ChemSusChem* **2017**, *10*, 3284–3303.
53. Bährle, C.; Nick, T.U.; Bennati, M.; Jeschke, G.; Vogel, F. High-Field Electron Paramagnetic Resonance and Density Functional Theory Study of Stable Organic Radicals in Lignin: Influence of the Extraction Process, Botanical Origin, and

- Protonation Reactions on the Radical g Tensor. *J. Phys. Chem. A* **2015**, *119*, 6475–6482.
54. Chakar, F.S.; Ragauskas, A.J. Review of current and future softwood kraft lignin process chemistry. *Ind. Crops Prod.* **2004**, *20*, 131–141.
55. *Monomers, Polymers and Composites from Renewable Resources*; Elsevier, 2008; ISBN 978-0-08-045316-3.
56. Kim, J.S.; Lee, Y.Y.; Kim, T.H. A review on alkaline pretreatment technology for bioconversion of lignocellulosic biomass. *Bioresour. Technol.* **2016**, *199*, 42–48.
57. Bunzel, M.; Schüßler, A.; Tchetseubu Saha, G. Chemical Characterization of Klason Lignin Preparations from Plant-Based Foods. *J. Agric. Food Chem.* **2011**, *59*, 12506–12513.
58. Sun, Z.; Fridrich, B.; de Santi, A.; Elangovan, S.; Barta, K. Bright Side of Lignin Depolymerization: Toward New Platform Chemicals. *Chem. Rev.* **2018**, *118*, 614–678.
59. Owen, M.J. Elastomers: Siloxane. In *Encyclopedia of Materials: Science and Technology*; Buschow, K.H.J., Cahn, R.W., Flemings, M.C., Ilschner, B., Kramer, E.J., Mahajan, S., Veyssi re, P., Eds.; Elsevier: Oxford, 2001; pp. 2480–2482 ISBN 978-0-08-043152-9.
60. Waheed, S.; Cabot, J.M.; Macdonald, N.P.; Kalsoom, U.; Farajikhah, S.; Innis, P.C.; Nesterenko, P.N.; Lewis, T.W.; Breadmore, M.C.; Paull, B. Enhanced physicochemical properties of polydimethylsiloxane based microfluidic devices and thin films by incorporating synthetic micro-diamond. *Sci. Rep.* **2017**, *7*, 15109.

61. Adly, N.; Weidlich, S.; Seyock, S.; Brings, F.; Yakushenko, A.; Offenhäusser, A.; Wolfrum, B. Printed microelectrode arrays on soft materials: from PDMS to hydrogels. *Npj Flex. Electron.* **2018**, *2*, 15.
62. Bedük, T. Lignin as an antistatic additive for common polymers. Thesis, Bilkent University, 2018.
63. Argyropoulos, D.S. Quantitative Phosphorus-31 NMR Analysis of Lignins, a New Tool for the Lignin Chemist. *J. Wood Chem. Technol.* **2006**.
64. Lin, S.Y.; Dence, C.W. *Methods in Lignin Chemistry*; Springer Berlin Heidelberg: Berlin, Heidelberg, 1992; ISBN 978-3-642-74065-7.
65. Zhao, X.; Huang, Z.; Zhang, Y.; Yang, M.; Chen, D.; Huang, K.; Hu, H.; Huang, A.; Qin, X.; Feng, Z. Efficient solid-phase synthesis of acetylated lignin and a comparison of the properties of different modified lignins. *J. Appl. Polym. Sci.* **2017**, *134*.
66. Graham, H.D. Stabilization of the Prussian blue color in the determination of polyphenols. *J. Agric. Food Chem.* **1992**, *40*, 801–805.
67. Cyr, N.; Eloffson, R.M.; Ripmeester, J.A.; Mathison, G.W. Study of lignin in forages and wood by carbon-13 CP/MAS NMR. 1. Some evidence of polymerization and depolymerization. *J. Agric. Food Chem.* **1988**, *36*, 1197–1201.
68. Gao, X.; Laskar, D.D.; Zeng, J.; Helms, G.L.; Chen, S. A ¹³ C CP/MAS-Based Nondegradative Method for Lignin Content Analysis. *ACS Sustain. Chem. Eng.* **2015**, *3*, 153–162.
69. Davis, M.F.; Schroeder, H.A.; Maciel, G.E. Solid-State ¹³ C Nuclear Magnetic Resonance Studies of Wood Decay. III. Decay of Colorado Blue Spruce and Paper Birch by *Postia placenta*. *Holzforschung* **1994**, *48*, 301–307.

70. Archipov, Y.; Argyropoulos, D.S.; Bolker, H.I.; Heitner, C. ^{31}P NMR Spectroscopy in Wood Chemistry. I. Model Compounds. *J. Wood Chem. Technol.* **1991**, *11*, 137–157.
71. Argyropoulos, D.S.; Bolker, H.I.; Heitner, C.; Archipov, Y. ^{31}P NMR Spectroscopy in Wood Chemistry Part V. Qualitative Analysis of Lignin Functional Groups. *J. Wood Chem. Technol.* **1993**, *13*, 187–212.
72. Balakshin, M.; Capanema, E. On the Quantification of Lignin Hydroxyl Groups With ^{31}P and ^{13}C NMR Spectroscopy. *J. Wood Chem. Technol.* **2015**, *35*, 220–237.
73. Argyropoulos, D.S. ^{31}P NMR in wood chemistry: A review of recent progress. *Res. Chem. Intermed.* **1995**, *21*, 373–395.
74. Musa, U.G.; Cezan, S.D.; Baytekin, B.; Baytekin, H.T. The Charging Events in Contact-Separation Electrification. *Sci. Rep.* **2018**, *8*, 2472.
75. Cezan, S.D.; Nalbant, A.A.; Buyuktemiz, M.; Dede, Y.; Baytekin, H.T.; Baytekin, B. Control of triboelectric charges on common polymers by photoexcitation of organic dyes. *Nat. Commun.* **2019**, *10*, 276.
76. Zhu, M.; Song, J.; Li, T.; Gong, A.; Wang, Y.; Dai, J.; Yao, Y.; Luo, W.; Henderson, D.; Hu, L. Highly Anisotropic, Highly Transparent Wood Composites. *Adv. Mater.* **2016**, *28*, 5181–5187.